

2024-05-01

Selective Transfection Of A Transferrin Receptor-Expressing Cell Line With Dna-Lipid Nanoparticles And Synthesis Of Parasite-Derived Glycans As Biomarkers For Leishmaniasis

Irodiel Vinales Lozano
University of Texas at El Paso

Follow this and additional works at: https://scholarworks.utep.edu/open_etd



Part of the [Allergy and Immunology Commons](#), [Biomedical Commons](#), [Chemistry Commons](#), [Immunology and Infectious Disease Commons](#), and the [Medical Immunology Commons](#)

Recommended Citation

Vinales Lozano, Irodiel, "Selective Transfection Of A Transferrin Receptor-Expressing Cell Line With Dna-Lipid Nanoparticles And Synthesis Of Parasite-Derived Glycans As Biomarkers For Leishmaniasis" (2024). *Open Access Theses & Dissertations*. 4164.
https://scholarworks.utep.edu/open_etd/4164

This is brought to you for free and open access by ScholarWorks@UTEP. It has been accepted for inclusion in Open Access Theses & Dissertations by an authorized administrator of ScholarWorks@UTEP. For more information, please contact lweber@utep.edu.

SELECTIVE TRANSFECTION OF A TRANSFERRIN RECEPTOR-EXPRESSING CELL
LINE WITH DNA-LIPID NANOPARTICLES AND SYNTHESIS OF PARASITE-DERIVED
GLYCANS AS BIOMARKERS FOR LEISHMANIASIS

IRODIEL VINALES LOZANO

Doctoral Program in Chemistry

APPROVED:

Katja Michael, Ph.D., Chair

Igor C. Almeida, Ph.D.

Sreeprasad T. Sreenivasan, Ph.D.

Manuel L. Penichet, MD Ph.D.

Stephen L. Crites, Jr., Ph.D.
Dean of the Graduate School

Copyright 2024 Irodiel Vinales Lozano

SELECTIVE TRANSFECTION OF A TRANSFERRIN RECEPTOR-EXPRESSING CELL
LINE WITH DNA-LIPID NANOPARTICLES AND SYNTHESIS OF PARASITE-DERIVED
GLYCANS AS BIOMARKERS FOR LEISHMANIASIS

by

IRODIEL VINALES LOZANO, BSc.

DISSERTATION

Presented to the Faculty of the Graduate School of

The University of Texas at El Paso

in Partial Fulfillment

of the Requirements

for the Degree of

DOCTOR OF PHILOSOPHY

Department of Chemistry and Biochemistry

THE UNIVERSITY OF TEXAS AT EL PASO

May 2024

ACKNOWLEDGMENTS

In the culmination of my academic journey, I extend my deepest gratitude to those who have supported and inspired me along the way.

Dr. Katja Michael. As my mentor and research advisor, she has consistently provided invaluable guidance and support over the course of my Ph.D. journey. Her trust in my capabilities and relentless push for excellence have had a transformative effect on my academic and personal growth. Dr. Michael has enriched my life culturally and acted as my personal Grammarly (most of the English I currently know is because of her). As she emphasizes, mentorship entails a lifelong commitment, and I am deeply appreciative of her ongoing support. Thank you sincerely for everything.

Dr. Igor Almeida. I extend my sincerest gratitude for your unwavering support throughout my research journey. Your generous sharing of knowledge and access to lab resources have been fundamental to the progress of my work. I am deeply appreciative of the guidance you have provided and the trust you have placed in me.

Dr. Sreeprasad T. Sreenivasan. Your guidance during my doctoral years as a member of my committee has been remarkable. Your approachability and dedication to teaching the Advanced Analytical course have been exemplary, serving as an example of academic excellence. You have set a shining example of success in academia.

Dr. Manuel L. Penichet. I extend my heartfelt thanks for your guidance and mentorship during the final years of my PhD journey. Your technical expertise, support, and wealth of knowledge have been instrumental in shaping the success of my research endeavors. Moreover, your insightful teachings, including the revelation that Cuba had more than one discoverer, have enriched my understanding beyond the confines of academia.

Dr. Zhu Young Kim. I extend my sincere gratitude for your support as a member of my committee, particularly during the challenging comprehensive exam part B. Your guidance and expertise were instrumental in navigating this critical phase of my academic journey.

Dr. Rosa A. Maldonado. I wish to express my gratitude for your approachability and transparency throughout our interactions. Your willingness to share lab resources generously and treat me with the same care as your own student has been immensely appreciated. Moreover, your insightful history lessons and unwavering optimism have not only enriched my academic journey but also inspired me to approach challenges with a positive mindset.

Dr. Wilson Poon. Your dedication to teaching and guiding me through the intricacies of the realm of lipid nanoparticles has been essential to my growth as a researcher. I am profoundly grateful for your generosity in sharing your resources and for fostering an environment of honesty and enthusiasm within your lab. Moreover, your commitment to maintaining a beautifully organized workspace and cultivating a healthy, friendly atmosphere is a testament to your exemplary leadership.

Dr. Alba Lucia Montoya. I extend my heartfelt thanks to Dr. Alba Lucia Montoya for her guidance in synthesizing carbohydrates and for exemplifying dedication and hard work during her tenure in Dr. Michael's Lab.

Eileni Rodriguez Gil. Your constant presence and invaluable life and work lessons have been a source of strength and wisdom. Your emotional support has carried me through the challenges of this journey.

Juan Enrique Martinez Urbay. To my very best friend of over 15 years, Juan Enrique Martinez Urbay, your honesty, integrity, and unwavering support have been a constant source of inspiration and strength.

Dr. Cameron C. Ellis. Your readiness to assist without hesitation, coupled with your exemplary character, has been a guiding light.

Dr. Priscila Silva Grijo Farany. Your support and organizational prowess have been invaluable. Your dedication sets a high standard for excellence.

Dr. Igor Estevao Da Silva. Your support in running the ELISAs and measuring our samples has been indispensable to the success of our endeavors.

Miguel A. Beltran. Thank you for the invaluable support while working on our cancer project.

Dr. Colin D. Knight. Your support, particularly during the initial phases of our cancer project, has been deeply appreciated.

Dante Salinas. Your assistance during MaxiPrep has been crucial to our progress.

Juan Carlos Silva Espinoza. Your optimism and willingness to assist have been a constant source of encouragement. Your emotional support has provided strength during challenging times, and your wealth of knowledge has enriched my understanding of our field. You are an exceptional biologist and human being, and I am profoundly grateful for your presence in my life.

Diana Gonzalez Garcia. Your support during experiments and willingness to share resources have been deeply appreciated.

Dr. James Salvador. Your excellence in teaching and support in organic chemistry has been instrumental in shaping my academic journey.

Dr. Keelung Hong and the Yen Chuang Foundation. I extend my deepest gratitude to Dr. Keelung Hong and the Yen Chuang Foundation for their generous support, which has been instrumental in enabling our research endeavors. Dr. Hong's guidance and introduction to the

intricate world of liposome synthesis have opened new avenues of exploration and learning for me.

Dr. Ricardo A. Bernal and Dr. Marco A. Ramirez-Ramos. My thanks to both of you for your support in capturing CryoEM images.

Graduate School and School of Sciences. Thank you for all the activities and for the economic support through the Dr. Keelung Hong Chemistry Graduate Research Fellowship.

Dr. Jose A. Hernandez. Thank you very much for your technical support with measuring the first genosphere formulations.

Maria H. Rodriguez. Maria, your support with paperwork and problem-solving skills have been indispensable throughout this journey.

Veronica Fortier. Your guidance and support have been invaluable assets during this journey.

Guillermo A. Campos. Your unwavering assistance and readiness to help have been deeply appreciated.

Dr. Sohan R. Jankuru Hennadige. Your support with NMR and MS measurements has been instrumental to the success of my research.

Dr. Mahesh Narayan. I am grateful for your support and guidance as my graduate advisor during my first year in the program.

Department of Chemistry and Biochemistry. Our department deserves heartfelt appreciation for its support throughout my journey, particularly for the teaching assistant position it provided me when I needed it.

This acknowledgment is a testament to the profound impact each of you has had on my academic and personal growth. Your support and encouragement have been indispensable, and for that, I am eternally grateful.

CONTENTS

ACKNOWLEDGMENTS.....	iv
LIST OF FIGURES.....	xii
LIST OF TABLES	xvi
LIST OF SCHEMES.....	xvii
CHAPTER 1. PEPTIDE-DECORATED LIPID NANOPARTICLES WITH ENCAPSULATED PDNA ENABLE SELECTIVE TRANSFECTION OF CELLS	1
1.1. ABSTRACT.....	1
1.2. HYPOTHESIS AND SPECIFIC AIMS	2
1.3. INTRODUCTION	4
1.3.1. A POTENTIAL TREATMENT AGAINST MELANOMA AND THE ORIGIN OF OUR LIPID NANOPARTICLE JOURNEY	4
1.3.1.1. PRELIMINARY EXPERIMENTS	7
1.3.2. GENE DELIVERY METHODS.....	11
1.3.3. ACHIEVING SELECTIVITY	13
1.3.4. PHYSICOCHEMICAL CHARACTERISTICS AND SYNTHESIS OF LNPS	15
1.4. MATERIALS AND METHODS.....	18
1.4.1. REAGENTS AND CELL LINES	18
1.4.2. SYNTHESIS OF LNPS	20
1.4.3. LNP CHARACTERIZATION.....	21

1.4.4. <i>IN VITRO</i> TRANSFECTION ASSAY AND CELL IMAGES	23
1.4.5. FLOW CYTOMETRY	24
1.4.6. STATISTICAL ANALYSIS	24
1.5. RESULTS AND DISCUSSION	26
1.5.1. SYNTHESIS OF LNPS	26
1.5.2. CHARACTERIZATION OF LNPS.....	29
1.5.3. <i>IN VITRO</i> TRANSFECTION ASSAY	35
1.5.4. TRANSFECTION EFFICIENCY ASSESSED BY FLOW CYTOMETRY	37
1.6. CONCLUSIONS.....	41
1.7. IMPACT STATEMENT AND FUTURE DIRECTIONS.....	43
CHAPTER 2. IMPROVED SYNTHESIS OF <i>LEISHMANIA</i> PARASITE-DERIVED GLYCANS (G27 _{SH} AND G28 _{SH}) AND ITS CONJUGATION TO LIPIDS	44
2.1. ABSTRACT.....	44
2.2. HYPOTHESIS AND SPECIFIC AIMS	45
2.3. INTRODUCTION	48
2.3.1. GLYCOSCIENCES	48
2.3.2. LEISHMANIASIS OVERVIEW	50
2.3.3. G27 _{SH} AND G28 _{SH} IN cELISA	53
2.4. MATERIALS AND METHODS.....	54
2.5. RESULTS AND DISCUSSION	56

2.5.1. PREVIOUS SYNTHESIS OF <i>O</i> -ALLYL- β -D-GALACTOFURANOSIDE (5).....	56
2.5.2. NEW SYNTHESIS OF <i>O</i> -ALLYL- β -D-GALACTOFURANOSIDE (5)	58
2.5.3. PREVIOUS SYNTHETIC PROCEDURE FOR THE THIOL-ENE REACTION.....	60
2.5.4. NEW SYNTHETIC PROCEDURE FOR THE THIOL-ENE REACTION	62
2.5.5. PREVIOUS DEACYLATION PROCEDURE	63
2.5.6. NEW DEACYLATION PROCEDURE.....	66
2.5.7. NGP INSTABILITY OVERVIEW	70
2.5.8. SYNTHESIS OF THE NEOGLYCOLIPIDS (NGLS)	72
2.6. CONCLUSIONS.....	81
2.7. ADDITIONAL PROJECT: CONJUGATION OF G28 _{SH} TO CRM197 PROTEIN	83
REFERENCES	86
VITA.....	112

LIST OF FIGURES

Figure 1. Chemical structure and schematic representation of the α Gal epitope	5
Figure 2. Schematic representation of our ideal approach for a melanoma treatment	6
Figure 3. Result of the transfection of B16 cells with murine ggta1 DNA with an HA-tag at the C-terminus using a mammalian expression vector. The expression of α 1,3GalT with HA-tag was analyzed using Western Blot and protein was found at the expected 51 kDa (A); and α Gal expression was detected using fluorescence microscopy (B). Untransfected (wt) and ggta1-transfected B16 cells were coincubated with Griffonia simplicifolia Lectin I (GSL I) Isolectin B4, Dylight 594 (Vector Labs) and visualized via fluorescence (B) using a Cytation 7 Cell Imaging Multi-Mode Reader (Biotek, Agilent).	8
Figure 4. Transfection of hTfR1-expressing CHO cells with mCherry mRNA using two different LNPs. A: untransfected negative control; B: LNP without DT7. C: LNP with DT7. The mCherry fluorescence was visualized using a Cytation 7 Cell Imaging Multi-Mode reader (Biotek, Agilent). Live cell microscopy images were collected at 20X, bright field, and fluorescence images for mCherry (593/618 nm).	9
Figure 5. Transfection experiments of CHO TfR1 (+) cells (A, B) and CHO TfR1 (-) cells (C, D) with LNP DT7 (+) and mGreenLantern (mGL) coding DNA as a gene reporter using a mammalian expression plasmid vector. The cells were fixed using 4% PFA at 60 hpt and incubated with DAPI. A and C: Detection of the fluorescence of mGL; B and D: merged images of mGL and DAPI detection. CHO cells were visualized via fluorescence using a Cytation 7 Imaging Multi-Mode Reader (Biotek, Agilent).	10

Figure 6. Cytotoxicity effect of pooled NHS on α Gal-negative (top) and α Gal-positive (bottom). The cytotoxicity assay was performed using the aCella TOX kit (CLATOX100, Cell Technology). The kit quantitatively measures the release of glyceraldehyde-3-phosphate dehydrogenase (GAPDH) from mammalian cells. GAPDH catalyzes the oxidative phosphorylation of glyceraldehyde-3-phosphate (GAP) to 1,3-bisphosphoglycerate kinase (PGK) to produce ATP, which is then detected via luciferase/luciferin bioluminescence using a Cytation 7 Cell Imaging Multi-Mode Reader (Biotek, Agilent) Statistical analysis: Mixed-effects model with Geisser-Greenhouse correction and Turkey's multiple comparison test. **, $p < 0.001$	11
Figure 7. Schematic representation of a) the preparation of LNPs with maleimide functionalization (LNP-Mal) by the pipetting mixing method (Figure 1a created with BioRender); and b) post-assembly modification with the DT7 peptide to yield the LNP-DT7 particles.	29
Figure 8. Characterization of LNP-Mal and LNP-DT7 at different DMG-PEG2000 concentrations and N/P ratios. a, b, and c) Size (intensity-weighted), ζ -potential, and EE% at different DMG-PEG2000 concentrations, respectively. d, e, and f) Size (intensity-weighted), ζ -potential, and EE% at different N/P ratios, respectively. Data indicate mean \pm SD of three replicates.....	33
Figure 9. CryoEM image of a) LNP-Mal and b) LNP-DT7. Both particles were formulated with 3 mol% of DMG-PEG2000 and an N/P ratio = 6.	34
Figure 10. mGL protein expression in CHO-TRVb-neo (top row) and CHO-TRVb-hTfR1 cells (bottom row). At 48 h post-transfection of 600 ng of mGL-pDNA LNP-DT7, cells were stained with Hoechst 33342 (second column) and imaged in the Cytation 7 microscope mode, using the filters for DAPI (Hoechst 33342) and GFP (mGL).	37
Figure 11. Percentage of mGL-positive cells at different concentrations of pDNA. CHO-TRVb-neo and CHO-TRVb-hTfR1 cells transfected with 0, 100, 200, 400, 600, 800, and 1000 ng of	

mGL-pDNA encapsulated in LNP-DT7. As a positive control, transfection of 100 ng mGL-pDNA with Lipofectamine 2000 was performed in both cell lines. The percentage of mGL transfected cells was evaluated by flow cytometry. Data were represented as mean \pm SD of biological replicates (n = 3). Statistical analysis was performed by Bonferroni's multiple comparisons test: *** p <0.001; **** p <0.0001..... 38

Figure 12. Percentage of mGL-positive CHO-TRVb-hTfR1 cells at different concentrations of pDNA encapsulated in LNP-2ME and LNP-DT7. CHO-TRVb-hTfR1 cells were transfected with 0, 100, 200, 400, 600, 800, and 1000 ng of mGL-pDNA encapsulated in LNP-2ME (nontargeting LNPs) and LNP-DT7 (active targeting LNPs). As a positive control, transfection of 100 ng mGL-pDNA with Lipofectamine 2000 (Lf-2000) was performed. The percentage of mGL transfected cells was evaluated by flow cytometry by counting 10,000 events..... 40

Figure 13. Structures of a) G27_{SH} and b) G28_{SH} used for conjugation..... 45

Figure 14. Schematic representation of Leishmania surface glycoconjugates (GPLs) 53

Figure 15. a) Cross-titration showing the response of NGP27b and NGP28b against L. major serum pool, L. tropica serum pool, and healthy serum pool b) Cross-titration showing the response of NGP27b and NGP28b against L. braziliensis serum pool and healthy serum pool..... 54

Figure 16. ¹H-NMR, 600 MHz, D₂O, compound (G28_S)₂..... 68

Figure 17. ¹³C-NMR, 150 MHz, D₂O, compound (G28_S)₂..... 69

Figure 18. ESI-TOF HR mass spectrum of compound (G28_S)₂ 70

Figure 19. Circular Dichroism measurements and α -helix percentage of a) NGP28b and b) NGP29b..... 71

Figure 20. ESI-MS HR spectra of DSPE-PEG2000-Mal and its product of conjugation DSPE-PEG2000-G28..... 74

Figure 21. ^1H -NMR, 400 MHz, CDCl_3 , spectra (top) DSPE-PEG2000-G28, and (bottom) DSPE-PEG2000-Mal	75
Figure 22. ESI-MS HR spectrum of DSPE-G28	76
Figure 23. ^1H -NMR, 400 MHz, CDCl_3 , spectra (top) DSPE-G28, and (bottom) DSPE-Mal	77
Figure 24. ESI-MS HR spectrum of DSPE-4PEG-G28.....	78
Figure 25. ^1H -NMR, 400 MHz, CDCl_3 , spectra (top) DSPE-4PEG-G28, and (bottom) DSPE-4PEG-Mal	79
Figure 26. ^1H -NMR, 400 MHz, CDCl_3 , spectra (top) DSPE-PEG3400-G28,	80
Figure 27. Chemical structure of the heterobifunctional crosslinker Sulfo-GMBS.	83
Figure 28. MALDI-TOF MS of CRM197 (blue) and CRM197-G28 (red).....	85

LIST OF TABLES

Table 1. List of chemical abbreviations, their composition, and sources.	18
Table 2. Monosaccharide symbol nomenclature for glycans.....	50

LIST OF SCHEMES

Scheme 1. Excerpt from Montoya et al. JACS Au showing the synthetic scheme for G27 _{SH} and G28 _{SH}	46
Scheme 2. Synthesis of galactofuranoside 5, a precursor for synthesizing G27 _{SH} and G28 _{SH} . Alba Montoya's dissertation provides a complete description.	57
Scheme 3. Optimized Fischer-Lubineau D-Galf synthesis.	59
Scheme 4. Thiol-ene photoadditions following the old procedure.	60
Scheme 5. Decomposition of AIBN and DPAP initiators.	61
Scheme 6. Optimized thiol-ene photoaddition.	63
Scheme 7. Zemplen deacylation following the previous procedure.	64
Scheme 8. Optimized Zemplen deacylation.	66
Scheme 9. Structures of the maleimide-derivatized phospholipids and their corresponding NGLs after conjugation with G28 _{SH}	73

CHAPTER 1. PEPTIDE-DECORATED LIPID NANOPARTICLES WITH ENCAPSULATED PDNA ENABLE SELECTIVE TRANSFECTION OF CELLS

1.1. ABSTRACT

Despite notable progress in lipid nanoparticle (LNP)-mediated gene delivery, achieving selective transfection of specific cell types, such as cancer cells, remains a significant hurdle, hindering the advancement of innovative gene therapies. In this study, we engineered an LNP formulation encapsulating plasmid DNA (pDNA) encoding the monomeric Green Lantern (mGL) fluorescent reporter protein. The DT7 peptide ligand targeting human transferrin receptor 1 (hTfR1) was also conjugated to the LNP surface for targeted delivery to hTfR1-expressing cells. Optimization of LNP composition yielded favorable particle diameter, ζ -potential, yield, and pDNA encapsulation efficiency. Evaluation of transfection selectivity using a panel of two engineered cell lines, CHO-TRVb-hTfR1 expressing hTfR1 and CHO-TRVb-neo lacking this receptor, was accomplished through flow cytometry, measuring the expression of the fluorescent mGL protein. Our experiments revealed a dose-dependent mGL expression in the evaluated range of LNP concentrations, with up to 20% transfection efficiency in CHO-TRVb-hTfR1 cells and markedly lower efficiency (up to 4%) in CHO-TRVb-neo cells, indicating a five-fold enhanced selectivity for hTfR1-expressing cells. These findings suggest the potential of this LNP platform, or similar ones modified with DT7, for *in vivo* applications, particularly in the selective targeting of malignant cells overexpressing hTfR1. Further work aims to enhance LNP selectivity, including the development of dual-targeting LNPs and exploring additional ligands for improved therapeutic precision.

1.2. HYPOTHESIS AND SPECIFIC AIMS

Utilizing nucleic acids as therapeutic agents is advertised as a pivotal avenue in molecular medicine's future. Non-viral gene therapy modalities, including lipid nanoparticles (LNPs) and other nucleic acid carriers, are proposed to address severe ailments necessitating systemic administration for genetic disease, viral infection, or cancer cell targeting.¹ However, the development of efficient gene delivery vectors remains a critical bottleneck, constraining the efficacy of gene-based therapeutics in clinical trials.

Two notable instances of successful LNPs delivering nucleic acids are the vaccines against SARS-CoV-2, namely BNT162b2² (Pfizer-BioNTech) and mRNA-1273³ (Moderna). In contrast to conventional vaccines, these mRNA-based LNP vaccines exhibited exceptional efficacy, exceeding 94 %, highlighting their potential in addressing current and future SARS-CoV-2 variants.^{4,5} Besides mRNA, DNA-based LNPs have emerged as promising candidates for nucleic acid delivery therapies, with at least ten clinical trials currently in Phase I-III.^{6,7} Some of the advantages of DNA-based LNP technology can be attributed to DNA offers cost-effectiveness, ease of production, and greater stability compared to mRNA, factors particularly relevant for remote regions and developing countries.^{8,9}

Although unspecific delivery of genetic material into various cells may not be a significant concern in certain applications, such as SARS-CoV-2 vaccines, achieving selective targeting remains a persistent challenge for enhancing the efficacy of gene therapies in diverse medical scenarios.¹⁰ With appropriate design and formulation, LNPs present the advantage of being engineered to target the desired tissue selectively. Selective targeting can be achieved through two methods: passive targeting, which involves altering the lipid formulation,^{11,12} and active targeting,

which entails modifying the LNP surface with a ligand that binds specifically to a receptor on the target cell.¹³

The human transferrin receptor (hTfR1), also known as CD71, is highly expressed on tumor cells due to their rapid proliferation and elevated iron demand,^{14, 15} making it a universal cancer biomarker and a promising target for active targeting approaches.^{14, 16} While the natural ligand for hTfR1, human transferrin protein (Tf), has been widely used in targeting therapeutic agents to tumors, its effectiveness may be limited by the presence of high concentrations of endogenous Tf in human serum.¹⁷ However, the retro-inverso peptide DT7, engineered from the T7 peptide, exhibits enhanced stability and affinity to hTfR1 without competitive interference from endogenous Tf, making it a promising candidate for targeted drug delivery applications.¹⁸

Hypothesis: In this research project, **we hypothesize that lipid nanoparticles (LNPs) encapsulating plasmid-DNA (pDNA) and incorporating the peptide ligand DT7 can be synthesized and selectively transfect cells expressing human transferrin receptor 1 (hTfR1) efficiently to overcome the lack of specificity in current approaches.**

To address the hypothesis raised above, we propose the following specific aims:

Specific Aim 1

To synthesize lipid nanoparticles (LNPs) encapsulating plasmid-DNA (pDNA) encoding the reporter mGL protein using the pipetting mixing method and post-assembly derivatize them with the DT7 peptide, employing thiol-maleimide click chemistry to enable selective targeting of cells expressing human transferrin receptor 1 (hTfR1).

Specific Aim 2

To assess the *in vitro* transfection efficiency and selectivity of the LNP-DT7 formulations using two different cell lines engineered to express and not express the hTfR1.

1.3. INTRODUCTION

1.3.1. A POTENTIAL TREATMENT AGAINST MELANOMA AND THE ORIGIN OF OUR LIPID NANOPARTICLE JOURNEY

In the United States, it is projected that there will be approximately 100,640 new cases of melanoma diagnosed and 8,290 related fatalities in the year 2024.¹⁹ Advanced melanoma poses significant treatment challenges; however, immunotherapy has emerged as a promising therapeutic avenue in recent times.²⁰ Specifically, there exist three primary categories of immunotherapy for advanced-stage melanoma: cytokine therapy, oncolytic virus therapy, and checkpoint inhibitor therapy. One such example is Pembrolizumab (Keytruda), a monoclonal antibody that targets the PD-1 receptor on cytotoxic T cells, enhancing their ability to eliminate melanoma cells.²⁰ Although Pembrolizumab and combination therapies have shown efficacy in extending survival, the majority of individuals with advanced melanoma continue to face a relentless and incurable progression of the disease. Consequently, there exists an imperative for the development of innovative therapeutic strategies to address the unmet needs of individuals with advanced melanoma.

Autologous therapeutic vaccines are another form of immunotherapy that primarily relies on tumor-specific antigens (TSAs). However, TSAs typically exhibit low immunogenicity. Various adjuvant-based strategies have been investigated to augment the immunogenicity of TSAs.²¹⁻²⁸ For instance, in a phase-1 clinical trial involving an autologous melanoma vaccine, anti- α Gal antibodies were utilized as an endogenous adjuvant. Stage-III melanoma patients received intratumoral injections of α Gal-bearing glycolipids.²⁵ Regrettably, this approach failed to yield significant tumor regression or cure. Nevertheless, it is noteworthy that none of the patients developed autoimmune conditions, and enzyme-linked immunosorbent assay (ELISA) analyses revealed no autoantibodies against normal tissue antigens, using skeletal muscle or human colon

homogenates as immobilized antigens.²⁹ Despite the partial success observed with the autologous melanoma vaccine strategy, a more comprehensive and robust immune response is imperative.

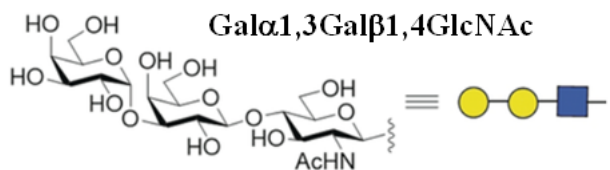


Figure 1. Chemical structure and schematic representation of the α Gal epitope

The α Gal epitope (**Figure 1**) is synthesized by the enzyme α 1,3-galactosyltransferase (α 1,3GalT, or GGTA1), which is entirely absent in humans. Therefore, the α Gal epitope is also absent in human glycoproteins, and it is highly immunogenic and antigenic. Anti- α Gal Abs, which accounts for up to 1% of IgG in normal human serum (NHS), is responsible for the hyperacute rejection of xenografts by human recipients. For example, when a pig kidney expressing approximately 10^7 α Gal epitopes per cell on its surface glycoproteins is transplanted into a human recipient, rejection typically occurs within minutes to hours.^{30, 31} This rejection process is primarily mediated by the opsonization of pig cells by anti- α Gal antibodies, leading to complement-dependent cytotoxicity (CDC). Additionally, antibody-dependent cell-mediated cytotoxicity (ADCC) and antibody-dependent cell-mediated phagocytosis (ADCP) contribute to the mechanism of hyperacute rejection.

Kiessling^{32, 33} and Fukase³⁴ pioneered the development of bifunctional anti- α Gal antibody-recruiting molecules comprising a cancer-binding component and an α Gal component. These molecules were designed to bind to various types of cultured cancer cells, thereby decorating them with antigenic α Gal moieties. In the presence of NHS (normal human serum), containing anti- α Gal antibodies and rabbit complement, a substantial proportion of the cancer cells underwent complement-dependent cytotoxicity (CDC).³²⁻³⁵

The rapid and potent lysis/rejection observed in xenotransplantation due to anti- α Gal antibody-mediated processes underscores the remarkable capabilities of the immune system. Our research team is focused on introducing a novel gene therapy for melanoma, which leverages the interactions between α Gal and anti- α Gal antibodies. This innovative approach integrates the principles of autologous anti-melanoma vaccines with the destructive potential of anti- α Gal antibodies. Our idea is that melanoma cells could become immunological magnets through the forced expression of a highly antigenic cell surface glycotope: the α Gal.

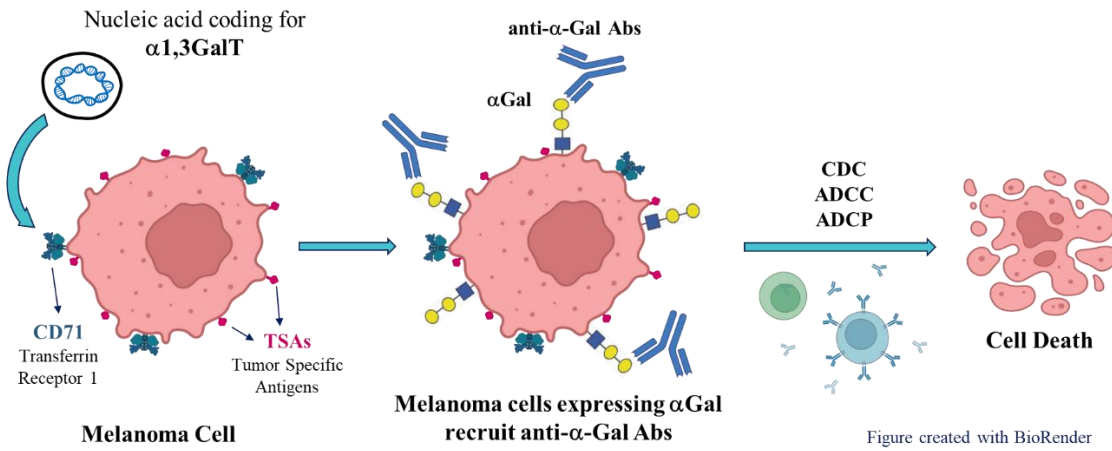


Figure 2. Schematic representation of our ideal approach for a melanoma treatment

Figure 2 provides a schematic representation of our most ambitious approach. Initially, we propose the *in vivo* selective transfection of melanoma cells with the murine α 1,3GalT gene (ggtal1) by actively targeting the human transferrin receptor (hTfR1/CD71). In this process, when expressed in α 1,3GalT-knockout (KO) mice, melanoma cells will exhibit the α Gal epitope. Consequently, these melanoma cells become susceptible to destruction by the innate immune system's anti- α Gal antibody-mediated responses, including complement-dependent cytotoxicity (CDC), antibody-dependent cell-mediated cytotoxicity (ADCC), or antibody-dependent cell-mediated phagocytosis (ADCP). Following phagocytosis by antigen-presenting cells (APCs), melanoma cells undergo processing, and their tumor-specific antigen (TSA) peptides are presented

via major histocompatibility complex (MHC) class I and II complexes. This presentation subsequently triggers the activation of CD8⁺ cytotoxic T cells and CD4⁺ helper T cells, initiating a cascade of immune responses. Ultimately, this immune activation stimulates B cells, fostering the development of specific anti-tumor immunity. Notably, transfection of all melanoma cells is not a prerequisite, as the anti-tumor immunity generated can effectively target melanoma cells regardless of α Gal expression.

1.3.1.1. PRELIMINARY EXPERIMENTS

Prior to delving into more intricate tasks, our lab conducted a set of preliminary experiments in partnership with Dr. Almeida's Lab.

Transfection of B16 melanoma cells with murine *ggta1* in vitro results in α Gal expression. (Miguel A. Beltran from Dr. Almeida's Lab accomplished this work). The B16F10Luc2 (B16) is the only commercially available mouse cancer cell line suitable because it lacks α Gal, resembling human cancer cells. A gene fragment containing *ggta1* labeled with an in-frame C-terminal human influenza hemagglutinin (HA)-tag was synthesized and inserted into a mammalian expression vector. Whole plasmid sequencing was used to validate the plasmid construct. The plasmid was transfected into B16 cells using LipofectamineTM 3000, and expression of α 1,3GalT was verified by immunoblot using an anti-HA Ab (**Figure 3A**). Note that only the *ggta1*-transfected cells express α 1,3GalT (*ggta1*⁺, right lane), and that two Ggta1 bands are observed. This agrees with two Ggta1 isoforms, which differ in length, i.e., 406 and 394 aa (<https://www.uniprot.org/uniprotkb/Q9DBU1/entry>; <https://www.uniprot.org/uniprotkb/Q3TXW0/entry>). To validate the expression and function of the enzyme, α Gal expression was visualized with a fluorescent *G. simplicifolia* isolectin 4 (IB4) that specifically binds to α Gal residues (red) (**Figure 3B**). Note that only the B16_{*ggta1*⁺} cells show fluorescence (right), while the wild-type B16

(B16_{wt}) (left) do not. These data prove that B16 cells transfected with our *ggta1*-vector express active α 1,3GalT and that the enzyme is indeed catalyzing α -galactosylation.

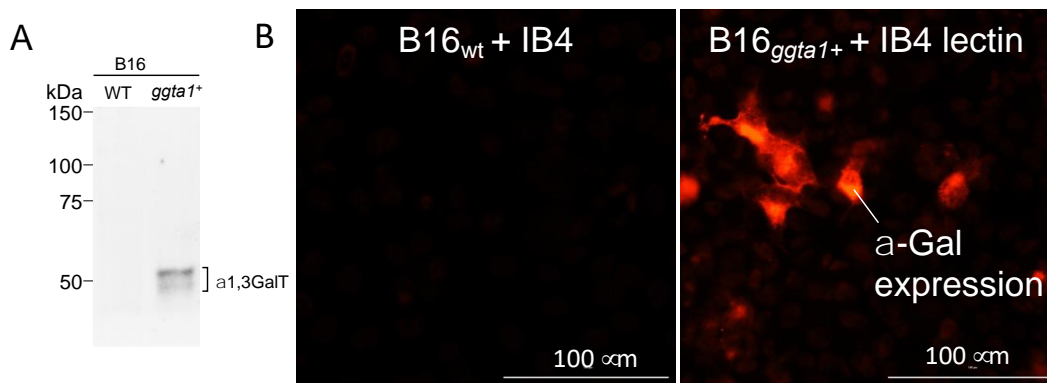


Figure 3. Result of the transfection of B16 cells with murine *ggta1* DNA with an HA-tag at the C-terminus using a mammalian expression vector. The expression of α 1,3GalT with HA-tag was analyzed using Western Blot and protein was found at the expected 51 kDa (A); and α Gal expression was detected using fluorescence microscopy (B). Untransfected (wt) and *ggta1*-transfected B16 cells were coincubated with *Griffonia simplicifolia* Lectin I (GSL I) Isolectin B4, Dylight 594 (Vector Labs) and visualized via fluorescence (B) using a Cytation 7 Cell Imaging Multi-Mode Reader (Biotek, Agilent).

LNPs equipped with DT7 infect CHO cells that express TfR1. (This work was accomplished in collaboration with Miguel A. Beltran). The DT7 peptide binds to hTfR1 and is internalized by the hTfR1 receptor via active transport. We have assembled LNPs with encapsulated mRNA coding for the fluorescent protein mCherry, with [LNP DT7 (+)] or without [LNP DT7 (-)] DT7 peptide on its surface. The LNPs were synthesized by microfluidic mixing, and their size (~ 100 nm), ζ -potential (near zero), and encapsulation efficiencies [60% for LNP DT7 (+), and 76% for LNP DT7 (-)] were validated before transfection of TfR1 expressing CHO cells. **Figure 4** shows that the DT7 ligand is necessary for transfection via TfR1 internalization (**Figure 4, bottom**) and that LNPs without the DT7 peptide only show a weak background transfection (**Figure 4, middle**). Note that the LNP synthesis and the transfection protocol have not yet been optimized.

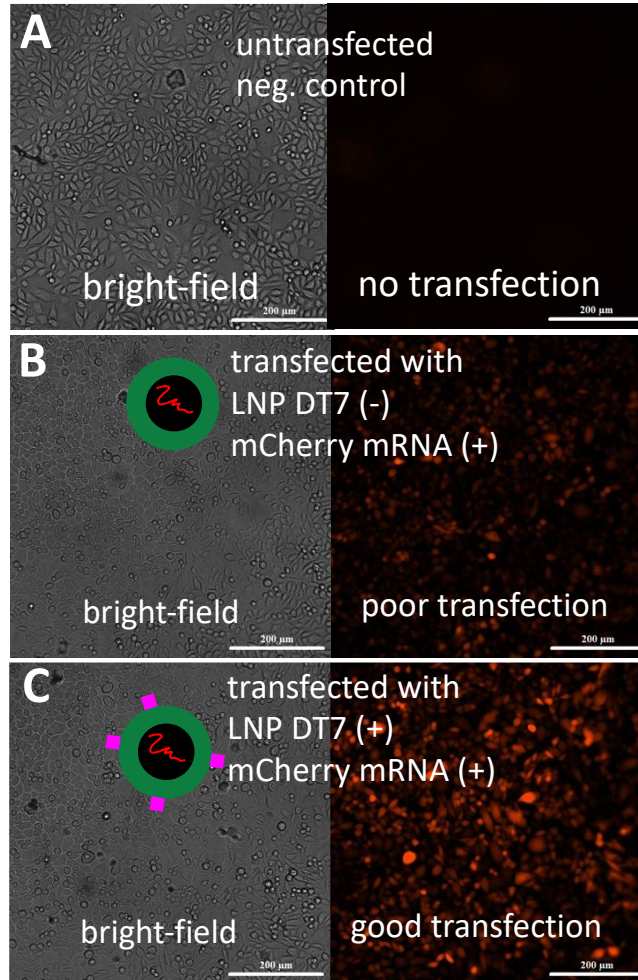


Figure 4. Transfection of hTfR1-expressing CHO cells with mCherry mRNA using two different LNPs. **A:** untransfected negative control; **B:** LNP without DT7. **C:** LNP with DT7. The mCherry fluorescence was visualized using a Cytation 7 Cell Imaging Multi-Mode reader (Biotek, Agilent). Live cell microscopy images were collected at 20X, bright field, and fluorescence images for mCherry (593/618 nm).

Our LNPs transfect hTfR1-expressing cells selectively. (This work was accomplished in collaboration with Miguel A. Beltran). To test whether our LNPs can selectively transfect cells with hTfR1 receptors over cells that lack them, we tested the transfection of CHO TfR1 (+) and CHO TfR (-) cells (kindly provided by M. Penichet) using a pDNA coding for the fluorescent protein mGreenLantern (**Figure 5**). These LNPs were synthesized using the pipetting mixing method. The LNPs were fully characterized prior to use (diameter ~100 nm, ζ -potential -7 mV,

encapsulation efficiency 60%). The transfection of CHO TfR1 (+) cells was significantly more efficient than the transfection of CHO TfR1 (-) cells. This can be attributed to the targeted delivery via DT7/hTfR1 binding. This shows that the selective targeting of hTfR1-expressing cells with DT7-modified LNPs is possible.

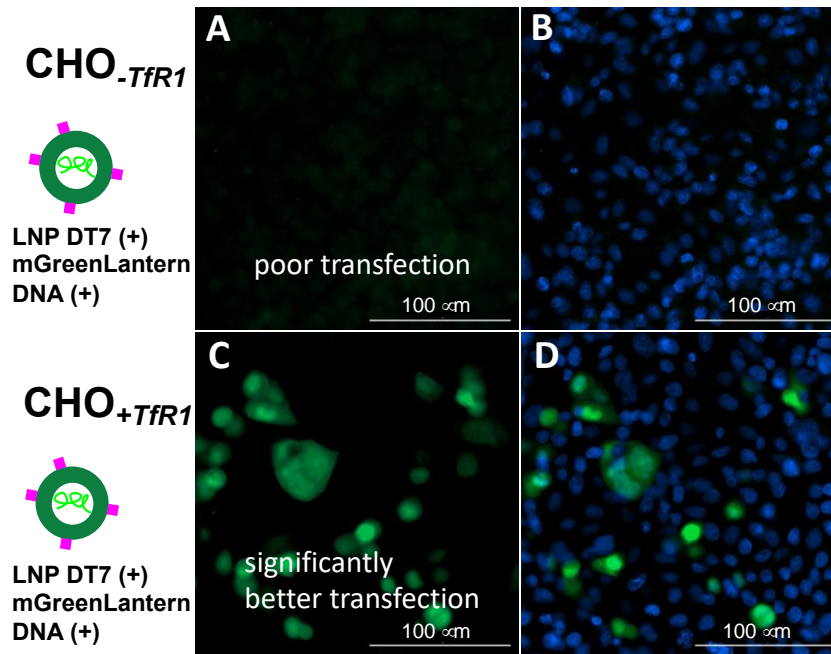


Figure 5. Transfection experiments of CHO TfR1 (+) cells (A, B) and CHO TfR1 (-) cells (C, D) with LNP DT7 (+) and mGreenLantern (mGL) coding DNA as a gene reporter using a mammalian expression plasmid vector. The cells were fixed using 4% PFA at 60 hpt and incubated with DAPI. A and C: Detection of the fluorescence of mGL; B and D: merged images of mGL and DAPI detection. CHO cells were visualized via fluorescence using a Cytation 7 Imaging Multi-Mode Reader (Biotek, Agilent).

Anti- α Gal Ab-mediated CDC *in vitro*. (This work was accomplished in collaboration with Colin D. Knight and Miguel A. Beltran from Dr. Almeida's Lab). We assessed the CDC of NHS in the presence of complement (C') on wild-type B16 (B16_{wt}) and α Gal-expressing B16 (B16_{ggta1+}) cells that had been transfected with a mammalian expression vector containing the murine *ggta1* (**Figure 6**). Our data show that B16_{ggta1+} are more effectively killed by pooled NHS (NHSP) than B16_{wt}, which lack α Gal. This supports anti- α Gal Ab-mediated CDC in B16 cells.

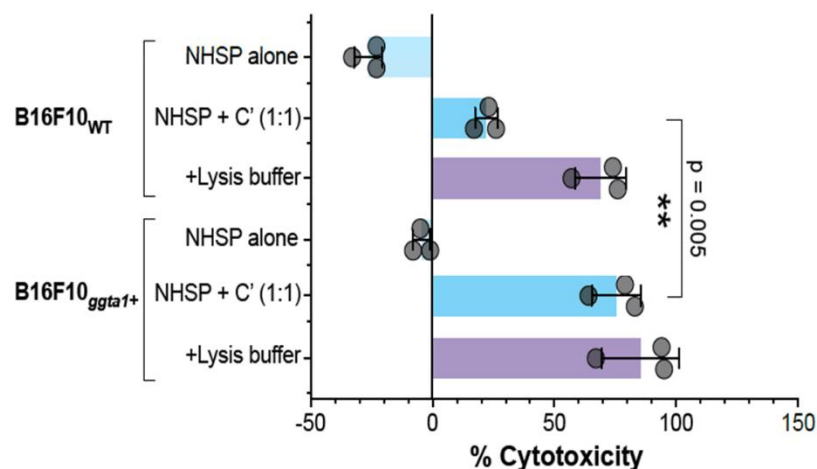


Figure 6. Cytotoxicity effect of pooled NHS on α Gal-negative (top) and α Gal-positive (bottom). The cytotoxicity assay was performed using the aCella TOX kit (CLATOX100, Cell Technology). The kit quantitatively measures the release of glyceraldehyde-3-phosphate dehydrogenase (GAPDH) from mammalian cells. GAPDH catalyzes the oxidative phosphorylation of glyceraldehyde-3-phosphate (GAP) to 1,3-bisphosphoglycerate kinase (PGK) to produce ATP, which is then detected via luciferase/luciferin bioluminescence using a Cytation 7 Cell Imaging Multi-Mode Reader (Biotek, Agilent) Statistical analysis: Mixed-effects model with Geisser-Greenhouse correction and Turkey's multiple comparison test. **, $p < 0.001$.

This ambitious concept serves as the foundation for our ongoing research project, which concentrates on enhancing the initial step of the process: the precise and effective delivery of genetic material into target cells.

1.3.2. GENE DELIVERY METHODS

In contemporary biomedical research, gene therapy has garnered increased attention due to its capacity to potentially address a spectrum of diseases, ranging from genetic disorders to various manifestations of cancer.¹ An essential stage in gene therapy involves proficiently delivering genes to specific tissues or cells, a task executed by specialized carriers known as gene delivery vectors. Gene therapies are commonly classified into viral and nonviral formulations based on their delivery vectors. Viral formulations utilize viruses to deliver genetic material into cells.³⁶ Notably, on December 8th, 2023, the U.S. FDA approved the first cell-based gene-editing therapy targeting sickle cell disease. This innovative approach involves the extraction,

modification, and reintroduction of the patient's blood stem cells.³⁷ Despite this advancement, numerous forthcoming gene therapies are anticipated to necessitate precise gene delivery to particular tissues or cells *in vivo*.³⁸

Clinical trials have explored different viral vectors, including lentiviruses, retroviruses, and adeno-associated viruses (AAV).^{38,36} AAV-mediated delivery is efficient for genetic diseases requiring long-term gene expression or genome integration. However, it is less suitable for conditions caused by point mutations.³⁸ Although viral transduction commonly results in enduring genome integration,³⁹ poses risks of off-target effects, including hepatotoxicity, undesired immune reactions, and, in rare instances, death.⁴⁰ Furthermore, AAVs exhibit restricted transgene carrying capacity (~4.8 kb), limiting their compatibility with larger CRISPR-based editors and other genetic payloads.⁴¹ Other challenges associated with viral vectors are the low productivity of AAV from host cells, the challenging scalability of the AAV-producing bioprocess, and the emergence of high levels of impurities during production.^{40, 42}

In recent years, there has been a growing recognition of nonviral formulations in the field of gene delivery, predominantly employing engineered lipid nanoparticles (LNPs). This shift aims to mitigate viral formulations' immunogenicity and off-target risks.⁴³ The appeal of nonviral therapies lies in their impressive ability to engineer stable nanostructures and the adaptability to modify their surfaces chemically.⁴⁴ This versatility enables the efficient encapsulation of nucleic acids, facilitating cellular delivery and endosomal release. Moreover, tailored nonviral formulations can prolong blood circulation, attenuate immune response, and reduce renal clearance.⁴³ The covalent attachment of active targeting ligands to LNPs can be achieved through various commercially available functionalized lipids.¹³

While LNP formulations encapsulating siRNA or mRNA have demonstrated effectiveness in cellular uptake and endosomal escape, exploring LNPs with plasmid DNA (pDNA) encapsulation remains underexplored. Notably, pDNA delivery provides the advantage of sustained transgene expression.^{45, 46} Compared to RNA, pDNA exhibits greater resistance to enzymatic degradation,⁴⁷ and its production is more cost-effective.⁸ These attributes are particularly pertinent for regions with limited resources and developing nations.⁹

1.3.3. ACHIEVING SELECTIVITY

Traditional LNPs, however, face a significant limitation due to their physicochemical resemblance to low-density lipoproteins (LDL) and their propensity to adsorb apolipoprotein E (Apo-E) in blood plasma.⁴⁸ This characteristic leads to their preferential accumulation in the liver and hepatocytic uptake via the low-density lipoprotein receptor (LDL-R). While traditional LNP technologies effectively target hepatocytes, their specific characteristics limit their application to non-liver tissues. The development of LNPs capable of delivering nucleic acids to tissues beyond the liver poses a considerable challenge. Overcoming this barrier is imperative for fully realizing the potential of nucleic acid delivery technologies.¹⁰

Remarkable advancements have been made in controlling essential parameters such as size, ζ -potential, nucleic acid encapsulation, and polydispersity index (PDI) in LNP-mediated gene therapy.^{1, 46} Nevertheless, a significant challenge remains in achieving selective targeting of specific tissues or cell types. Both active and passive targeting approaches have been proposed for LNPs. However, quantitative data are scarce on selectivity.

Passive targeting mechanisms in LNPs are primarily governed by size and charge, modifiable through alterations in lipid molar compositions. For instance, incorporating negatively

charged LNPs with increased DMG-PEG2000, a synthetic neutral lipid with a polyethylene glycol (PEG) chain, has enhanced cellular uptake by CD8⁺ dendritic cells in lymph nodes.⁴⁹ In specific cases, passive targeting is achieved by introducing an additional lipid, termed selective organ targeting (SORT) lipids.^{11, 12} These SORT lipids are incorporated into the LNP formulation by dissolving them in the organic solvent at varying molar ratios before mixing with the nucleic acid component. The resulting LNP targets organs such as the liver, spleen, and lungs.^{12, 50} The composition of lipids and the type of ionizable lipid utilized in the formulation significantly influence pDNA-LNP transfection.^{46, 51}

In the pursuit of active targeting, various ligands have been utilized to modify LNPs. Several research groups have employed whole antibodies (Abs) or fragment antigen-binding regions (Fabs), incorporating functionalized DSPE-PEG during LNP formulation and chemically grafting the antibodies onto the particles after synthesis.⁵²⁻⁵⁴ Carbohydrates have also played a crucial role in active targeting strategies. For instance, DSPE-PEG2000-mannose was integrated into a formulation to facilitate the selective delivery of LNPs to liver sinusoidal endothelial cells.⁵⁵ Small molecules, aptamers, peptides, and proteins have also been employed to modify the surface of actively targeting LNPs.¹³

The human transferrin receptor (hTfR1), CD71, is a crucial transmembrane glycoprotein facilitating iron transport. hTfR1 is highly expressed on tumor cells due to their rapid proliferation and elevated iron demand.^{14, 15} This receptor has been recognized as a universal cancer biomarker.¹⁶ It has become a promising target for active targeting approaches in cancer research and other conditions.^{14, 16} The natural ligand for the hTfR1 is the human transferrin protein (Tf); it plays a vital role in the iron transport process and exhibits a strong affinity for hTfR1.^{14, 56} Tf has been widely utilized as a targeting ligand for delivering therapeutic agents to tumors.⁵⁷ However,

its application might be limited by the presence of high concentrations of endogenous Tf in human serum.⁵⁸ Consequently, the naturally occurring Tf can competitively impede Tf-modified drug delivery systems, potentially reducing targeting efficiency *in vivo*,¹⁷ limiting the use of Tf as a hTfR1-targeting ligand in drug delivery systems.

The T7 peptide (HAIYPRH), a heptapeptide synthesized after phage display technology,⁵⁹ has exhibited significant binding affinity with the hTfR1.⁶⁰⁻⁶² However, the proteolytic susceptibility of all-L-configured peptides diminishes their bioavailability and effectiveness.⁶³ As a solution to this limitation, the *retro-inverso* peptide DT7 (hrpyiah, all-D-configured amino acids) has been engineered, displaying enhanced stability and affinity to the hTfR1 ($K_D = 22 \pm 1$ nM), even surpassing that of its L-form T7 peptide ($K_D = 120 \pm 5$ nM).¹⁸ Moreover, it has been established that there is no competitive interference between DT7 and endogenous Tf, further emphasizing its potential in targeted drug delivery applications.¹⁸

1.3.4. PHYSICOCHEMICAL CHARACTERISTICS AND SYNTHESIS OF LNPS

Various fundamental properties play a pivotal role in influencing the performance of LNPs, dictating their efficacy and behavior across diverse applications. Key factors affecting LNP performance encompass:

(a) Particle size: The dimensions of LNPs critically impact both their *in vitro* and *in vivo* functionality. Typically, LNPs exhibit average diameters ranging from 100 to 400 nm, with diameters falling within the 10 to 200 nm range considered optimal for systemic drug delivery via intravenous injection.^{64, 65} Particles smaller than 200 nm are preferable, facilitating passage through liver sinusoidal endothelial fenestrae and permitting sterilization by filtration.⁶⁶⁻⁶⁸

(b) Surface charge: The surface charge of LNPs, experimentally assessed through ζ -potential measurements, significantly governs their interactions with cellular membranes. A ζ -potential exceeding +30 mV or falling below -30 mV ensures robust electrostatic stability, preventing LNP aggregation.^{69, 70} While cationic LNPs may directly disrupt cellular membranes, inducing cytotoxicity, anionic cell membranes generally repel anionic LNPs. This charge plays a vital role in membrane interactions and endosomal escape, with neutral LNPs ($-10 \text{ mV} < \zeta\text{-potential} < 10 \text{ mV}$) often preferred to mitigate cytotoxicity concerns associated with anionic or cationic LNPs.⁶⁵ The incorporation of cationic ionizable lipids into the LNP formulation is essential as the surface charge of the LNPs is determined by the environmental pH; like this, undesirable electrostatic interactions between the LNP and the cell membrane can be avoided.⁷¹

(c) The polydispersity index (PDI): A $\text{PDI} < 0.2$ indicates a uniform LNP size distribution, contributing to formulation homogeneity and reproducibility.⁷¹ Achieving a desirable PDI for LNPs with nucleic acid encapsulation involves careful consideration of lipid composition, the protocol for mixing the organic lipid phase with the aqueous nucleic acid phase, the flow rate ratio (FRR), and total flow rate (TFR).⁷²

(d) Surface modification (e.g., PEGylation): Integration of polyethylene glycol (PEG) into LNPs imparts an external polymeric layer to the LNP surface, effectively preventing the adoption of serum protein (like Apo-E and albumins) and components of the phagocytic system.⁷³ LNP PEGylation extends the *in vivo* circulation time and enhance stability by preventing particle aggregation, even when the charge of the LNP is neutral.⁷³ However, excessive PEG can hinder cellular internalization and intracellular release of nucleic acids, emphasizing the need for optimal formulation.⁷⁴ In addition, concerns have been raised regarding inflammatory responses and potential obstacles to particle uptake associated with PEGylated lipids, commonly called the “PEG

dilemma.”⁷⁵ The immunogenicity of PEGylated lipids may trigger PEG-related hypersensitivities, leading to the generation of anti-PEG IgM and IgG antibodies.⁷⁵ Paradoxically, this immune response, counter to the intended purpose of PEGylated lipids, accelerates the blood clearance of LNPs.⁷⁶ Understanding and fine-tuning these properties is imperative to tailor LNPs for specific biomedical applications, enhancing their efficacy in therapeutic or diagnostic scenarios.

The ethanol dilution method stands as a well-established technique for LNP assembly, involving the prompt combination of an ethanol lipid solution with an aqueous buffer containing the nucleic acid component.^{65, 77} This process, facilitated through various mixing methods such as pipette mixing, vortex mixing, and microfluidic mixing, offers versatility for different scales of LNP production.^{12, 72} Pipette mixing, characterized by manual up-and-down pipetting, is particularly favored for small-scale LNP batches, proving simplicity in optimization, *in vitro* studies, and low-dose *in vivo* experiments.¹²

1.4. MATERIALS AND METHODS

1.4.1. REAGENTS AND CELL LINES

Table 1 shows a list of the chemicals used in this study.

Table 1. List of chemical abbreviations, their composition, and sources.

Abbreviation	Chemical Name/Composition	Source/Manufacturer
DLin-MC3-DMA	4-(Dimethylamino)-butanoic acid, (10Z,13Z)-1-(9Z,12Z)-9,12-octadecadien-1-yl-10,13-nonadecadien-1-yl ester	Cayman Chemicals
DMG-PEG2000	α -[(2R)-2,3-bis[(1-oxotetradecyl)oxy]propyl]- ω -methoxy-poly(oxy-1,2-ethanediyl)	Cayman Chemicals
Cho	Cholesterol	Avanti Polar Lipids (CRODA)
DSPC	1,2-distearoyl-sn-glycero-3-phosphatidylcholine	Avanti Polar Lipids (CRODA)
DSPE-PEG2000-Mal	1,2-distearoyl-sn-glycero-3-phosphoethanolamine-N-[maleimide(polyethylene glycol)-2000]	Laysan Bio Inc
EtOH	Ethanol 200-proof	Thermo Fisher Scientific
TCEP	Bond-Breaker TCEP Solution, Neutral pH	Thermo Fisher Scientific
Water	Molecular Grade Water, Cytiva Hyclone	Thermo Fisher Scientific
PBS	Gibco PBS, pH 7.4	Thermo Fisher Scientific
Acetate Buffer	Sodium Acetate (3 M), pH 5.5, RNase-free	Thermo Fisher Scientific
PicoGreen (PG)	Quant-iT PicoGreen dsDNA assay kit	Thermo Fisher Scientific
TE	Tris (10 mM, pH 7.5) and EDTA (1 mM) RNase-free	Thermo Fisher Scientific
Triton	Triton X-100	Thermo Fisher Scientific

Lipid stock solutions were made by dissolving each lipid in 200-proof ethanol, then stored at -20 °C. Before using them, the stock solutions were warmed to room temperature.

An additional D-cysteine amino acid was added to the C-terminus of the DT7 peptide (hrpyiah) to allow the conjugation of the thiol-derivatized peptide to the surface of the maleimide-derivatized LNP. The synthesis, purification, and characterization were custom-made by GenScript. From now on, DT7 will refer to the cysteine-derivatized peptide (hrpyiahc).

The plasmid pcDNA3.1-mGreenLantern (mGL-pDNA) was a gift from Gregory Petsko (Addgene plasmid #161912; <http://n2t.net/addgene:161912>; RRID: Addgene_161912).⁷⁸ *Escherichia coli* (*E. coli*) DH5alpha (Top10) bacterial cells (Thermo Fisher Scientific) underwent transformation and cultivation on Luria-Bertani (LB) agar medium supplemented with 50 µg/mL kanamycin. Subsequently, selected colonies were inoculated in 5 mL LB medium with kanamycin and incubated under shaking at 37°C for 12 h. Following incubation, a miniprep (Promega) was conducted, and EcoRI and ApaI double digestion was performed to verify the presence of a 739-base pair DNA fragment corresponding to the mGreenLantern gene. Finally, the GeneJET plasmid Maxiprep kit (Thermo Fisher Scientific) was utilized to obtain ample quantities of pDNA for the LNP preparations.

Derived from the original CHO-TRVb cells, a TfR-deficient Chinese hamster ovary cells,⁷⁹ CHO-TRVb-hTfR1⁸⁰ cells expressing hTfR1 (excluding hTfR2), and CHO-TRVb-neo⁸⁰ cells transfected with an empty neomycin vector were generously provided by Dr. Phillip Koeffler (Cedars Sinai Medical Center, Los Angeles, CA). The cell lines were cultured in an F-12 (HAM) medium (Thermo Fisher Scientific), supplemented with 10% fetal bovine serum (FBS) (Corning) and 1 mg/mL G418 (neomycin, Corning) as a selecting marker. Gibco StemPro Accutase Cell

Dissociation Reagent (Thermo Fisher Scientific) was used for cell detachment before passages and flow cytometry analysis.

1.4.2. SYNTHESIS OF LNPS

The synthesis of maleimide-derivatized LNPs encapsulating mGL-pDNA, which encodes the monomeric Green Lantern (mGL) fluorescent protein,⁷⁸ was conducted using the pipetting mixing method. Initially, various lipid formulations were prepared, including the ionizable lipid DLin-MC3-DMA, cholesterol, helper lipid DSPC, PEGylated-lipid DMG-PEG2000, and maleimide-derivatized lipid DSPE-PEG2000-Mal, in different molar ratios to achieve the final lipid concentration of 6.2 mg/mL in absolute ethanol 200-proof. Simultaneously, the aqueous solution was made by diluting mGL-pDNA in nuclease-free water and adjusting the pH to 4 using a 25 mM sodium acetate buffer. The pDNA concentration was determined using NanoDrop (Thermo Fisher Scientific), and adjustments were made to achieve the desired ionizable cationic lipid (positive charges) to phosphates from pDNA (negative charges) (N/P mol/mol ratio) for the corresponding batch. Subsequently, the aqueous and alcoholic phases were rapidly mixed at a 3:1 (v/v) ratio by vigorous pipetting for approximately 30 s. Following synthesis, the LNP solution was further dissolved in 1X PBS pH 7.4 to reach an ethanol concentration of 2 vol%. Purification and concentration were performed through Amicon filtration (30 kDa MWCO, MilliporeSigma Amicon Ultra-0.5 Centrifugal Filter Units). The final volume of each LNP preparation was adjusted with fresh 1X PBS pH 7.4 to reach a total lipid concentration of 3 mg/mL. The samples were preserved at 4°C until utilization for a maximum duration of one week.

For DT7 peptide modification, maleimide-derivatized LNPs were combined post-synthesis with 10 equiv of DT7 and 10 equiv of the reducing agent neutral-TCEP in 1X PBS for 2 h at rt.

Post-reaction, excess DT7, and TCEP were eliminated through washing with fresh 1X PBS pH 7.4 in an Amicon filter (30 kDa MWCO, MilliporeSigma Amicon Ultra-0.5 Centrifugal Filter Units). The final volume of each LNP preparation was adjusted with fresh 1X PBS pH 7.4 to reach a total lipid concentration of 3 mg/mL. The samples were preserved at 4°C until utilization for a maximum duration of one week. Simultaneously, an additional set of maleimide-functionalized LNPs underwent treatment with beta-mercaptoethanol (2ME) using identical conditions to those used for the DT7 modification. The new group of particles, designated as LNP-2ME, was utilized as negative controls (nontargeting particles) in subsequent transfection assays.

1.4.3. LNP CHARACTERIZATION

Hydrodynamic size, PDI, and ζ -potential. The three measurements were carried out utilizing dynamic light scattering (DLS) in a Zetasizer Ultra Red Label instrument from Malvern Instruments. The measurements aimed to characterize the average hydrodynamic intensity-weighted size of LNPs, expressed as the average LNP diameter in nanometers based on light scattering by intensity. ZEN0040 disposable cuvettes (Malvern Panalytical) were utilized for DLS measurements in pure water at a dilution of 1:1000 v/v (LNP solution/pure water). To determine ζ -potential, LNPs were appropriately diluted 1:100 v/v in nuclease-free water and subjected to analysis using a DTS1070 disposable folded capillary cell (Malvern Panalytical, Malvern, UK).

Encapsulation Efficiency (EE). The EE measures the percentage of the total pDNA encapsulated into the LNPs; it was assessed using the PicoGreen (PG) reagent. Initial preparations involved two buffers; the TE-buffer and the Triton/TE-buffer (0.2% v/v Triton X-100 in TE buffer). Triton is added to lyse the LNPs, releasing the encapsulated pDNA and making it detectable to the PG reagent. Both buffers were triplicated to a black microplate (Nunc 96-Well

Solid Polystyrene Microplate). Depending on the formulation, the concentration of pDNA in the LNP samples was adjusted with TE to approximately 60 ng/mL and added to each TE and TE/Triton well. The EE assay incorporated two standard curves, one with mGL-pDNA in TE-buffer and the other with mGL-pDNA in Triton/TE. Each standard curve enabled the calculation of pDNA concentration in its respective buffer. The two standard curves approach is crucial for accurately determining the EE and pDNA concentration, as a single standard curve approach using only Triton/TE-buffer may lead to an overestimation of encapsulation by 5-10%, owing to the higher background fluorescence of PG due to the interference with Triton. Microplates were incubated at 40 °C for 15 min under continuous stirring at 200 rpm to facilitate the extraction of the encapsulated pDNA with the Triton. The PG reagent, originally in DMSO, was diluted 200-fold using a TE-buffer and added to each well. Adjustments were made to ensure a final volume of 200 µL per well.

Subsequent incubation at 25 °C for 5 min under continuous shaking was followed by endpoint fluorescence intensity measurement in a BioTek Cytation 7 Cell Imaging Multi-Mode Reader (Agilent) at 485/528 nm (excitation/emission), bandwidth of 20 nm. The EE percentage of mGL-pDNA in the LNPs was calculated using the following equation:

$$EE\% = \left(1 - \frac{C_o}{C_t}\right) * 100\%$$

C_o represents the concentration of unencapsulated mGL-pDNA when the TE-buffer was used exclusively, and C_t denotes the total mGL-pDNA concentration after LNP lysis with Triton/TE-buffer. EE was reported as an average after measuring three replicates of each sample. The reported mean EE percentages were obtained from separate experiments, validating the reproducibility of the LNP formulations.

Cryo-Electron Microscopy (CryoEM). The vitrification of the LNP samples was accomplished by dispensing 6 μL of sample solution onto a glow-discharged 300 mesh grid (continuous carbon film gold grid); pure water was used as the dispersant. Subsequently, grids were subjected to blotting with filter paper for 7 s at 25°C, keeping the relative humidity at 100%. This was followed by fast immersion into a liquid ethane/propane mixture cooled by liquid nitrogen to achieve rapid freezing. Once vitrified, the frozen grids were kept below -170°C using liquid nitrogen until further analysis. Imaging was taken on a JEOL 3200FS using the Minimum Dose System (MSD) at 30 $\text{e}^-/\text{\AA}^2$ electron dose, 300 kV as accelerating voltage, and 80 kX magnification.

1.4.4. *IN VITRO* TRANSFECTION ASSAY AND CELL IMAGES

(This work was done in collaboration with Juan Carlos Silva-Espinoza from Dr. Rosa Maldonado's Lab). Both cell lines, CHO-TRVb-neo and CHO-TRVb-hTfR1, were seeded at a density of 10,000 cells per well in 96-well black/clear bottom plates using F-12 (HAM) medium supplemented with 10% FBS and 1 mg/mL G418. Cells were incubated at 37 °C and 5% CO₂ for 12 h. Following incubation, the cells were washed twice with F-12 (HAM) basal medium before adding LNPs. mGL-pDNA-loaded LNPs, modified with the ligand DT7, were diluted in F-12 (HAM) basal medium at concentrations of 100, 200, 400, 600, 800, and 1000 ng of encapsulated mGL-pDNA in a final volume of 100 μL . Simultaneously, a cell group transfected with the gold standard reagent for *in vitro* transfections, Lipofectamine 2000 using 100 ng of mGL-pDNA, was used as a positive control, and an untreated cell group was included as a negative control. Transfections were performed in triplicate for each LNP dose, including the untreated and positive control groups. 4-hour post-transfection, the medium containing LNPs was removed, and the wells

were thoroughly washed with F-12 (HAM) basal medium. Finally, 100 μ L of complete medium was added, and the cells were allowed to grow at 37 °C and 5% CO₂ for 48 h. After this incubation, the cell nuclei were stained with 100 μ L Hoechst 33342 in PBS at a concentration of 0.5 μ g/mL at 37 °C for 20 min. Microplates were imaged using a Cytation 7 (BioTek, Agilent, Santa Clara, CA), employing the DAPI and GFP filters.

1.4.5. FLOW CYTOMETRY

(This work was done in collaboration with Juan Carlos Silva-Espinoza from Dr. Rosa Maldonado's Lab). After image acquisition, cells were carefully rinsed with PBS, and 100 μ L of Accutase was added to each well. The plate underwent a 5-minute incubation at 37 °C to facilitate cell detachment. Cells were then gently pipetted up and down and transferred to tubes containing 1 mL of complete F-12 (HAM) medium. Following a 2 min centrifugation at 2000 rpm, the cells were fixed with FACS-Fix buffer (1X PBS, 1% BSA, 2% paraformaldehyde) and incubated for another 30 min. Lastly, the cells were washed with FACS buffer (1X PBS, 1% BSA). A Gallios Flow Cytometer (Beckman Coulter) was employed to determine the percentage of transfected cells, counting 2000 events and using channels FL9 for Hoechst 33342 and FL1 for mGL expression (Figure S1). FlowJo™ software 10.8.1 was used on a Mac® workstation to analyze the Flow Cytometry Standard (FCS) files.

1.4.6. STATISTICAL ANALYSIS

Graphical representation and statistical analyses were conducted using GraphPad Prism 9.5.1 (GraphPad Software, Inc., La Jolla, CA). A two-way ANOVA Bonferroni's multiple

comparisons was used to compare the means of two independent samples against each other. Significance was established at $p < 0.05$.

1.5. RESULTS AND DISCUSSION

Specific Aim 1. To synthesize lipid nanoparticles (LNPs) encapsulating plasmid-DNA (pDNA) encoding the reporter mGL protein using the pipetting mixing method and post-assembly derivatize them with the DT7 peptide, employing thiol-maleimide click chemistry to enable selective targeting of cells expressing human transferrin receptor 1 (hTfR1).

1.5.1. SYNTHESIS OF LNPS

LNPs were formulated using DLin-MC3-DMA as the essential ionizable cationic lipid. Cationic lipids play a vital role in LNPs designed for nucleic acid encapsulation, including mRNA, siRNA, or pDNA, by counteracting their negative charges.⁸¹ In earlier LNP designs, cationic lipids displaying a permanent positive charge, such as DOTAP (1,2-dioleoyl-3-trimethylammonium propane), DOTMA (N-[1-(2,3-dioleoyloxy)propyl]-N,N,N-trimethylammonium chloride) and DDAB (Didecyldimethylammonium bromide), were commonly utilized. However, the enduring positive charge of these lipids presented challenges *in vivo* due to their cytotoxicity and non-specific targeting.^{50, 82} On the other hand, ionizable cationic lipids, such as DLin-MC3-DMA, exhibit pH-dependent properties.⁸³ At acidic pH (~ pH 4.0), the majority of DLin-MC3-DMA molecules are protonated, facilitating electrostatic complexation with the negative-charged nucleic acids. However, at physiological pH 7.4, only a tiny fraction of their amines remain protonated.⁸³ The ionizable lipid DLin-MC3-DMA has notably been utilized in the pioneering FDA-approved siRNA-LNP therapy, Onpattro, designated for managing the polyneuropathy associated with hereditary transthyretin-mediated (hATTR) amyloidosis in adult patients.^{84, 85} Onpattro stands as the premier RNA interference (RNAi) therapeutic sanctioned by the FDA to address this specific medical condition.^{84, 85}

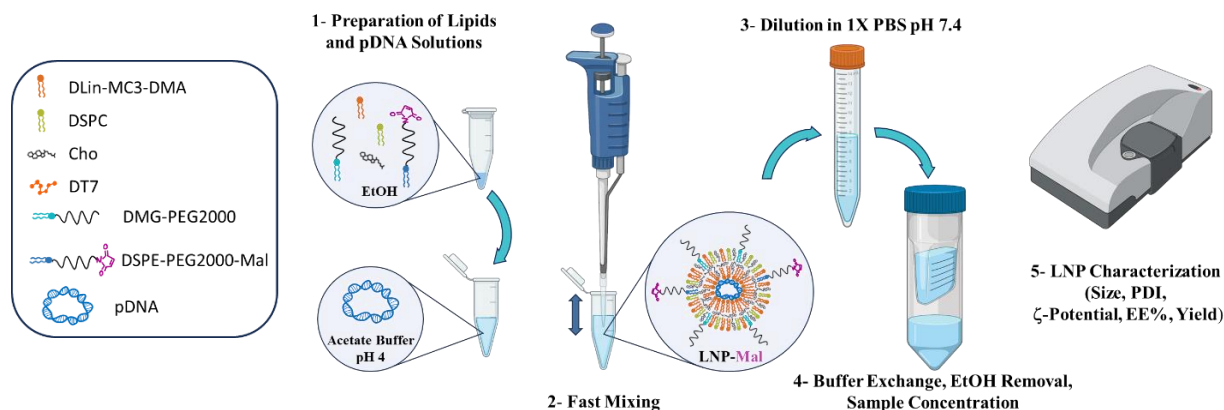
Cholesterol was integrated into the formulation to bolster LNP stability and facilitate endosomal escape, complementing the function of the ionizable lipid.⁸⁶ Additionally, DSPC acted as a neutral helper lipid, aiding LNP assembly.⁸⁷ DMG-PEG2000, a well-established pegylated lipid, was incorporated to decorate the surface of the LNPs, enhancing stability and preventing aggregation via steric hindrance mechanisms.⁸⁸ Lastly, the maleimide-derivatized lipid DSPE-PEG2000-Mal was introduced in the formulation at 0.5 mol% to enable the subsequent conjugation of the DT7 ligand to the LNP surface. Consequently, the DT7-modified LNPs exhibit selective targeting towards cells expressing hTfR1.

We decided to start the LNP synthesis with a specific molar ratio of DLin-MC3-DMA/ Cholesterol/ DSPC/ DMG-PEG2000/ DSPE-PEG2000-Mal, established as 50/ 38.5/ 10/ 1/ 0.5, respectively. While this formulation has been utilized for various applications, it has primarily incorporated mRNA as the nucleic acid component. However, as we are utilizing pDNA, we have opted to synthesize a range of formulations with DMG-PEG2000 mol% varying from 1 to 5 mol%. This approach enables us to attain the optimal physicochemical properties of LNPs. Throughout these formulations, the N/P ratio, representing the ratio of ionizable cationic lipid to negative charges in the pDNA, was maintained at 6, while the proportions of DLin-MC3-DMA, DSPE-PEG2000-Mal, and DSPC remained constant. The consecutive increments in the DMG-PEG2000 mol% were counterbalanced by the proportionate reduction in the cholesterol content. Once we determined the optimal lipid formulation based on the DMG-PEG2000 mol%, we decided to test various N/P ratios, keeping the lipid formulation constant and aiming to enhance the properties of LNPs further.

The mGL-pDNA carrying the gene sequence for the fluorescent reporter protein monomeric GreenLantern was dissolved in a nuclease-free acetate buffer of 25 mM and pH 4.

Previously dissolved in absolute ethanol, the lipids were combined with the aqueous mGL-pDNA solution in a microcentrifuge tube utilizing the pipetting mixing technique (**Figure 7a**). The mGL was preferred as the fluorescent protein due to its heightened brightness within cells, displaying up to sixfold greater intensity than the more commonly used enhanced green fluorescent protein (EGFP).⁷⁸ Following pH switch with PBS, ethanol removal, and LNP concentration via an Amicon filter, the maleimide functionalized LNPs (LNP-Mal) were produced and subjected to characterization, including determination of their average hydrodynamic diameter, PDI, ζ -potential, DNA encapsulation efficiency, and total DNA recovery yields. Once LNP-Mal were prepared, they were conjugated with the DT7 peptide to yield the desired DT7-derivatized LNPs (LNP-DT7) (**Figure 7b**), poised to assess their targeting capabilities further.

a)



b)

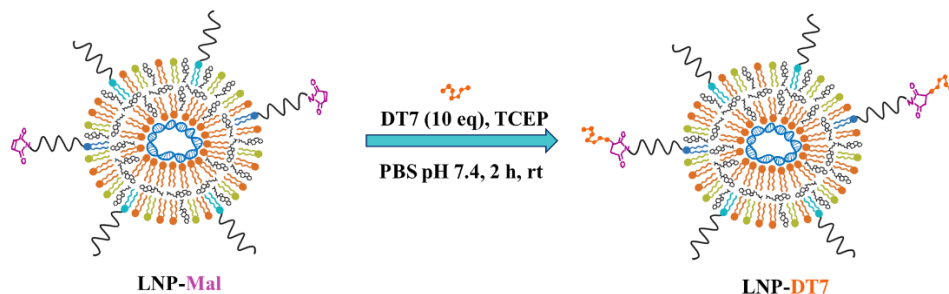


Figure 7. Schematic representation of a) the preparation of LNPs with maleimide functionalization (LNP-Mal) by the pipetting mixing method (Figure 1a created with BioRender); and b) post-assembly modification with the DT7 peptide to yield the LNP-DT7 particles.

1.5.2. CHARACTERIZATION OF LNPS

Both the LNP-Mal and LNP-DT7 groups underwent comprehensive characterization using DLS, ζ -potential analysis, and our adapted PicoGreen pDNA EE assay. Maintaining a fixed N/P ratio of 6, five distinct formulations were explored to determine the optimal amount of pegylated lipid DMG-PEG2000 for particle formation and mGL-pDNA encapsulation (**Figure 8a-c**). Starting at the lower concentration of 1 mol% of DMG-PEG2000, LNP-Mal with a hydrodynamic size of approximately 115 nm and a PDI of 0.08 were obtained. However, following DT7 conjugation, visible particle aggregation occurred, suggesting that only a concentration of 1 mol% of DMG-PEG2000 compromised the stability of LNP-DT7 (**Figure 8a**). This issue was addressed by progressively increasing the DMG-PEG2000 concentration in the overall lipid formulation. A consistent reduction in size was noted across all LNPs as the concentration of DMG-PEG2000 increased from 2 to 5 mol% (**Figure 8a**). This relationship between particle size and PEG percentage has been previously documented.⁸⁹ Furthermore, LNP-DT7 particles displayed a steady rise of approximately 59 nm in hydrodynamic size across all formulations compared to their precursors (LNP-Mal) while maintaining PDIs below 0.2 in all instances (**Figure 8a**).

As anticipated, both LNP-Mal and LNP-DT7 groups maintained a neutral charge independently of the presence of DT7, with ζ -potential values falling from -10 to 10 mV⁶⁵ (**Figure 8b**). These measurements were conducted at pH 7.4, where the ionizable lipid DLin-MC3-DMA (pKa = 6.44)⁸³ was predominantly deprotonated, resulting in a neutral ζ -potential for the LNPs. An interesting observation was that ζ -potentials shifted from positive to negative values after the DT7 was conjugated (**Figure 8b**), a phenomenon that has been previously reported in liposomes decorated with DT7.¹⁸

The correlation between pDNA EE and the DMG-PEG2000 content was assessed at concentrations of DMG-PEG2000 from 2 and 5 mol%. **Figure 8c** shows that LNPs containing 2, 2.5, or 3 mol% DMG-PEG2000 had similar EEs of about 90%, while 5 mol% DMG-PEG2000 LNPs displayed a significantly lower EE. This observation suggests that the higher concentration of DMG-PEG2000 may impact the assembly mechanism of the LNPs. However, the pDNA recovery yield continued to be consistent across all preparations, ranging from 82% to 96% (**Figure 8c**). Our findings suggest that LNPs containing DMG-PEG2000 at concentrations of 2, 2.5, and 3 mol% displayed closely similar physicochemical characteristics, with the LNP formulation containing 3 mol% exhibiting marginally better overall properties. A set of preliminary transfection experiments (not shown here) was conducted to reveal that 3 mol% DMG-PEG2000 LNPs yielded the most promising outcomes. Furthermore, the choice to advance with the higher concentration of DMG-PEG2000 at 3 mol% was influenced by its potential to mitigate protein corona formation and diminish the probability of nonspecific uptake in a future *in vivo* scenario. This decision aligns with previous research emphasizing the role of PEGylation in enhancing nanoparticle stability and reducing off-target effects in biological systems.⁷¹

Once we established the DMG-PEG2000 concentration at 3 mol% in the LNP formulations, we explored the optimal quantity of ionizable lipid (DLin-MC3-DMA) for particle optimization, a parameter better described by the N/P ratio. Four conditions (N/P = 4, 6, 8, and 10) were investigated (**Figure 8d,e,f**). Transitioning from an N/P ratio of 4 to 6 led to a significant reduction in LNP size and a notable improvement in PDI (**Figure 8d**).

Given that most amine groups from the DLin-MC3-DMA display a positive charge at pH 4,⁹⁰ the robust electrostatic binding between the negatively charged pDNA and the positively charged ionizable lipids at an elevated N/P ratio facilitated the creation of compacted LNPs with reduced diameters. This observation implies that at an N/P ratio of 4, there might be insufficient positively charged lipids to bind with all the negatively charged pDNA, resulting in some pDNA molecules remaining unbound in the solution. To validate this hypothesis, the pDNA EE% was measured, which improved from approximately 60% at N/P = 4 to approximately 90% at N/P = 6 (**Figure 8f**).

The size remained relatively consistent with the N/P ratio increase from 6 to 8 and 10, but the PDI rose to undesirable levels, especially post-DT7 conjugation (**Figure 8d**). Moreover, higher N/P ratios, such as 8 and 10, are thought to reduce the pDNA endosomal escape capacities, thereby diminishing the transfection efficiency.⁹¹

In terms of ζ -potential, all particles displayed neutrality, with values falling within the range of -10 to +10 mV. A consistent transition from positive to negative ζ -potential values was noted when contrasting the LNP-Mal group with the LNP-DT7 group (**Figure 8e**).

LNP-Mal particles typically exhibited more advantageous physicochemical characteristics than their related LNP-DT7 particles. The latter exhibited an increase in PDI and size, coupled with a decline in overall yield and EE%. This trend can be ascribed to the additional manipulation

and purification steps the LNP-DT7 particles underwent during their synthesis. LNP-DT7 featuring 3 mol% of DMG-PEG2000 and an N/P = 6 were selected for further experiments. LNPs synthesized under these conditions demonstrated suitable particle sizes for *in vivo* gene delivery (approximately 150 nm), a desirable low PDI post-conjugation (approximately 0.145), high encapsulation efficiency (> 80%), and a yield exceeding 90%.

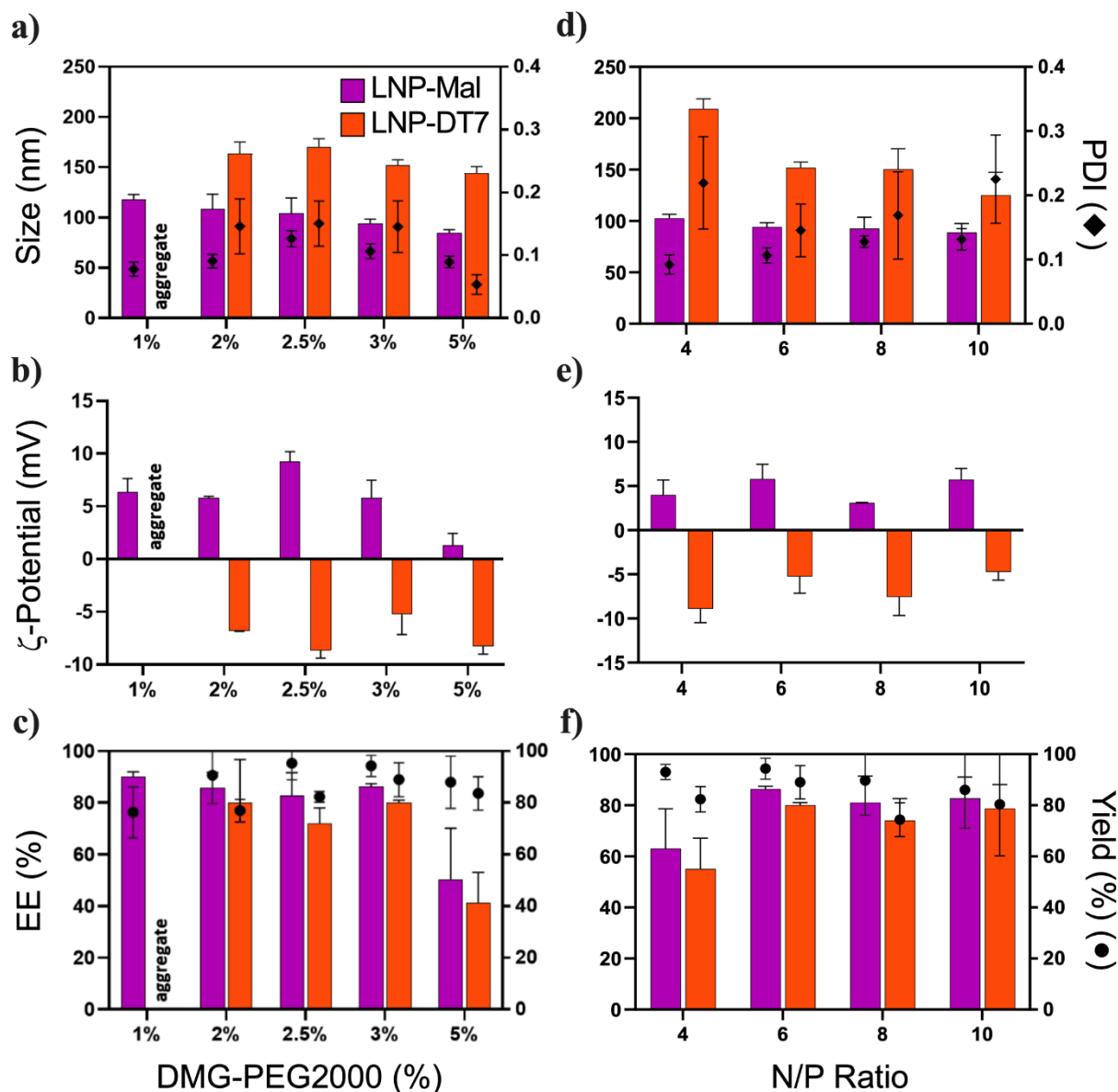


Figure 8. Characterization of LNP-Mal and LNP-DT7 at different DMG-PEG2000 concentrations and N/P ratios. a, b, and c) Size (intensity-weighted), ζ -potential, and EE% at different DMG-PEG2000 concentrations, respectively. d, e, and f) Size (intensity-weighted), ζ -potential, and EE% at different N/P ratios, respectively. Data indicate mean \pm SD of three replicates.

The spherical morphology of the selected LNP-Mal and LNP-DT7 particles was confirmed by cryo-electron microscopy (CryoEM) imaging (**Figure 9**). Notably, the core diameter of both LNPs, as assessed via CryoEM analysis, was found to be less than 100 nm; conversely, DLS

measurements suggested sizes of about 94 nm and 150 nm for the LNP-Mal and LNP-DT7, respectively. These discrepancies can be attributed to the distinct principles guiding the two measurement approaches.⁹² CryoEM solely assesses the LNP lipidic core, thus rendering the attached DT7 and PEG branches indistinguishable at the utilized magnification. Consequently, this results in an underestimation of the total LNP diameter. On the other hand, DLS computes the intensity-weighted size using the equivalent sphere model, where each particle is represented as a sphere. The intensity-weighted hydrodynamic size of LNPs is significantly affected by several factors, including LNP concentration, temperature, sedimentation, buffer viscosity, pH, presence of aggregates, and surface characteristics (e.g., PEGylation and DT7 conjugation).⁹³ Given that scattering intensity is proportional to the square of the particle molecular weight, any polydispersity or breadth in particle size distributions tends to skew the size average toward larger particle sizes. Additionally, since scattering intensity is proportional to the square of the particle molecular weight, any variability or polydispersity in particle size distribution tends to bias the LNP average diameters toward larger particle sizes.^{93, 94}

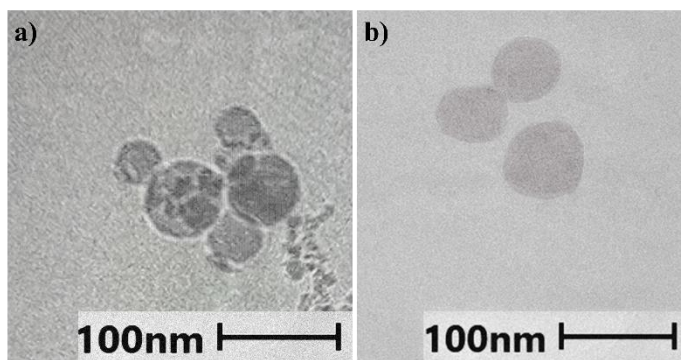


Figure 9. CryoEM image of a) LNP-Mal and b) LNP-DT7. Both particles were formulated with 3 mol% of DMG-PEG2000 and an N/P ratio = 6.

Specific Aim 2. To assess the *in vitro* transfection efficiency and selectivity of the LNP-DT7 formulations using two different cell lines engineered to express and not express the hTfR1.

1.5.3. *IN VITRO* TRANSFECTION ASSAY

Two exceptional cell lines, CHO-TRVb-neo and CHO-TRVb-hTfR1,^{79, 80} were utilized to conduct the selective transfection experiment using the LNP-DT7. The CHO-TRVb-hTfR1 cell line has been genetically modified to express hTfR1 exclusively. In contrast, CHO-TRVb-neo cells were transfected with an empty vector and showed no detectable transferrin receptor on their surface. This two-cell panel provides a robust negative control (CHO-TRVb-neo) and positive control (CHO-TRVb-hTfR1) in terms of hTfR1 expression, circumventing challenges to establish an appropriate negative control for transfection experiments since most commercially available human cell lines express some level of hTfR1. Furthermore, this two-cell panel enables the assessment of unbiased quantitative information during transfection selectivity experiments, as cellular uptake depends solely on the presence or absence of the DT7/hTfR1 interaction.

For the *in vitro* transfection assays, CHO-TRVb-neo and CHO-TRVb-hTfR1 cells were plated at a density of 1×10^4 cells per well. After cells adhered, they were exposed to six different LNP-DT7 concentrations, resulting in progressive encapsulated pDNA amounts ranging from 100 to 1000 ng per well, specifically at 100, 200, 400, 600, 800, and 1000 ng/well. This strategy allowed for the investigation of dose/response correlation. Cells were treated with LNP-DT7 particles in a basal serum-free F-12 (HAM) medium for a duration of 4 hours to reduce the undesirable nonspecific uptake mediated by the ApoE/LDL-R pathway.

Concurrently, a positive control transfection experiment was conducted employing Lipofectamine 2000 and the same mGL-pDNA at 100 ng/well concentration in Opti-MEM

medium as per the manufacturer's instructions. After the 4-hour exposure period, all wells underwent thorough washing with basal medium and were allowed to recover in F-12 (HAM) supplemented with 10% FBS and 1 mg/mL G418 as a selecting marker.

Forty-eight hours post-transfection, the mGL protein expression was qualitatively evaluated by fluorescence microscopy in a Cytation 7 Cell Imaging. Live cell nuclei were stained with Hoechst 33342.⁹⁵ Subsequently, microscopy images were captured using the DAPI filter cube for nuclear identification (Hoechst 33342 ex/em: 361/497 nm), the GFP filter cube for mGL expression (ex/em: 503/514 nm), and brightfield. **Figure 10** illustrates representative images of both cell lines, with CHO-TRVb-neo shown in the top row and CHO-TRVb-hTfR1 in the bottom row, after exposure to 600 ng/well of mGL-pDNA employing LNP-DT7 as the transfection vehicle. A notable difference in mGL protein expression is observed between the two cell lines, with CHO-TRVb-hTfR1 cells exhibiting higher protein expression than CHO-TRVb-neo cells. Quantitative assessment of transfected cells was performed using flow cytometry.

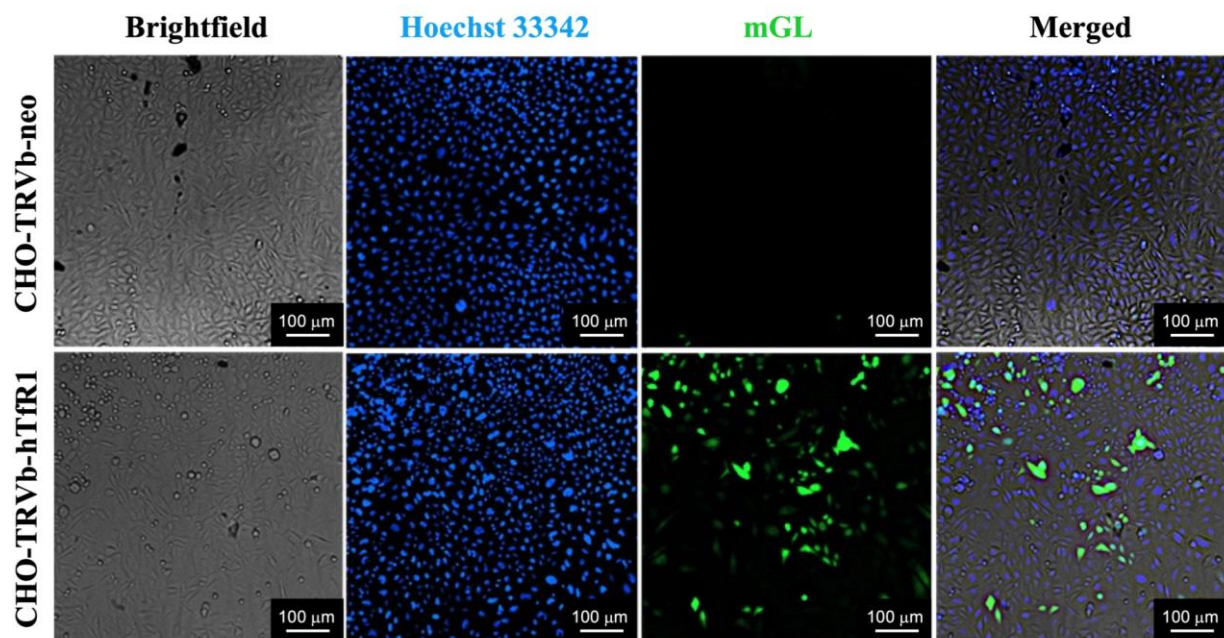


Figure 10. mGL protein expression in CHO-TRVb-neo (top row) and CHO-TRVb-hTfR1 cells (bottom row). At 48 h post-transfection of 600 ng of mGL-pDNA LNP-DT7, cells were stained with Hoechst 33342 (second column) and imaged in the Cytation 7 microscope mode, using the filters for DAPI (Hoechst 33342) and GFP (mGL).

1.5.4. TRANSFECTION EFFICIENCY ASSESSED BY FLOW CYTOMETRY

Right after imaging, cells from each well were detached using Accutase, which contains proteolytic and collagenolytic enzymes. Accutase is known for its gentler nature than trypsin, making it more preservative with the cell surfaces; this is particularly important during flow cytometry analysis.⁹⁶ Once detached, cells were transferred to 1 mL of complete F-12 medium, fixed using FACS fix solution, and resuspended in FACS PBS before flow cytometry analysis to quantify the mGL protein expression by flow cytometry. A positive control group of cells, stained only with Hoechst 33342, was utilized to quantify the number of cells based on the number of nuclei. **Figure 11** compares the percentages of mGL-positive cells at different mGL-pDNA concentrations in both cell lines, CHO-TRVb (-neo and -hTfR1).

The graph consistently shows low mGL expression, averaging approximately 4%, in all experiments where CHO-TRVb-neo cells were treated with LNP-DT7. In contrast, when Lipofectamine 2000 was used as the transfection reagent at a pDNA concentration of 100 ng/well, the percentage of transfected cells reached approximately 24%. These results confirmed that LNP-DT7 particles have a limited affinity towards CHO-TRVb-neo cells, which do not express hTfR1.

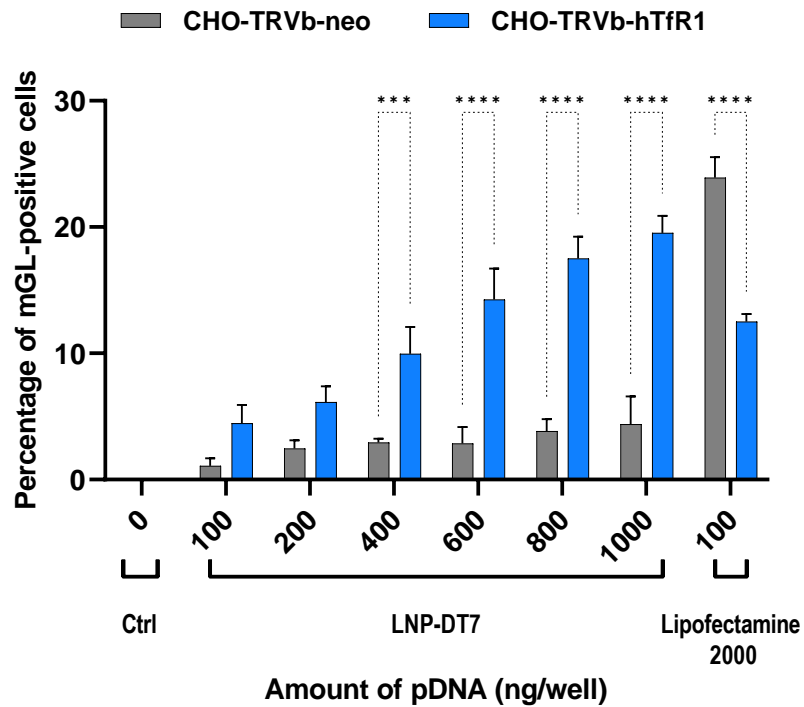


Figure 11. Percentage of mGL-positive cells at different concentrations of pDNA. CHO-TRVb-neo and CHO-TRVb-hTfR1 cells transfected with 0, 100, 200, 400, 600, 800, and 1000 ng of mGL-pDNA encapsulated in LNP-DT7. As a positive control, transfection of 100 ng mGL-pDNA with Lipofectamine 2000 was performed in both cell lines. The percentage of mGL transfected cells was evaluated by flow cytometry. Data were represented as mean \pm SD of biological replicates ($n = 3$). Statistical analysis was performed by Bonferroni's multiple comparisons test: *** $p < 0.001$; **** $p < 0.0001$.

In contrast, the percentage of mGL-positive CHO-TRVb-hTfR1 cells increased dose-dependent. At a mGL-pDNA dose of 1000 ng/well, the transfection efficiency reached approximately 20%. Remarkably, achieving a 20% transfection efficiency at 1000 ng/well dose

using pDNA encapsulated in an LNP is a remarkable outcome. This result exceeds the reported outcomes in existing literature, where similar percentages were only achieved using higher pDNA doses, such as 5000 ng, and only via the ApoE/LDL-R pathway.^{97, 98}

In general, selective transfection between cell types remains relatively unexplored, with most literature focusing on selective cellular uptake. However, cellular uptake alone does not guarantee successful endosomal escape and further expression of the edited or new gene product, which are crucial hurdles that a nucleic acid-LNP must overcome. Although this research did not directly investigate cellular uptake, our high transfection efficiency suggests that cellular uptake of LNP-DT7 by CHO-TRVb-hTfR1 cells must have been at least 20% or higher. Interestingly, when Lipofectamine 2000 was used as the transfection method, the transfection efficiency was lower in CHO-TRVb-hTfR1 cells compared to CHO-TRVb-neo cells.

This observation implies that CHO-TRVb-neo cells are more easily transfected than CHO-TRVb-hTfR1 cells when employing Lipofectamine 2000, widely recognized as the benchmark for non-selective *in vitro* transfections. However, our findings have revealed the opposite pattern when utilizing LNPs modified with the DT7 peptide (LNP-DT7). The enhanced selectivity of LNP-DT7 particles toward hTfR1-expressing cells can be attributed to the strong interaction between pair DT7/hTfR1. This selectivity can be evaluated at a particular pDNA concentration by determining the ratio of mGL-positive CHO-TRVb-hTfR1 to mGL-positive CHO-TRVb-neo cells. Our experiments confirmed a selective transfection ranging from four to fivefold, exceeding analogous evaluations documented in the literature, which predominantly rely on cellular uptake.^{99, 100}

Drawing from the distinctive engineered cell lines employed in this investigation, the observed transfection selectivity stemmed exclusively from the DT7/hTfR1 interaction. Among the transfected cell population, CHO-TRVb-hTfR1 cells constituted 83%, with CHO-TRVb-neo

cells comprising the remaining 17%. When considering the transfection of CHO-TRVb-neo cells, our results suggest that 17% of the transfection occurred in a nonspecific manner. These findings imply that our existing LNP formulations could be enhanced through additional refinement, such as simultaneous targeting of two distinct receptors, and/or increased PEG shielding to minimize nonspecific uptake.

To validate further the transfection reliance on the interaction between the DT7 ligand and the hTfR1 receptor, CHO-TRVb-hTfR1 cells were individually exposed to varying concentrations of pDNA using LNP-2ME and LNP-DT7. As anticipated, LNP-DT7 demonstrated notably elevated transfection efficiencies compared to LNP-2ME, as illustrated in (**Figure 12**).

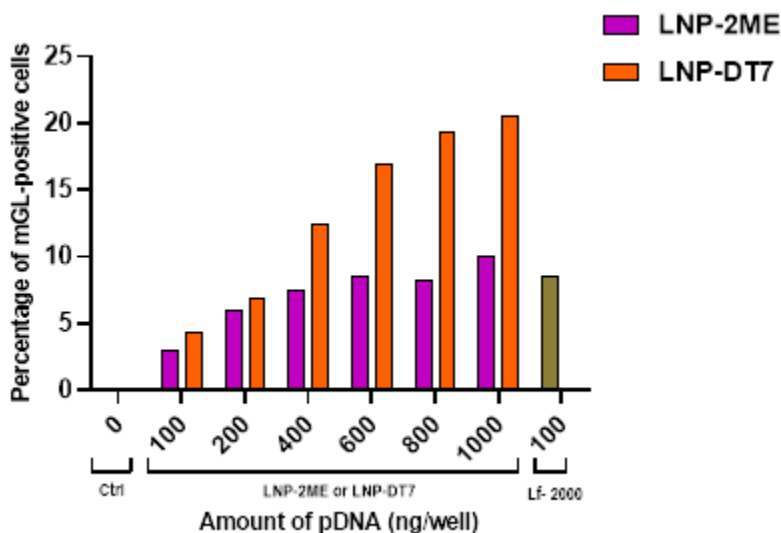


Figure 12. Percentage of mGL-positive CHO-TRVb-hTfR1 cells at different concentrations of pDNA encapsulated in LNP-2ME and LNP-DT7. CHO-TRVb-hTfR1 cells were transfected with 0, 100, 200, 400, 600, 800, and 1000 ng of mGL-pDNA encapsulated in LNP-2ME (nontargeting LNPs) and LNP-DT7 (active targeting LNPs). As a positive control, transfection of 100 ng mGL-pDNA with Lipofectamine 2000 (Lf-2000) was performed. The percentage of mGL transfected cells was evaluated by flow cytometry by counting 10,000 events.

1.6. CONCLUSIONS

In this investigation, we successfully synthesized LNPs incorporating a cell-targeting ligand and encapsulated pDNA encoding a fluorescent reporter mGL protein using the pipette mixing method. The formulation involved five lipids (DLin-MC3-DMA, cholesterol, DSPC, DMG-PEG2000, and DSPC-PEG2000-Mal) along with the pDNA. After the conjugation of the DT7 peptide, an hTfR1 receptor ligand onto the LNP surface was performed. By adjusting the DMG-PEG2000 mol% and N/P ratios, we optimized critical LNP parameters such as hydrodynamic size, ζ -potential, and pDNA encapsulation efficiency to achieve effective cell transfection. Optimization experiments identified LNPs with a formulation of DLin-MC3-DMA: Cho: DSPC: DMG-PEG200: DSPE-PEG2000-Mal (50: 10: 36.5: 3: 0.5) at an N/P ratio of 6 as optimal for pDNA encapsulation with desirable physicochemical properties.

Selective transfection experiments using CHO-TRVb-hTfR1 and CHO-TRVb-neo cell lines, representing positive and negative controls for hTfR1 expression, respectively, demonstrated significant and dose-dependent transfection efficiency (up to 20%) in CHO-TRVb-hTfR1 cells compared to lower efficiency (up to 4%) in CHO-TRVb-neo cells. These results directly translate to a five-fold selective transfection for hTfR1-expressing cells. Qualitative analysis via fluorescence microscopy further confirmed these findings, illustrating clear differences in the reporter protein expression between CHO-TRVb-hTfR1 and CHO-TRVb-neo cell lines. Furthermore, our calculations indicate that 17% of the transfection in our model took place through nonspecific interactions. These findings underscore the need for continued enhancements in both LNP formulation and synthetic procedures to optimize their suitability for *in vivo* applications.

Our experiments highlight the superior performance of the active targeting LNP-DT7 in CHO-TRVb-hTfR1 cells, which can be attributed to the strong interaction between the ligands

DT7 and the hTfR1, which in our model is only expressed on the surface of the CHO-TRVb-hTfR1 cells. To the best of our understanding, this investigation represents the first study documenting such unbiased selective transfection.

In summary, the formulated LNP-DT7 particles exhibit potential for precise gene delivery, notably within hTfR1-expressing cells. This investigation establishes a robust groundwork for forthcoming *in vivo* studies and emphasizes the translational prospects of active-targeting LNP strategies in selective gene therapy applications.

1.7. IMPACT STATEMENT AND FUTURE DIRECTIONS

The research outlined in **Chapter 1** has significantly advanced our research group's capabilities, laying the groundwork for the synthesis and engineering of functional lipid nanoparticles in our laboratory. This achievement provides us with a robust platform and established protocols for assembling LNPs that could find applications beyond cancer treatment, such as genetic disorders, Alzheimer's disease, and other areas of biomedical relevance.

While acknowledging the progress made, further refinement is necessary, particularly to enhance the selectivity of our current LNP-DT7 formulation. Our forthcoming endeavors will focus on synthesizing LNPs decorated with multiple ligands capable of targeting overexpressed receptors on specific cell types, such as cancer cells. Presently, our research concentrates on synthesizing a dual-targeting LNP, combining the DT7 peptide targeting hTfR1 and the folate moiety targeting the Folate Receptor alpha (FR α), both commonly overexpressed in cancer cells. This approach aims to heighten the selectivity of our particles toward the desired cellular targets.

Moreover, our future investigations will explore the integration of antibodies and other small molecules as potential ligands for further enhancing LNP selectivity and efficacy. Through these concerted efforts, we anticipate significant advancements in the design and application of targeted lipid nanoparticles, offering promising prospects for improved therapeutics.

CHAPTER 2. IMPROVED SYNTHESIS OF *LEISHMANIA* PARASITE-DERIVED GLYCANS (G27_{SH} AND G28_{SH}) AND ITS CONJUGATION TO LIPIDS

2.1. ABSTRACT

The most abundant antibodies naturally occurring in human serum, known as Anti- α Gal antibodies, are crucial for protecting against certain pathogens that express α Gal epitopes on their cell surfaces. In our investigation of cutaneous leishmaniasis patients from Argentina and Bolivia infected with *Leishmania braziliensis*, we discovered a distinct type of anti- α Gal antibody (L-Anti- α Gal) with a unique specificity profile compared to the Anti- α Gal antibodies found in natural human serum (NHS). Depending on the specific *Leishmania species* causing the infection, L-Anti- α Gal antibodies exhibit strong and specific reactions with synthetic neoglycoprotein antigens containing the disaccharide Galp α 1,3Gal β and the trisaccharide Galp α 1,6Galp α 1,3Gal β , derived from the cell surface glycoinositol phospholipids (GIPL-2 and GIPL-3) of the *Leishmania parasite*. To facilitate their use in research, we optimized the synthesis of these glycans previously established in our lab. Optimization involved implementing one-pot reactions using iron (III) chloride as a catalyst, employing a photoinitiator catalyst to enhance thiol-ene photo addition, and the accurate calculation of the deacylation reagent during the final deprotection step. Furthermore, we conjugated these glycans to a novel platform based on PEGylated phospholipids for further implementation in chemiluminescent enzyme-linked immunosorbent assays (cELISA).

2.2. HYPOTHESIS AND SPECIFIC AIMS

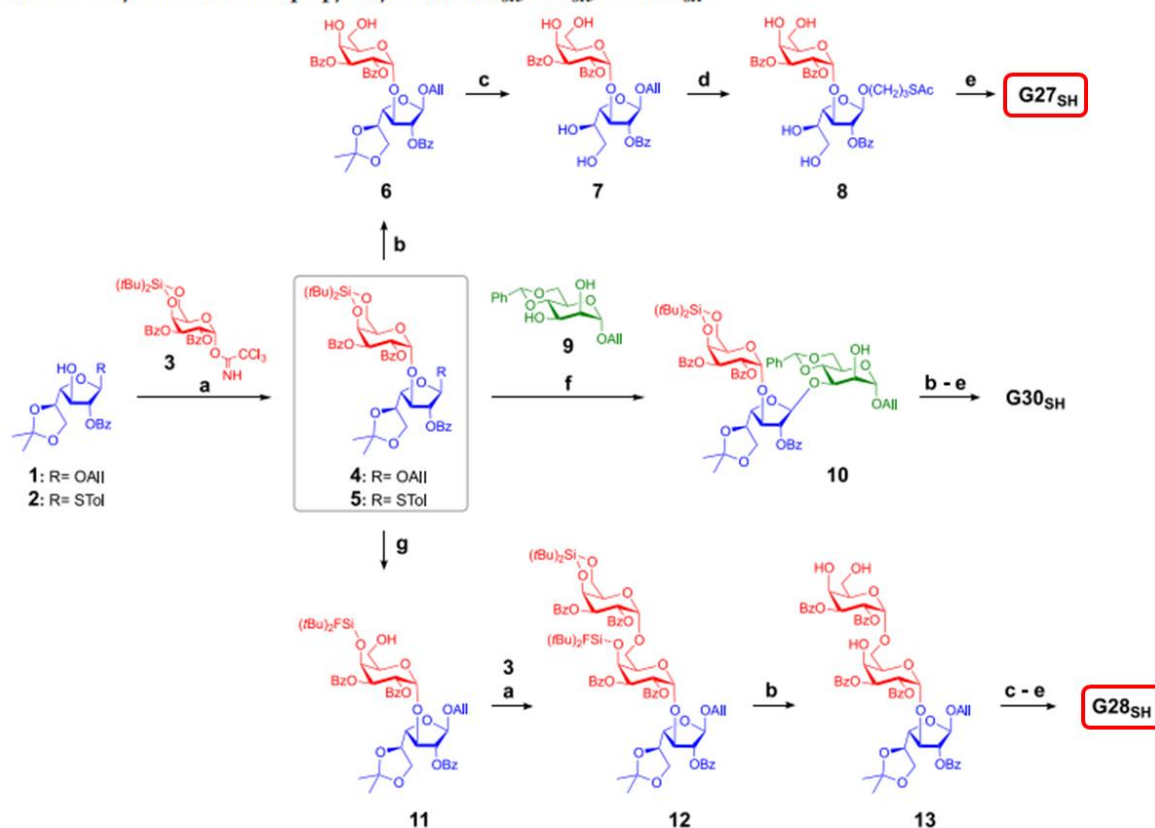
In the past decade, our group has been engaged in synthetic bioorganic chemistry with a focus on carbohydrate chemistry, particularly oligosaccharide and glycoconjugate synthesis. In an overall process that we call “reversed immunoglycomics,” our lab synthesizes terminal portions of parasite-derived glycans or suspected structures based on partial structural information.¹⁰¹⁻¹⁰⁸ These sugars are then conjugated to proteins to form glycoarrays of neoglycoproteins used as antigens in chemiluminescent Enzyme-Linked Immunosorbent Assay (cELISA) to identify diagnostic biomarkers.



Figure 13. Structures of a) **G27_{SH}** and b) **G28_{SH}** used for conjugation.

So far, we have achieved the complete synthesis of some essential parasite-derived glycans modified with thiol handles for conjugation.¹⁰⁹⁻¹¹⁵ Among them, the disaccharide Gal α 1,3Gal β (**G27_{SH}**) (*Figure 13*) and the trisaccharide Gal α 1,6Gal α 1,3Gal β (**G28_{SH}**) (*Figure 13*) are particularly important because their neoglycoprotein conjugates **NGP27b** and **NGP28b** have shown significant activity against sera of patients with *Leishmania major* and *Leishmania braziliensis* infection, respectively.¹¹⁶

Scheme 1. Synthesis of 3-Thiopropyl Glycosides $G27_{SH}$, $G30_{SH}$, and $G28_{SH}$



^aTMS-OTf, DCM, 0 °C to rt, 1 h, MS 4 Å (50–67%). ^bHF·pyridine, THF, 0 °C then rt, 1 h (65–88%). ^cTFA/H₂O/DCM 1:1:10, rt, 15 min (70–90%). ^dAcSH, AIBN or DPAP, THF, UV light (350 nm), 6–12 h (85–93%). ^eNaOMe, MeOH, rt, 2 h (quant.). ^fNIS, AgOTf, DCM, 0 °C to rt, 45 min, MS 4 Å (47%). ^gHF·pyridine (1.2 equiv), THF, 0 °C, 6 h or HF·pyridine (excess), THF, 0 °C, 2 h (60%).

Scheme 1. Excerpt from *Montoya et al. JACS Au* showing the synthetic scheme for $G27_{SH}$ and $G28_{SH}$

Even though our group has already published the complete syntheses of $G27_{SH}$ and $G28_{SH}$ (*Scheme 1*)^{115, 116} the current methodology is still not ideal. It is a tedious multistep synthetic route where most of the reactions are not high-yielding, and a lot of chromatography is still needed. The issues above affect the overall time needed to accomplish the syntheses, which is not very economical because many solvents and expensive reagents are required. Furthermore, neoglycoproteins **NGP27b** and **NGP28b** exhibited compromised stability, resulting in significant variations in CL-ELISA outcomes over time for the same batch.

Hypothesis: In this research project, we hypothesize that the use of different catalysts, radical initiators, and deprotection procedures will significantly improve our previously

established syntheses for G27_{SH} and G28_{SH} with respect to efficiency, reagent consumption, reagent toxicity, and production time. Moreover, conjugating the glycans to maleimide-derivatized phospholipids will yield neoglycolipids (NGLs) characterized by enhanced stability and controllability during synthesis compared to the currently employed neoglycoproteins (NGPs).

To address the hypothesis raised above, we propose the following specific aims:

Specific Aim 1

To synthesize the precursor *O*-allyl- β -D-galactofuranoside using anhydrous iron (III) chloride as a catalyst in a one-step Fischer-Lubineau glycosylation from allyl alcohol and D-galactose.

Specific Aim 2

To accomplish the thiol-ene photoaddition using the photocatalyst DPAP in DCM as solvent.

Specific Aim 3

To optimize the deprotection of the benzoate groups using catalytic amounts of sodium methoxide and a minimum quantity of Amberlyst-15H.

Specific Aim 4

To conjugate the thiol-derivatized glycan to the PEGylated and maleimide-derivatized phospholipids to generate the corresponding neoglycolipids (NGLs).

2.3. INTRODUCTION

2.3.1. GLYCOSCIENCES

In recent years, there has been broad acknowledgment of the critical role that glycans (or oligosaccharides) and glycoconjugates (glycolipids and glycoproteins) play in biological recognition processes.¹¹⁷⁻¹²⁰ The complex structure, diverse functionality, and dynamic nature of natural glycans enable them to participate in intermolecular interactions as biological information encoders.¹²¹ The process of carbohydrate recognition constitutes an essential aspect of biological development¹²² and the immune response against pathogens by identifying exogenous carbohydrates.^{123, 124} Conversely, numerous viral pathogens and bacteria (such as *Haemophilus influenzae* and *Escherichia coli*) initially adhere to the host-host tissues by specifically binding to glycans on the host cell surfaces.¹²⁵ Consequently, there exists a keen interest in the development of therapeutic drugs capable of modulating, interfering with, or taking advantage of carbohydrate-based pathogen-host interactions. Zanamivir and Oseltamivir, neuraminidase inhibitors utilized in the treatment of influenza infections, are two of many examples of therapeutic agents that disrupt carbohydrate-specific interactions.¹²⁶ Vaccines employing bacterial polysaccharides conjugated to carrier proteins have demonstrated notable efficacy against *H. influenzae*.¹²⁷

Given the involvement of glycans in numerous biological functions, research on carbohydrates has garnered unprecedented attention. However, it still represents only a fraction of the research devoted to nucleic acids and proteins. A major challenge stems from the difficulty in obtaining sufficient quantities of pure and structurally well-defined glycans and glycoconjugates, which often occur in nature in microheterogeneous forms and at low concentrations.^{128, 129} Consequently, the chemical synthesis of oligosaccharides represents a viable approach to address this challenge. Despite notable progress in the synthesis of complex oligosaccharides,^{120, 130-132}












their assembly remains intricate due to the absence of standardized methods for routine preparation.

While retrosynthetic analysis is more straightforward for oligosaccharides compared to other natural products, several challenges persist in their chemical synthesis, including (a) achieving stereoselectivity during the glycosidic bond formation (glycosylation reactions); (b) glycosylation of glycans with a high density of functional groups; (c) differentiation of multiple functional groups with orthogonal protection to regulate the regioselectivity of glycosylation, (d) extensive protection and deprotection steps that diminish the overall synthesis efficiency, rendering oligosaccharide synthesis a laborious and time-consuming process.

These technical hurdles, compounded by the need to address at least ten human-type monosaccharides and the extensive structural diversity of the targets, underscore the absence of a universal method for glycans assembly.^{130, 133} Nonetheless, given the paramount importance of glycans and their conjugates in glycomic research, advancements in carbohydrate chemistry persist, driving the development of novel and improved synthetic methodologies.

While nature boasts several hundred distinct monosaccharides, only a minority of these are prevalent in extensively studied glycans.¹³⁴ **Table 2** illustrates the symbol nomenclature for the most prevalent glycans found in *Leishmania* species surface glycoconjugates, accompanied by their standard abbreviations.¹³⁵

Table 2. Monosaccharide symbol nomenclature for glycans.

Shape	White (Generic)	Blue	Green	Yellow	Purple
Filled Circle	Hexose 	Glc 	Man 	Gal 	
Filled Square	HexNAc 	GlcNAc 		GalNAc 	
Crossed Square	Hexosamine 	GlcN 			
Filled Diamond	Deoxynonulosanate 				Neu5Ac 

2.3.2. LEISHMANIASIS OVERVIEW

Leishmania parasites can cause three clinical manifestations, depending on the infecting species. The first is localized cutaneous leishmaniasis (CL),¹³⁶ characterized by single or multiple skin ulcers along satellite lesions or nodular lymphangitis. The second manifestation is mucocutaneous leishmaniasis (MCL), involving mucosal tissue. The third and most severe form is visceral leishmaniasis (VL), which affects internal organs like bone marrow, spleen, and liver and can be fatal if left untreated.¹³⁷ Leishmaniasis affects not only humans but also dogs and various other mammals;¹³⁸ its transmission typically occurs through bites from infected female sandflies (*Phlebotomus lutzomyia*).¹³⁹

Cutaneous leishmaniasis is the most widespread form of leishmaniasis globally among its three clinical variants. Although 90% of CL cases are concentrated in seven countries -Algeria, Afghanistan, Iran, Brazil, Saudi Arabia, Peru, and Syria- CL is endemic in over 98 countries, posing a risk to approximately 350 million individuals. Its prevalence totals around 12 million cases, with an annual incidence ranging from 700,000 to 1 million cases.¹⁴⁰ However, these incidence figures are likely underestimated due to underrecognition and the absence of mandatory reporting in many countries.¹⁴¹ While CL is typically non-fatal, it results in significant disfiguring skin ulcers, often complicated by secondary infections that may require months to years to heal. The resulting scarring frequently leads to social ostracism and psychological distress.¹⁴²

Pentavalent antimonials¹⁴³ serve as the primary treatment for all leishmaniasis clinical presentations, emphasizing the importance of early diagnosis and intervention to achieve complete parasite eradication and prevent progression to severe forms of the disease.¹⁴⁴ Accurate diagnosis of CL poses challenges due to its resemblance to other skin conditions like syphilis, Hansen's disease, or skin cancer.¹⁴⁵ Biopsy specimen culturing is a standard diagnostic method, complemented by polymerase chain reaction (PCR) targeting parasite DNA, albeit with lower frequency due to variable parasite tissue distribution compromising sensitivity.¹⁴⁵ An alternative serological diagnostic approach involves ELISA targeting antibodies against the parasite, the effectiveness of which depends on the antigen selection and the applied technique. Numerous antigens have demonstrated efficacy for diagnostic purposes over time.¹⁴⁶⁻¹⁴⁹

A promising approach for diagnosing CL via serology involves utilizing specific carbohydrate antigens sourced from the parasite's cell surface. Like other protozoa, *Leishmania* parasites express species-specific glycoinositolphospholipids (GIPLs) and lipophosphoglycans (LPGs), with certain species like *L. (L.) major*, *L. (V.) panamensis*, and *L. (L.) mexicana* exhibiting

galactose-rich type-2 GIPLs.¹⁵⁰⁻¹⁵² The expression of LPGs is mainly confined to the promastigote stage, the insect-dwelling form of the parasite, where it constitutes a substantial portion of the densely arranged surface glycocalyx.¹⁵¹ Conversely, LPGs are present at minimal or undetectable levels in the amastigote stage, which infects mammalian macrophages.¹⁵¹ In contrast, GIPLs are plentiful in both key developmental stages of the parasite and are primarily expressed on the cell surface. These GIPLs frequently play a crucial role in determining parasite survival and infectivity. They feature at their glycans's non-reducing end α -galactopyranose (α -Galp) or β -galactofuranose (β -Galf) units,¹⁵²⁻¹⁵⁴ structures absent in humans but with strong antigenic and immunogenic properties.¹⁵²⁻¹⁵⁹ Consequently, patients infected with *L. (L.) major*, *L. (L.) mexicana*, or *L. (V.) braziliensis* often display elevated levels of anti- α -Gal and anti- β -Galf antibodies, which specifically target type-2 GIPLs or structurally similar motifs.

Most of the GIPLs and LPGs glycan structures of these parasites are unknown, but some of them have been studied and published (**Figure 14**).^{156, 160} For example, it is known that *L. major* and *L. mexicana* express unusual Galp α 1,3Galf β (GIPL-2) and Galp α 1,6Galp α 1,3Galf β (GIPL-3) moieties attached to the Manp α 1,3Manp α 1,4GlcN α trisaccharide. All GIPLs across all species share this component. They also express LPGs, which contain the same terminal Galp α 1,6Galp α 1,3Galf β trisaccharide as found in GIPL-3.¹⁵⁶ Furthermore, *L. major* GIPL-1 has a terminal Galf β 1,3Manp α , which lacks the Galp α moiety.

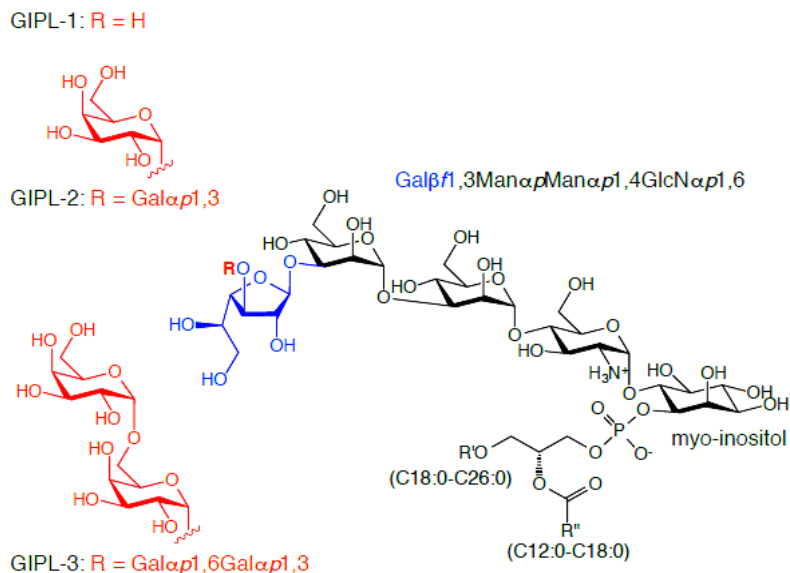


Figure 14. Schematic representation of *Leishmania* surface glycoconjugates (GPLs)

2.3.3. G27_{SH} AND G28_{SH} IN cELISA

Figure 15 a) and **b)** shows an excerpt of the cross-titrations when **NGP27b** (neoglycoprotein where **G27_{SH}** was attached on BSA) and **NGP28b** (neoglycoprotein where **G28_{SH}** was attached on BSA) were tested against patient sera with *L. major*, *L. tropica* and *L. braziliensis* in cELISA. Serum from healthy individuals was used as a control in all the experiments. **Figure 15 a)** shows how both **NGP27b** and **NGP28b** developed a high response when tested with sera from *L. major* infections, but they did not respond so well when sera from *L. tropica* infections or healthy individuals were used instead. In **Figure 15 b)** both NGPs were exposed to serum from patients with *L. braziliensis* infection and healthy individuals; in this experiment, **NGP28b** clearly showed a higher response than **NGP27b**. This last experiment showed that patients with *L. braziliensis* infection have a particular group of antibodies that adhere very strongly to the antigenic **G28** moiety.

More detailed cELISA results using individual sera of patients with *L. major* infection, *L. tropica* infection, and heterologous disease, Receiver-operating Characteristic analysis, as well as

sensitivity and specificity calculations are described in Alba Montoya's dissertation¹⁶¹ and our recent publication in *JACS Au*.¹¹⁵

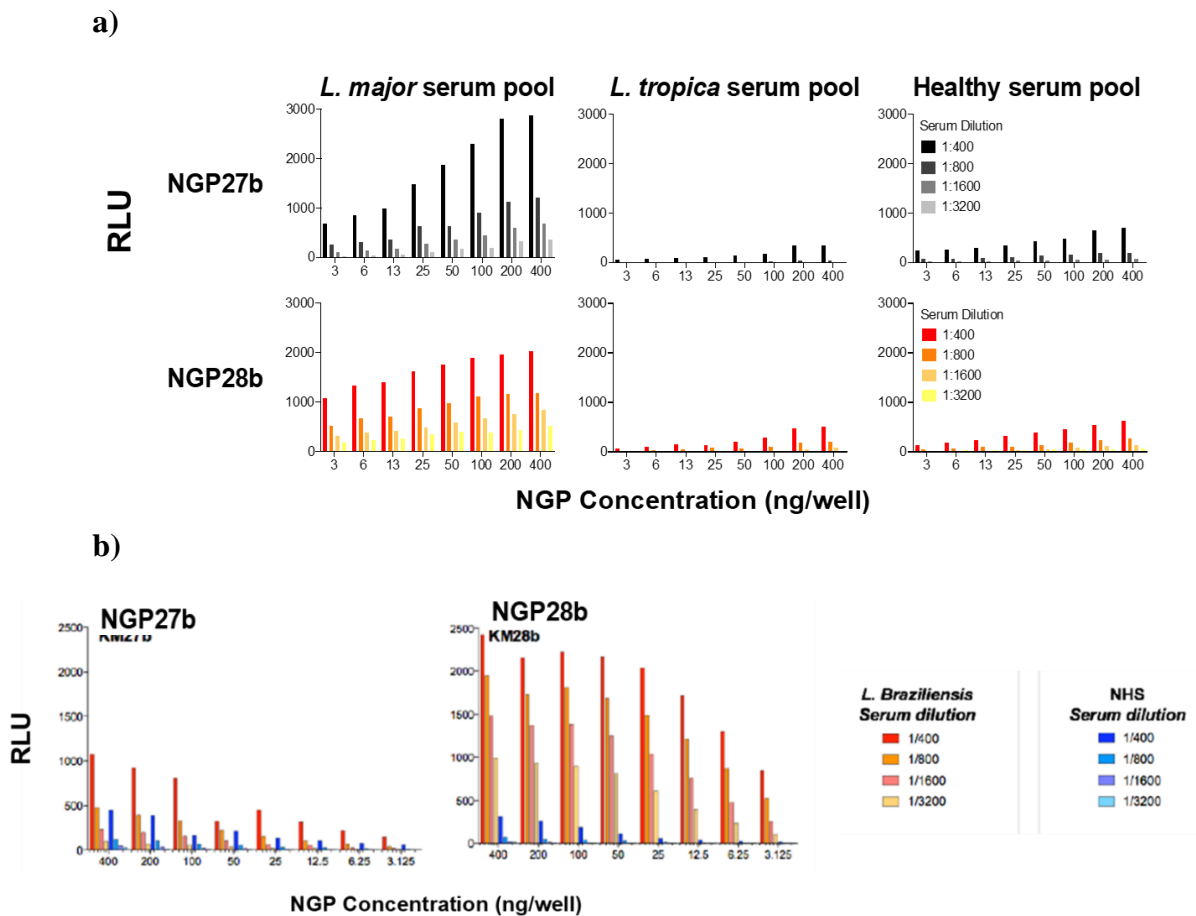


Figure 15. a) Cross-titration showing the response of NGP27b and NGP28b against *L. major* serum pool, *L. tropica* serum pool, and healthy serum pool b) Cross-titration showing the response of NGP27b and NGP28b against *L. braziliensis* serum pool and healthy serum pool.

2.4. MATERIALS AND METHODS

Excerpt from “*Reversed Immunoglycomics Identifies α -Galactosyl-Bearing Glycotopes Specific for Leishmania major infection*”¹¹⁵

All chemicals were purchased as reagent grade from Thermo Fisher Scientific, Sigma-Aldrich, or Acros Organic and used without further purification. The ACS-grade solvents used for reactions were obtained from Thermo Fisher Scientific and distilled from the appropriate drying agents. Molecular sieves (3 Å and 4 Å) were purchased from Alfa Aesar and Thermo Fisher Scientific, respectively, and activated under high vacuum and heat before use. Reactions were performed under an argon atmosphere, strictly anhydrous conditions, and monitored by TLC on silica gel 60 F254 plates from EMD Millipore or Dynamic Adsorbents, Inc. Spots were detected under UV light (254 nm) and/or by charring with 4% sulfuric acid in ethanol. The purification of the compounds was performed by flash column chromatography on silica gel (40-60 µm) from Thermo Fisher Scientific, and the ratio between silica and crude product ranged from 50:1 to 120:1 (dry w/w). FPLC purifications were performed with an AKTA Purifier 100 FPLC system from Cytiva (former GE Healthcare) using a Resource RPC column with a stationary phase of 15 µm polystyrene/divinylbenzene beads, solvent A: 2% CH₃CN/H₂O; solvent B: 85% CH₃CN/H₂O.

¹H and ¹³C-NMR spectra were recorded on a Bruker Avance III HD 400 MHz NMR spectrometer at 400 and 101 MHz or on a JEOL 600 MHz NMR spectrometer at 600 and 150 MHz, respectively. Chemical shifts (in ppm) were determined relative to tetramethylsilane (δ 0.00 ppm) as an internal standard in CDCl₃ and CD₃OD, or relative to the CDCl₃ signal (δ 77.0 ppm) in ¹³C-NMR spectra. In case of spectra measured in D₂O, a solution of tetramethylsilane in CDCl₃ in a sealed capillary was used as an external standard for calibration. Coupling constant(s) [Hz] were measured from one-dimensional ¹H-NMR spectra. Full or partial assignments were made by 1D spectra as well as standard COSY, HSQC, and TOCSY experiments. In disaccharides and trisaccharides, protons of galactopyranose are labeled with an italicized “*p*”, and protons of galactofuranose with an italicized “*f*”. Protons in the allyl group are labeled as “*a*” for the sp³-

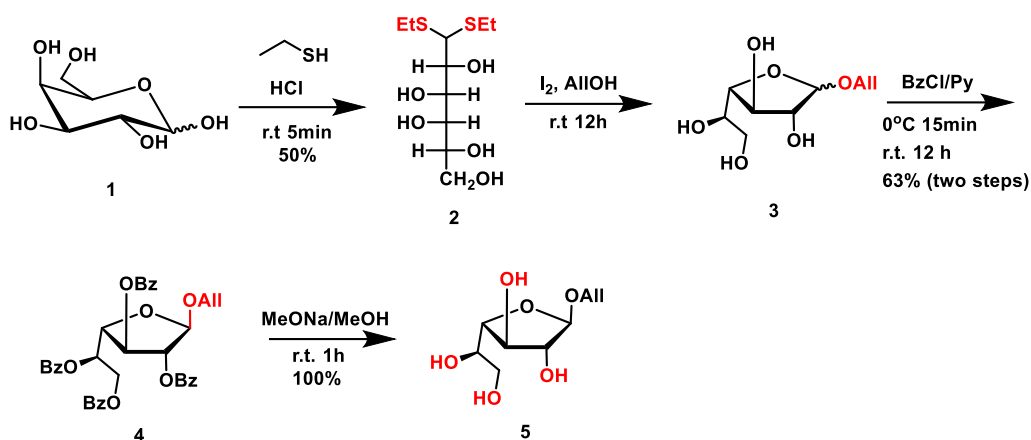
hybridized CH₂, “b” for the sp²-hybridized CH, and “c” for the terminal sp²-hybridized CH₂. MS analyses of the carbohydrate derivatives were performed on a high-resolution JEOL AccuTOF mass spectrometer using an electrospray ionization (ESI) source. The thiol-ene reactions were performed in a Rayonet RPR200 photochemical reactor (Southern New England Ultraviolet Company, Branford, CT) equipped with 16 UV lamps (350 nm). Bovine serum albumin (BSA) and BSA derivatives (neoglycoproteins (NGPs) and 2-mercaptoethanol-BSA) were measured by matrix-assisted laser/desorption/ionization mass spectrometer (MALDI)-TOF-MS (MALDI-8020, Shimadzu) using 10 mg/mL sinapinic acid, 0.1% trifluoroacetic acid, in 50% acetonitrile as a matrix. Polystyrene Nunc MaxiSorp 96-well ELISA plates and chemiluminescent ELISA reagents were purchased from Thermo Fisher Scientific or Jackson ImmunoResearch, and chemiluminescence was recorded on a Luminoskan Ascent, Thermo Fisher Scientific. Optical rotations were measured on an ATAGO AP-300 Automatic Polarimeter.

2.5. RESULTS AND DISCUSSION

Specific Aim 1. To synthesize the precursor *O*-allyl- β -D-galactofuranoside using anhydrous iron (III) chloride as a catalyst in a one-step Fischer-Lubineau glycosylation from allyl alcohol and D-galactose.

2.5.1. PREVIOUS SYNTHESIS OF *O*-ALLYL- β -D-GALACTOFURANOSIDE (5)

The previous synthetic procedure of the two target oligosaccharides, **G27_{SH}** and **G28_{SH}**, described in the dissertation of Dr. Alba Montoya,¹⁶¹ started synthesizing the monosaccharide precursor *O*-allyl- β -D-galactofuranoside (**5**), illustrated in (*Scheme 2*).



Scheme 2. Synthesis of galactofuranoside **5**, a precursor for synthesizing **G27_{SH}** and **G28_{SH}**. Alba Montoya's dissertation provides a complete description.

In this procedure, galactose (**1**) was first thioglycosylated in concentrated hydrochloric acid using ethanethiol as the acceptor. The exact timing was crucial when running the reaction; if the mixture is left for more than five minutes, many dark byproducts are formed, and consequently, the yield will be lower than 50 %. Working with the caustic fuming hydrochloric acid and pungent ethanethiol was the most significant inconvenience. When doing the work up, all the acid should be neutralized with a sodium bicarbonate solution, and the ethanethiol must be quenched with an oxidizing agent; for this purpose, we usually employ a bleach solution. All the materials (spatulas, Buchner funnel, round bottom flasks, beakers, syringes, needles, gloves) should also be bleached.

The second step was crucial because it ensured the final configuration was the desired galactofuranoside.^{162, 163} In this reaction, four isomers are formed: two furanose isomers and two pyranose ones. Based on our experience, running a silica column was not a good idea at this point because the four isomers were very polar and similar in *R_f* values, making the chromatography very difficult. That is why we performed a one-pot benzylation with benzoyl chloride in pyridine.

After a workup with sodium thiosulfate to quench the excess iodine and sodium bicarbonate to neutralize the solution, the desired benzoylated furanoside (**4**) was isolated using silica column chromatography with a 63% yield over two steps.

The final step to yield (**5**) was removing the benzoyl groups. This procedure was performed following the Zemplen diacylation reaction,¹⁶⁴ which involves treating the benzoylated starting material with sodium methoxide in methanol. The sodium methoxide solution must be prepared freshly by adding metallic sodium to anhydrous methanol.

To summarize, the previous route to synthesize compound (**5**) was a four-step synthesis with an overall yield of 32 %. It involved nine highly toxic reagents: ethanethiol, concentrated hydrochloric acid, iodine, allyl alcohol, benzoyl chloride, pyridine, elemental sodium, methanol, and sodium thiosulfate. It also had a deficient “atom economy,” meaning a tiny fraction was incorporated into the final product from all the reagents used.

2.5.2. NEW SYNTHESIS OF *O*-ALLYL- β -D-GALACTOFURANOSIDE (5**)**

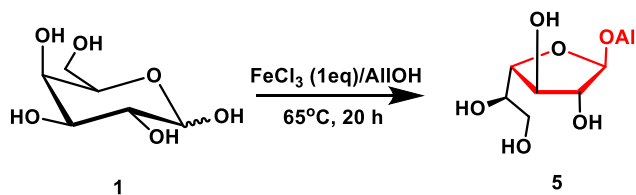
To improve the old synthesis, we needed to find a method to synthesize the galactofuranoside more efficiently. One drawback was that, unlike their thermodynamically favorable pyranoside counterparts, hexofuranosides were not commercially available.

Equilibration and anomeric control of hexopyranoside and hexofuranoside syntheses must be considered in addition to the competing donor/acceptor reactions for its construction. To this extent, pioneering work by H.E. Fischer from 1893 to 1895¹⁶⁵⁻¹⁶⁷ demonstrated that furanosides could be obtained from corresponding unprotected pyranoses using simple alcohols and Brønsted-Lowry acids. Further studies by J.C. Fischer and A. Lubineau¹⁶⁸ demonstrated that subjecting unprotected monosaccharides to thermal heating in the presence of the anhydrous Lewis acid FeCl₃

and methanol resulted in the formation of primarily methyl furanoside as the main product, with a mixture of α - and β -anomers. The reaction took approximately 28 hours, and in addition, the purification proved to be challenging and cumbersome.

Iron salts have garnered significant interest as cost-effective and environmentally sustainable agents in various selective processes within organic synthesis.¹⁶⁹ Over the past decade, FeCl_3 has shown to be an effective catalyst in forming carbon-carbon¹⁷⁰ or carbon-nitrogen bonds,¹⁷¹ in intramolecular Friedel-Craft reactions,¹⁷² and a reduction of ketones or allylic alcohols.¹⁷³

In this research, we chose to revisit the Fischer-Lubineau D-Galf synthesis, but instead of using methanol as the solvent, we decided to use allyl alcohol. In this reaction, the allyl alcohol worked as the solvent and reactant simultaneously. Different amounts of FeCl_3 were tested, but they showed better results when added in a stoichiometry ratio. (*Scheme 3*)



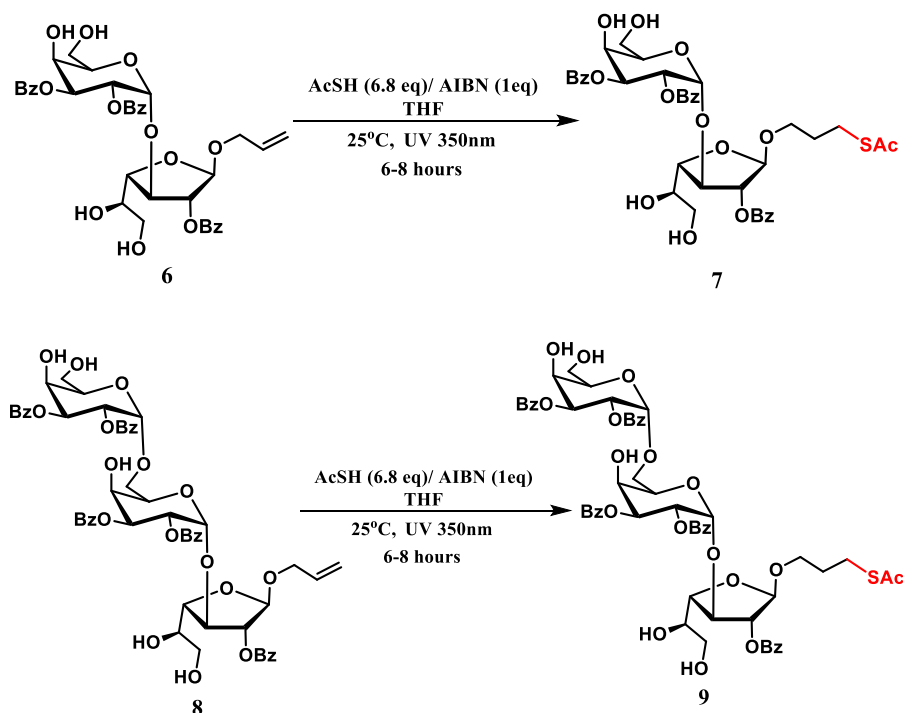
Scheme 3. Optimized Fischer-Lubineau D-Galf synthesis.

To summarize, the new route to synthesize compound (**5**) was a one-step synthesis with an overall yield of 45%. It involved three reagents that were not highly toxic or hazardous. In addition, it showed a better atom economy than the previous procedure.

Specific Aim 2. To accomplish the thiol-ene photoaddition using the photocatalyst DPAP in DCM as solvent.

2.5.3. PREVIOUS SYNTHETIC PROCEDURE FOR THE THIOL-ENE REACTION

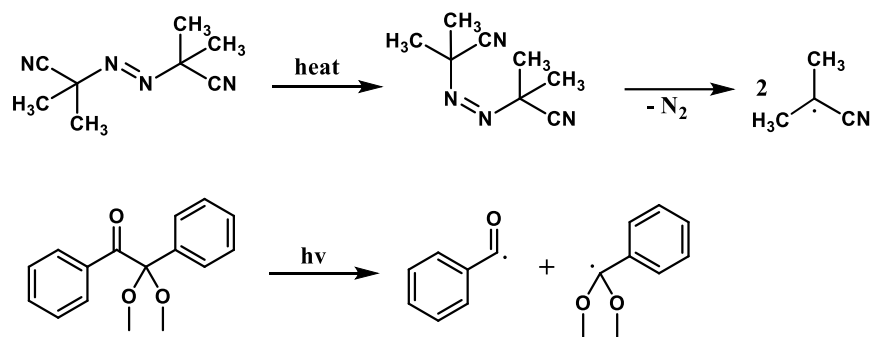
Close to the end of the previous synthetic route of both **G27_{SH}** and **G28_{SH}**, we performed a thiol-ene photoaddition (**Scheme 4**); this was a crucial step not only for the preparation of these two glycans but also for all the glycans that we synthesized in our lab because it ensured the further installation of the thiol functional group which was necessary when doing the final conjugation through thiol-maleimide coupling.



Scheme 4. Thiol-ene photoadditions following the old procedure.

Thiol-ene reactions have all the desirable features of a click reaction, being highly efficient, simple to execute with no side products, and proceeding rapidly to high yield.¹⁷⁴ When reactive olefinic substrates, that is, terminal olefins, are employed in thiol-ene chemistry, the reaction can be performed under mild conditions by only combining thiols and alkenes without the need for a radical initiator; that is, the reaction takes place through self-initiation, and light is used as the green catalyst.¹⁷⁵

In contrast to reactive alkenes, the thiol-ene reactions of less-reactive olefins can be initiated by adding radical initiators.¹⁷⁶ There are many possibilities for initiating thiol-ene addition, for example, the decay of an initiator molecule into radicals (*Scheme 5*). An initiator is a compound that fragments into radicals on heating to a specific temperature, termed “thermal initiation,” or irradiation with UV or visible light, termed “photoinitiation.” The two most common classes of thermal initiators are peroxides, such as di-tert-butylperoxide and benzoylperoxide, and azo compounds, such as 1,1-azobis(1-cyclohexanecarbonitrile) and 2,2-azobisisobutyronitrile (AIBN). In the case of photoinitiators, acetophenone derivatives, such as 2,2-dimethoxy-2-phenylacetophenone (DPAP), produce radicals through a rapid photochemical cleavage reaction.¹⁷⁷



Scheme 5. Decomposition of AIBN and DPAP initiators.

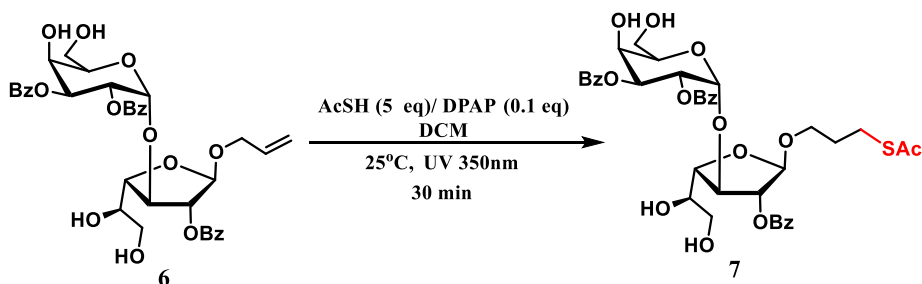
In a brief description, we did this reaction by mixing the olefinic sugar with 6.8 equivalents of the thioacetic acid in THF as the solvent. AIBN was used as the radical initiator in a 1:1 ratio to the olefinic sugar. The reaction was conducted under an inert atmosphere at rt for six hours and sometimes longer in the Rayonet UV reactor at 350 nm. (*Scheme 4*)

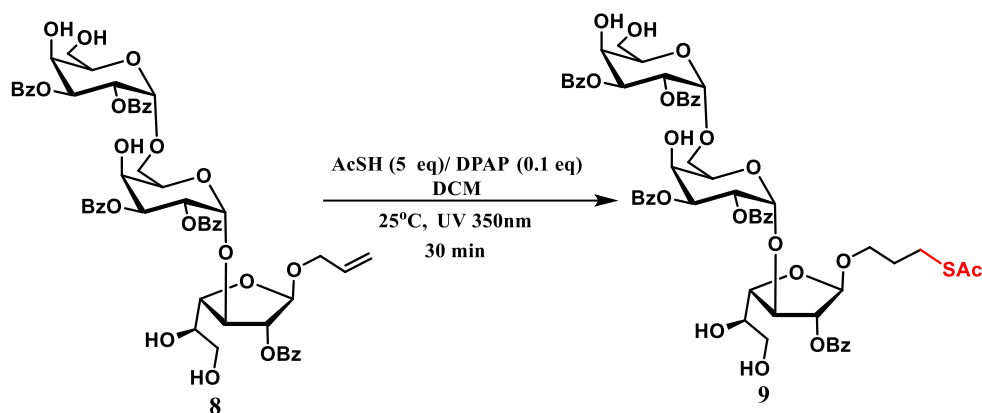
This procedure had some disadvantages: First, much thioacetic acid was used; it has a pK_a of 3.40, making it a stronger acid than acetic acid (pK_a = 4.75). Glycosidic bonds are incompatible with acid media; hydrolysis can quickly occur when small amounts of water are present. That is

why the THF needed to be anhydrous and under an argon atmosphere at all times for this reaction. THF was not a suitable solvent because it is hydrophilic and hygroscopic, especially after six hours of reaction. Another disadvantage is the use of AIBN; it is well known that AIBN is a thermoinitiator, which means the reaction would only occur under heating, but we run it under UV light at 25 °C. That is why AIBN was not used in a catalytic amount; we found the best results when used in a stoichiometric ratio. Finally, the yields were usually about 80 %, which is an attractive value in carbohydrate chemistry, but it falls behind the expected one for a click reaction.

2.5.4. NEW SYNTHETIC PROCEDURE FOR THE THIOL-ENE REACTION

In the new synthetic procedure, we decided to use a better photoinitiator; in this matter, the acetophenone derivative DPAP showed better results. As the solvent, we selected DCM because it is not hygroscopic, and hydrolysis would not be a problem. (*Scheme 6*)





Scheme 6. Optimized thiol-ene photoaddition.

The new route to synthesize compounds **7** and **9** was a more refined procedure with yields above 90 % after purification. The DPAP was used in catalytic amounts, and the reaction was completed after only 30 minutes of irradiation.

Specific Aim 3. To optimize the deprotection of the benzoate groups using catalytic amounts of sodium methoxide and a minimum quantity of Amberlyst-15H.

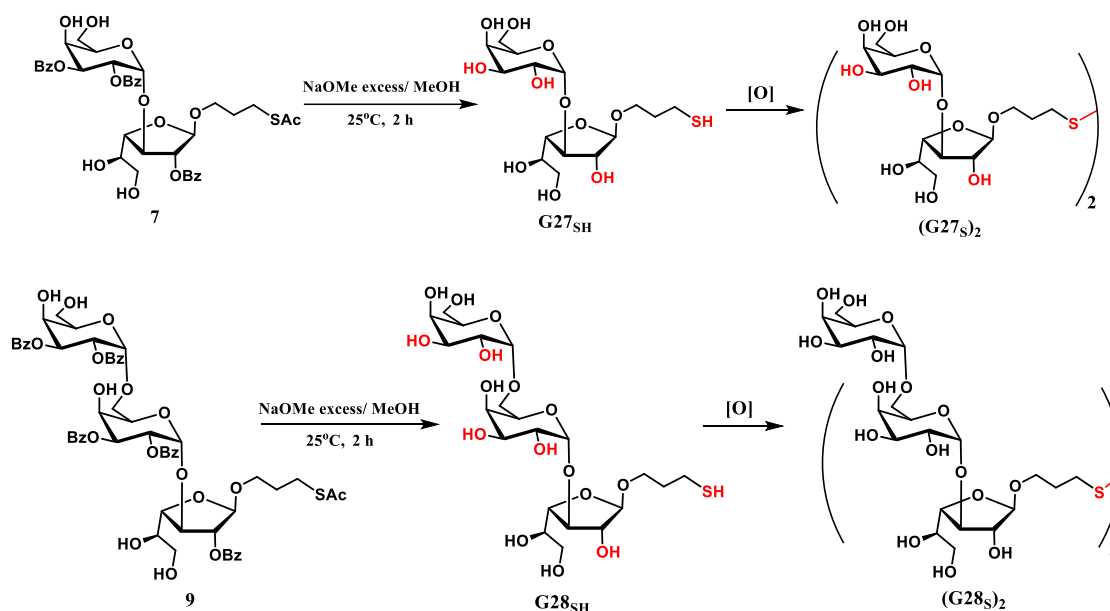
2.5.5. PREVIOUS DEACYLATION PROCEDURE

Acyl groups are widely used as protecting groups in organic synthesis strategies, especially in carbohydrate chemistry.^{178, 179} With the addition of acylation reagents under mild conditions, the hydroxyl groups of substrates readily form esters as intermediate products, and the esters are easily removed under a vast repertoire of different conditions when required.¹⁷⁹

Among all the available procedures to remove the acyl-protecting groups, we have decided to use the Zemlen diacylation. Zemlen and Kuntz first reported this reaction in 1924.¹⁶⁴ It describes the efficient removal of the *O*-acetyl-protecting groups of carbohydrates by treating the *O*-acetylated substrates in MeOH with a catalytic amount of sodium methoxide at rt. Today, it is a standard tool in laboratories and industry settings. Its inherent disadvantage is the retention of

sodium ions in solution. As the sodium ions can be removed using H^+ -exchanged resin, industrial diacylation techniques commonly involve ion-exchanged columns that can be regenerated with acid after ion exchange.¹⁸⁰

In our lab, we precisely plan the synthesis so that only acyl groups are present in the final deprotection. As shown in (*Scheme 7*), the Zemplen diacylation allowed us to remove in only one step the remaining acyl groups (typically acetyl and benzoyl) on the glycan skeleton and the acetyl from the thioacetyl moiety at the same time.



Scheme 7. Zemplen deacylation following the previous procedure.

Our previous procedure involved treating acyl-protected glycans (**7**) and (**9**) with 0.25 M NaOMe in anhydrous methanol and stirring for about three hours under argon-positive pressure. The removal of benzoyl and acetyl groups was monitored by mass spectrometry. The solution was then neutralized with the H^+ -ion exchange resin Amberlyst-15H, filtered through Celite,

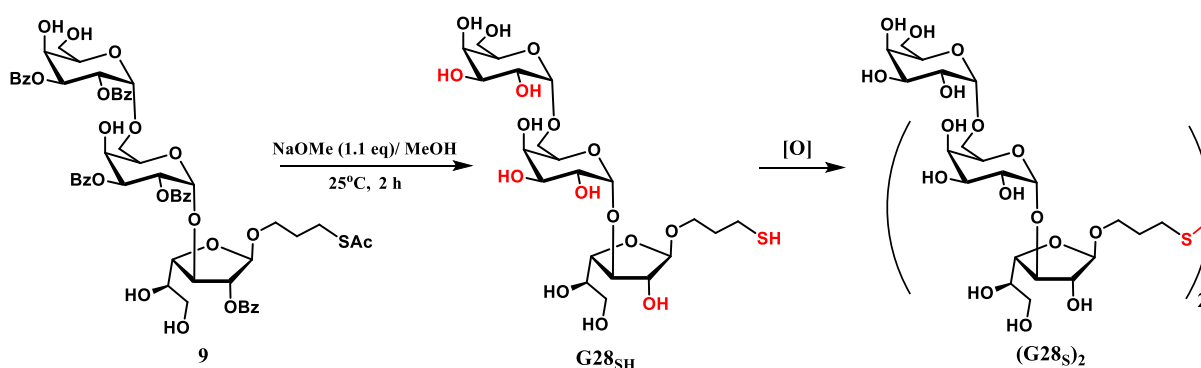
concentrated, dissolved in water, and lyophilized. Initially, the unprotected mercaptopropyl glycans **G27_{SH}** and **G28_{SH}** were produced, but they got oxidized by handling on air within hours to the disulfides (**G27s**)₂ and (**G28s**)₂, respectively. The final compounds were purified by reversed-phase FPLC on polystyrene/divinylbenzene beads using 2 % CH₃CN/H₂O (solvent A) and 85 % CH₃CN/H₂O (solvent B) in a gradient from 0 to 90 % of solvent B.

At first sight, the previous procedure appeared suitable, but it had some disadvantages. First, a considerable amount of sodium methoxide was used; for the synthesis of **G28_{SH}**, more than 20 equivalents were employed, and for **G27_{SH}**, more than 33 equivalents were used.¹⁶¹ Since the quantities of sodium methoxide solution were not standardized, they were always under the operator's estimation, giving this final deprotection a low reproducibility from batch to batch. In addition, more sodium methoxide means more H⁺-exchanging resin would be needed to reach the neutral pH. For this purpose, we used Amberlyst-15H, a strongly acidic ion exchange resin. Instead of packing a column with the Amberlyst-15H, the beads were added slowly and little by little to the sodium-enriched reaction mixture until all methoxide was neutralized as judged by pH indicator paper with an additional drop of water. By doing it like that, we saved some material and could control the reaction pH at any time. Based on our experience, adding a lot of Amberlyst-15H brought some extra inconveniences; if more than needed is accidentally added, the pH will drop below 7, and hydrolysis of the glycosidic bond could occur, on the other hand, after some time under magnetic stirring, some of the beads got crushed forming a suspension of residues that can even pass through Celite during filtration. Finally, the yield reported as quantitative was not an actual isolated yield after purification; at this point, the final compound was full of insoluble impurities and usually showed a grey-brown coloration that was not consistent with totally unprotected glycans. The actual yield after purification was often as low as 10 %.

2.5.6. NEW DEACYLATION PROCEDURE

In this situation, the solution to the problem did not involve a very sophisticated technique, and just by paying attention to small details, we could solve it successfully. A closer reading of the Zemplen deacetylation procedure revealed that the sodium methoxide should be added in catalytic amounts, which could potentially solve all our problems because there would be no need to add an excess of Amberlyst-15H, which can avoid undesired hydrolysis or solid impurities in the mixture.

It has been demonstrated by Bo Ren *et al.* that 0.1 equivalents of sodium methoxide to the acylated glycan give excellent results and that it works regardless of whether the protecting groups are benzoyl or acetyl groups.¹⁸⁰ In the case of the deacetylation of acetylated thio-containing glycosides, more than a stoichiometric amount of the base is necessary for each thioacetate group because the sulfhydryl group formed will neutralize the base. Therefore, 1.1 equivalents of sodium methoxide were used in the deacetylation of thioester-containing glycosides, producing free thiols in quantitative yields in two hours.¹⁸⁰ (*Scheme 8*)



Scheme 8. Optimized Zemplen deacylation.

To summarize, we came up with a general formula to calculate the optimal amount of sodium methoxide:

$$\text{Eq (NaOMe)} = 0.02 \times \text{A} + \text{S}$$

Where:

- **Eq (NaOMe)** represents the molar equivalents of NaOMe to accomplish the Zemplen deacylation to the protected glycan.
- **A** represents the number of acyl-protecting groups in the glycan structure; whether they are acetyl or benzoyls does not matter.
- **S** represents the number of thio-acyl units in the protected glycan.

For example, when running the deprotection of the thioester-containing disaccharide (**7**) (**A** = 3; **S** = 1) to afford **G27_{SH}**, the optimized equivalents of NaOMe that should be used are 1.06 eq. Adding the exact amount of NaOMe can be difficult; in those cases, adding a slight excess does not affect the overall yield.

Figures 16, 17, and 18 show the ¹H-NMR, ¹³C-NMR, and ESI-TOF HR mass spectra of compound (**G28s**)₂, respectively. This whole characterization was only possible after the improved synthetic procedure was implemented in our lab. A more complete characterization can be found in Montoya *et al.* (2021).¹¹⁵

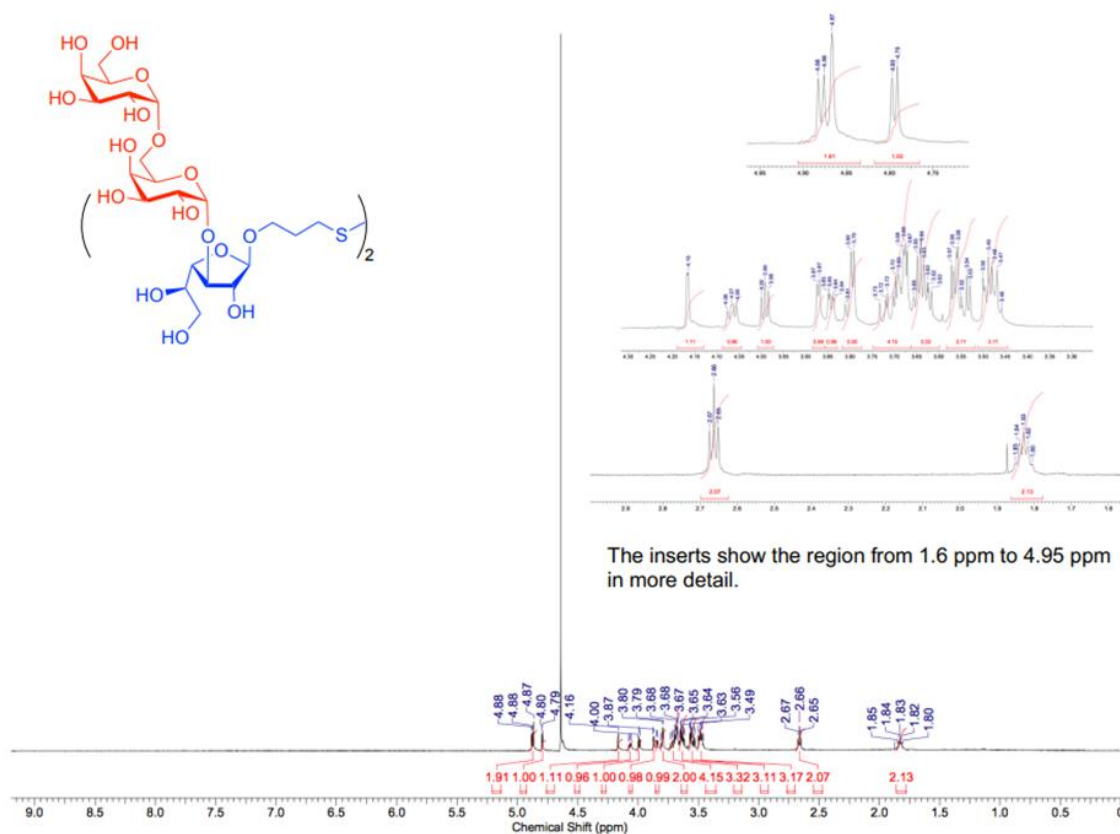


Figure 16. ^1H -NMR, 600 MHz, D_2O , compound $(\text{G28s})_2$

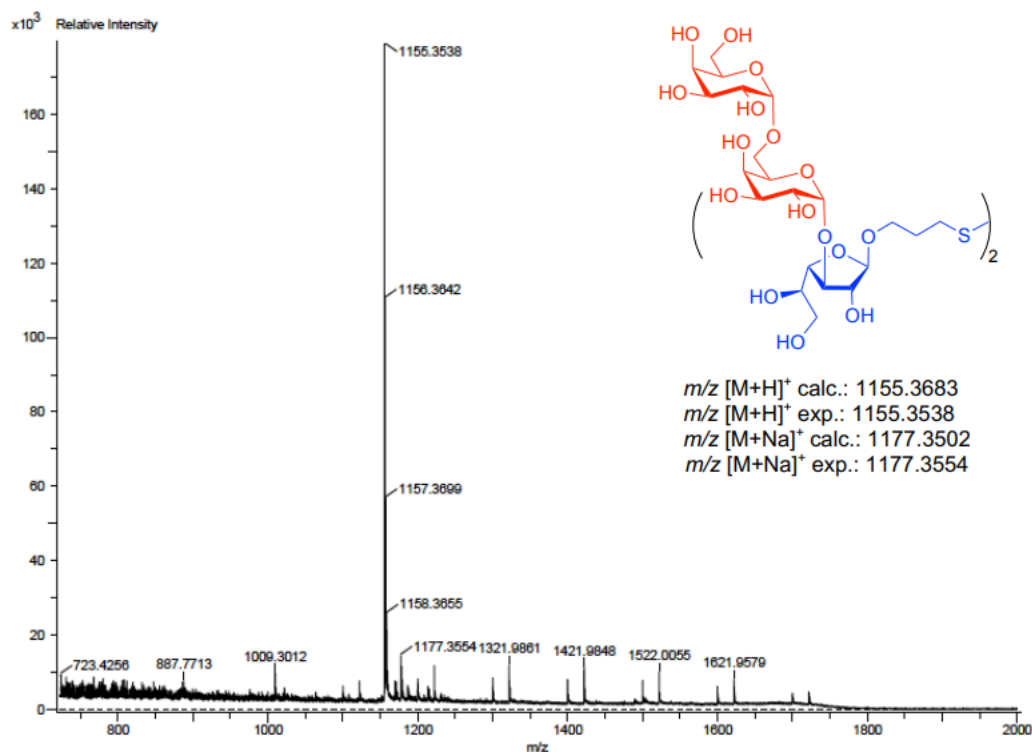


Figure 18. ESI-TOF HR mass spectrum of compound (G28s)₂

Specific Aim 4. To conjugate the thiol-derivatized glycan to the PEGylated and maleimide-derivatized phospholipids to generate the corresponding neoglycolipids (NGLs).

2.5.7. NGP INSTABILITY OVERVIEW

After synthesizing a new batch of oligosaccharide and derivatizing it with a thiol moiety, it is covalently conjugated to bovine serum albumin (BSA) using thiol-maleimide click chemistry, resulting in the formation of the corresponding neoglycoproteins (NGPs). These NGPs are subsequently assessed using chemiluminescent ELISA (cELISA) with patient sera, enabling the identification of NGPs exhibiting high antibody reactivity.^{115, 181} However, a decrease in the chemiluminescent response is occasionally noted over time for the identical batch of BSA-based NGPs during cELISA analysis. This observation suggests potential instability of the NGPs,

wherein disulfide bonds responsible for maintaining the protein's native conformation may become disrupted and reorganized upon exposure to TCEP or the free thiol-glycan, both of which act as reducing agents. Such alterations in conformation could lead to protein aggregation or the adoption of a configuration where the antigenic glycans are not properly displayed, resulting in reduced assay performance. Moreover, achieving precise control over the number of attached glycan units to a protein molecule proves challenging, as significant variations have been observed among batches produced from the same starting materials by the same operator.

Circular dichroism analysis was conducted on two different NGPs to assess the protein conformation changes over time: a freshly prepared batch of **NGP28b** (*Figure 19a*) and an older sample of **NGP29b** (*Figure 19b*). Each experiment included a standard of pure BSA and 2-mercaptoethanol-modified BSA (BSA-2ME) for comparison. The percentage of alpha-helix content was determined to evaluate the extent of protein misfolding.¹⁸² The analysis revealed that the alpha-helix content of **NGP28b** decreased from 70 to 60.2 % compared to unconjugated BSA, indicating some changes in protein conformation. On the other hand, a more pronounced decrease was observed in the older sample of **NGP29b**, where the alpha-helix percentage dropped from 65.7% to 31.4%, suggesting significant protein misfolding over time.

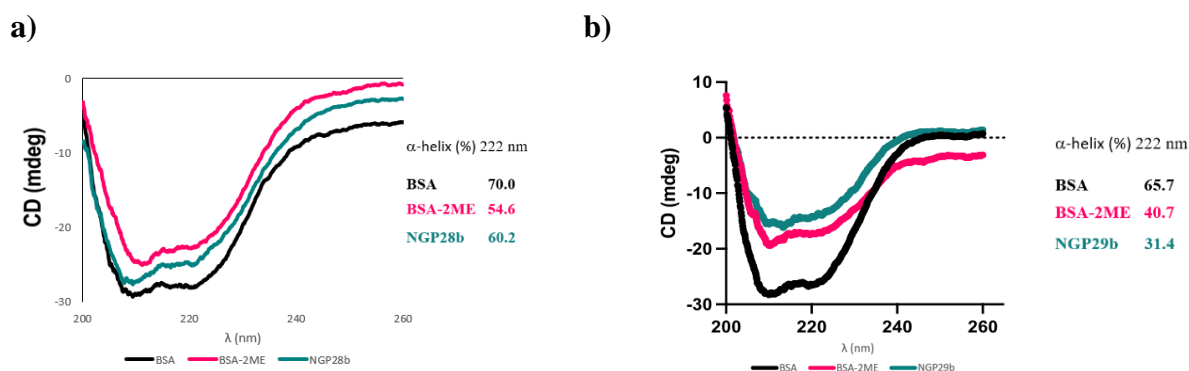
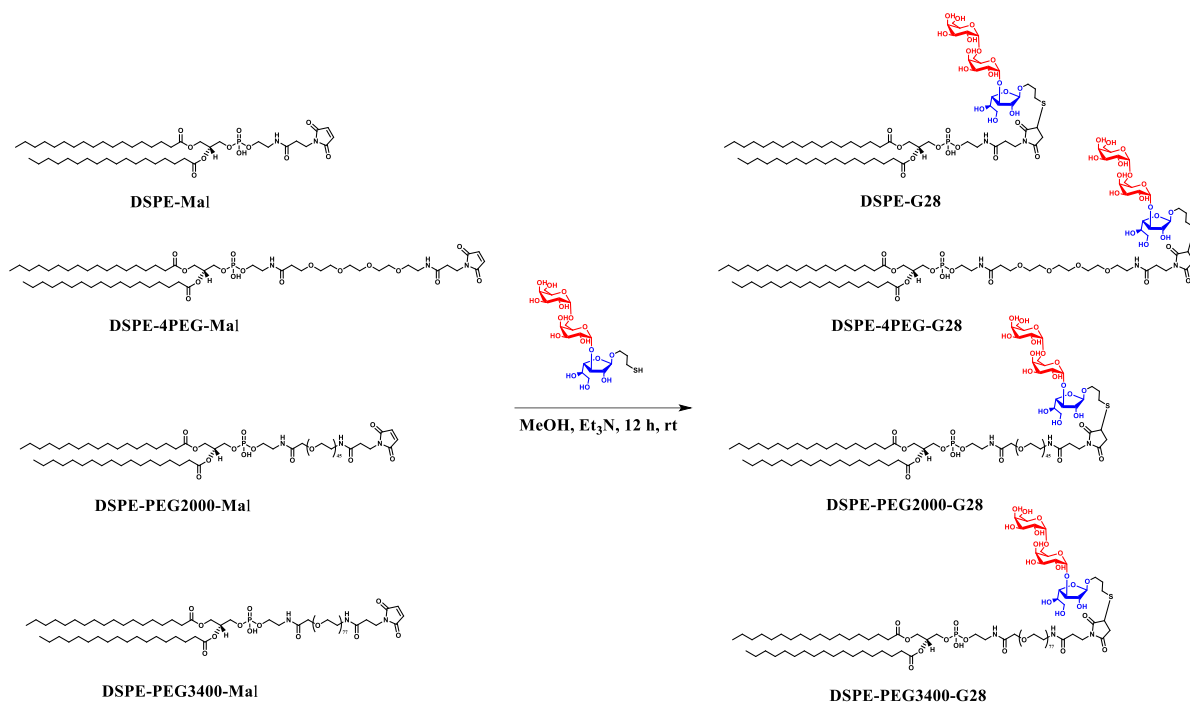


Figure 19. Circular Dichroism measurements and α -helix percentage of a) **NGP28b** and b) **NGP29b**.

2.5.8. SYNTHESIS OF THE NEOGLYCOLIPIDS (NGLS)

To overcome the instability observed in BSA-based NGPs, we conducted additional research into the conjugation of our glycans to lipidic anchoring tails, aiming to enhance their performance in cELISAs. The utilization of NGLs, serving as lipid-linked oligosaccharide probes, proved successful in exploring oligosaccharide ligands for discovery purposes.^{183, 184}

Due to the thiol functional group modification of our glycans, a lipid featuring a maleimide moiety emerged as the optimal choice for facilitating efficient conjugation via click coupling. We explored four maleimide-derivatized lipids (*Scheme 9*), including **DSPE-Mal**, wherein the glycan is positioned close to the lipid tail; **DSPE-4PEG-Mal**, incorporating four units of PEG between the glycan and the lipid; **DSPE-PEG2000-Mal**, where a PEG spacer of approximately 45 units separates the glycan from the lipid, and **DSPE-PEG3400-Mal** where a PEG spacer of approximately 77 units separates the glycan from the lipid. (*Scheme 9*)



Scheme 9. Structures of the maleimide-derivatized phospholipids and their corresponding NGLs after conjugation with **G28_{SH}**.

The synthetic procedure was very similar to all NGLs in *Scheme 9*. As a representative example **DSPE-PEG2000-G28**, a conjugate between the lipid **DSPE-PEG2000-Mal** and the trisaccharide **G28_{SH}** was synthesized as follows: In a glass vial, **DSPE-PEG2000-Mal** (5.5 mg) and previously reduced **G28_{SH}** (2.16 mg, 2 eq) were dissolved in 500 mL of methanol, and triethylamine (0.2 eq) was added as the catalyst. The vial was sealed under an argon atmosphere, protected from light, and stirred at room temperature for 48 hours. When the reaction was completed, the crude was concentrated under reduced pressure and further dried under a high vacuum for 8 hours. The remaining solid was resuspended in 1 mL of chloroform and centrifuged (20 minutes, 4 °C, 14000 g). The supernatant was carefully collected in a clean glass vial, reduced under low pressure, redissolved in pure water, and freeze-dried to yield **DSPE-PEG2000-G28** (6.1 mg, 94 % yield) as an off-white solid. The final product was characterized by ESI-MS to confirm

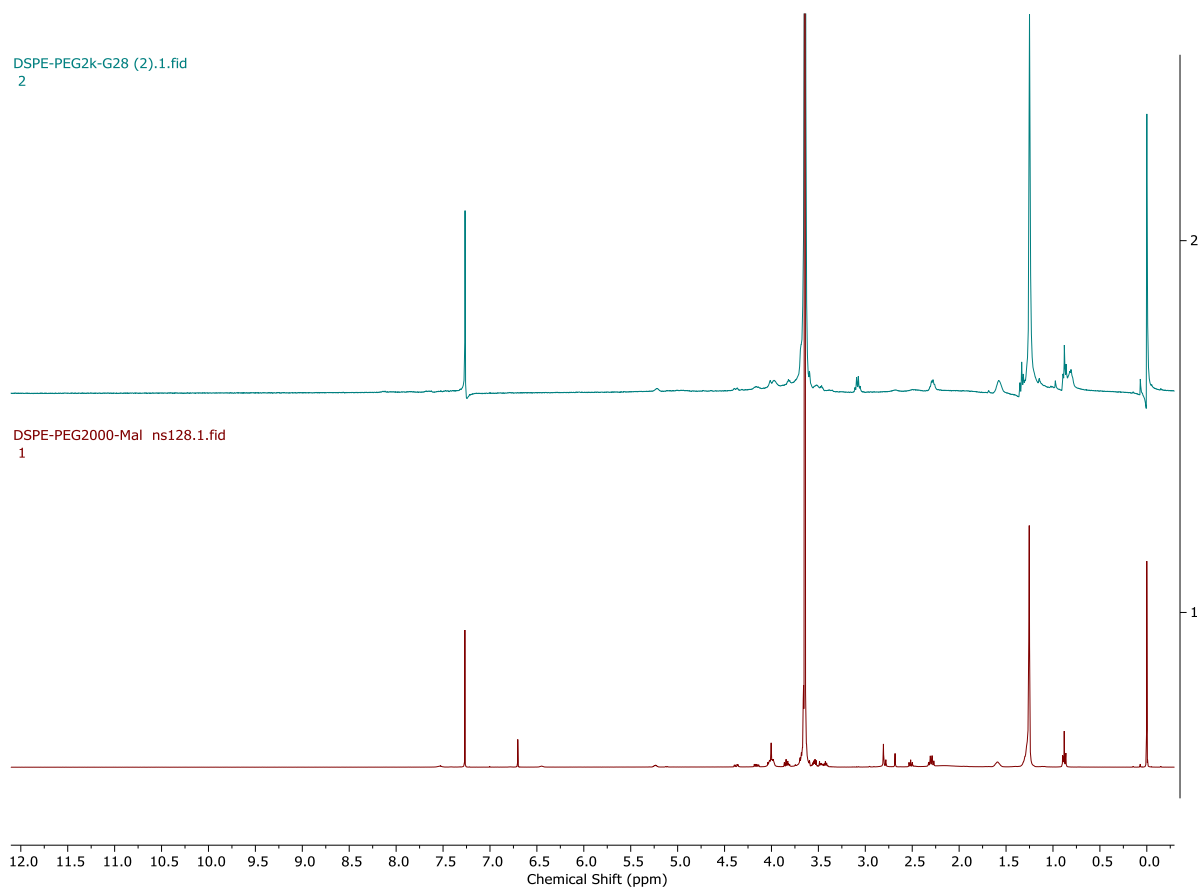


Figure 21. ^1H -NMR, 400 MHz, CDCl_3 , spectra (top) **DSPE-PEG2000-G28**, and (bottom) **DSPE-PEG2000-Mal**

Figure 22 shows the ESI-MS HR of **DSPE-G28**, and *Figure 23* shows the ^1H -NMR spectra of **DSPE-Mal** and **DSPE-G28** to confirm the disappearance of the maleimide signal at 6.7 ppm from the starting material.

Acq. Data Name: NGL project negative mode
Creation Parameters: Average(MS[1] Time:3.5700...3.8100)

Experiment Date/Time: 5/17/2023 3:23:31 PM
Ionization Mode: ESI-

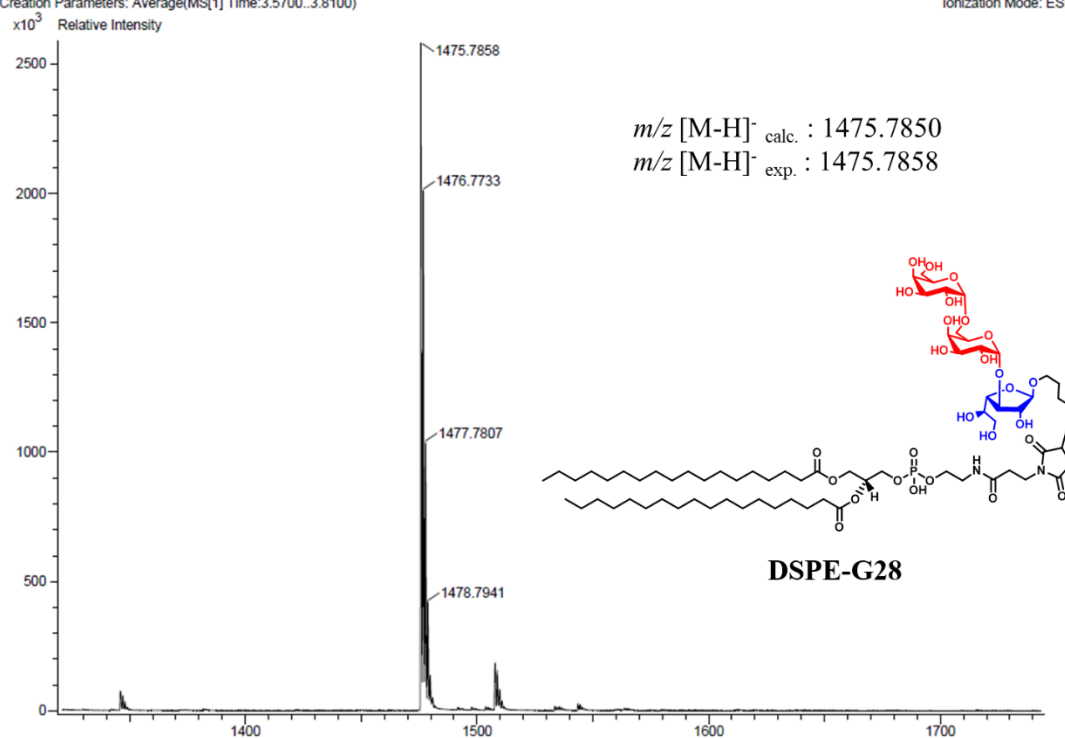


Figure 22. ESI-MS HR spectrum of **DSPE-G28**

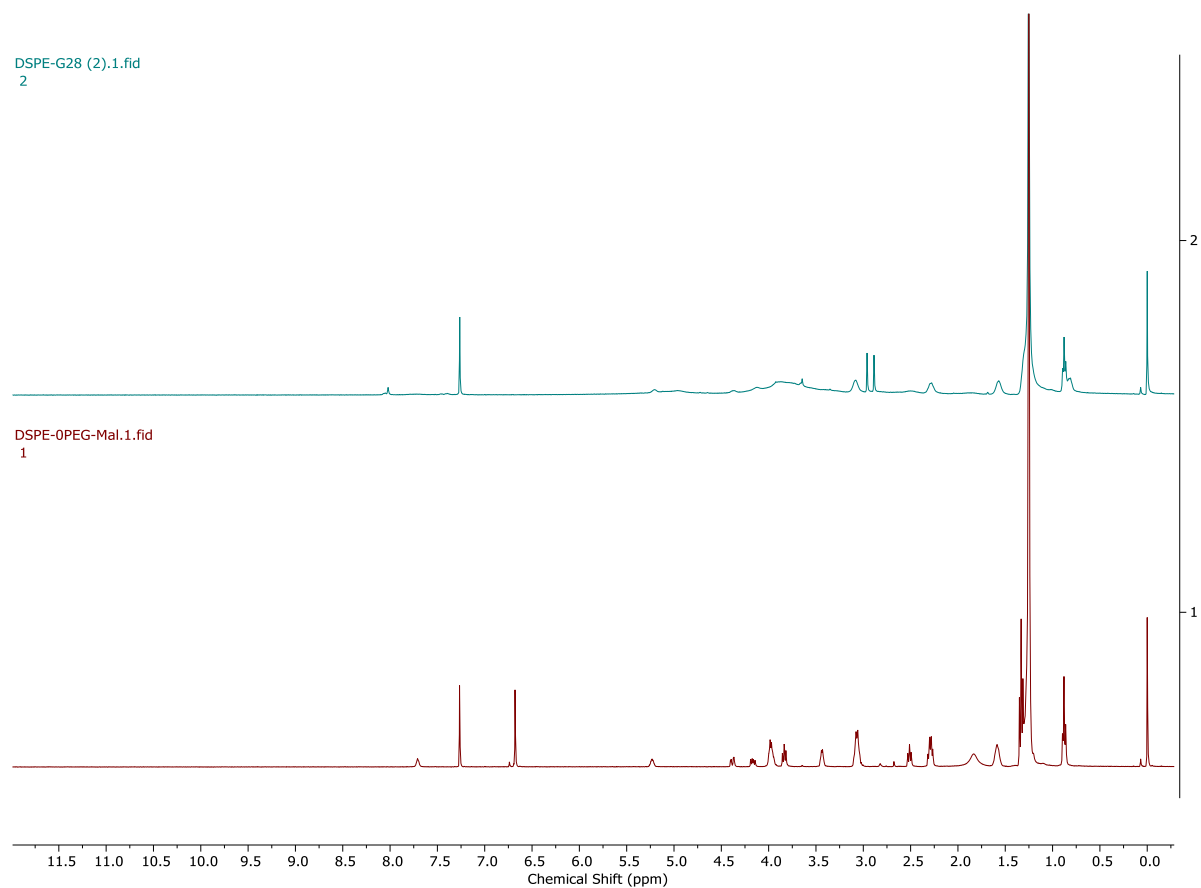


Figure 23. ^1H -NMR, 400 MHz, CDCl_3 , spectra (top) **DSPE-G28**, and (bottom) **DSPE-Mal**

Figure 24 shows the ESI-MS HR of **DSPE-4PEG-G28**, and *Figure 25* shows the ^1H -NMR spectra of **DSPE-4PEG-Mal** and **DSPE-4PEG-G28** to confirm the disappearance of the maleimide signal at 6.7 ppm from the starting material.

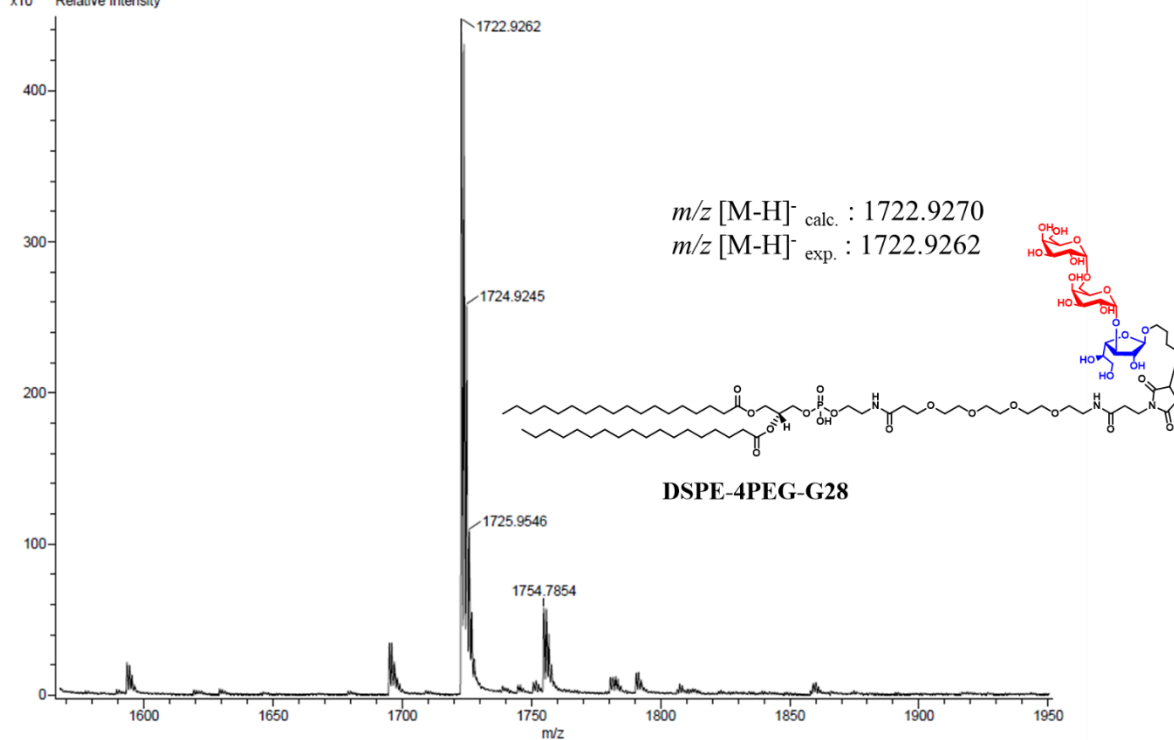


Figure 24. ESI-MS HR spectrum of **DSPE-4PEG-G28**

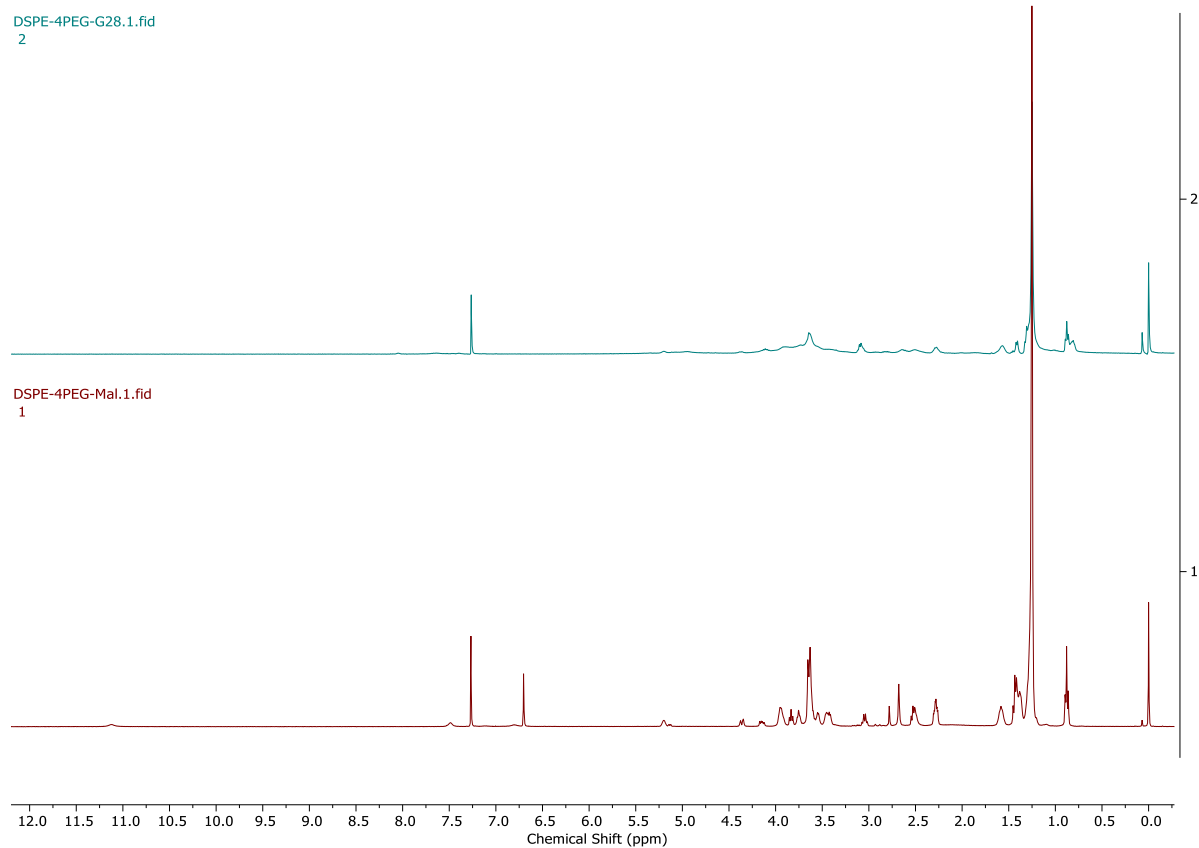


Figure 25. ^1H -NMR, 400 MHz, CDCl_3 , spectra (top) **DSPE-4PEG-G28**, and (bottom) **DSPE-4PEG-Mal**

Figure 26 shows the ^1H -NMR spectra of **DSPE-PEG3400-Mal** and **DSPE-PEG3400-G28** to confirm the disappearance of the maleimide signal at 6.7 ppm from the starting material.

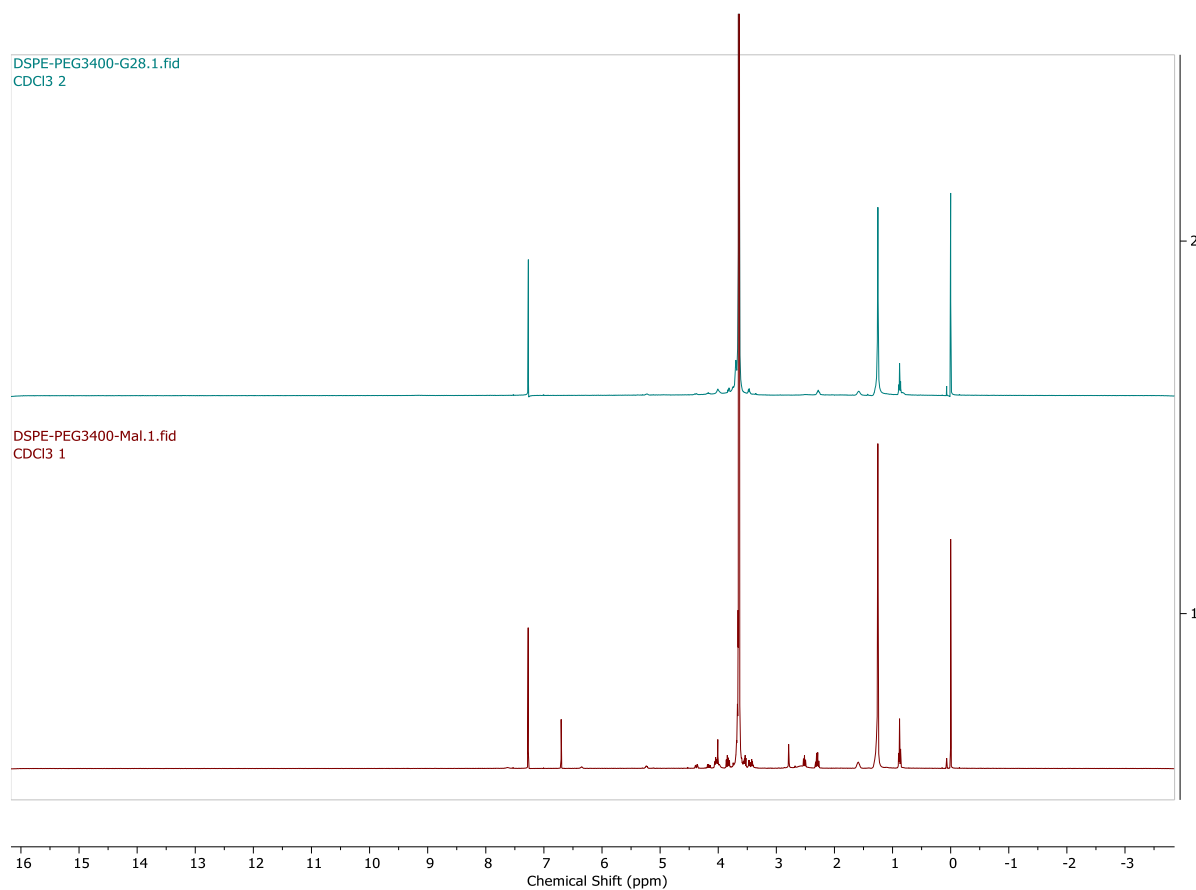


Figure 26. ¹H-NMR, 400 MHz, CDCl₃, spectra (top) **DSPE-PEG3400-G28**, and (bottom) **DSPE-PEG3400-Mal**

Our preliminary findings suggest that **DSPE-PEG2000-G28** exhibits superior performance compared to its homologs, **DSPE-G28** and **DSPE-4PEG-G28**. This observation implies that longer PEG chains may enhance solubility and improve antigen display, likely attributed to the antigen being positioned further from the plastic surface, thereby facilitating glycan-antibody binding. To determine the optimal platform, further experiments are warranted with even longer PEG spacers, such as **DSPE-PEG3400-Mal**.

2.6. CONCLUSIONS

The synthesis of the precursor *O*-allyl- β -D-galactofuranoside (**5**) was accomplished using anhydrous iron (III) chloride as a catalyst in a one-step Fischer-Lubineau glycosylation from allyl alcohol and D-galactose as starting materials. Iron salts are easily accessible, inexpensive, and abundant, and the metal itself is non-toxic; therefore, we came up with an improved procedure that is more attractive from an economic and environmental point of view than the previous one. The overall yield improved from 32% over four-step synthesis to 45% in only one step.

The thiol-ene photoaddition was improved by replacing the old radical initiator AIBN with the more efficient photocatalyst DPAP. Following the new procedure, we significantly reduced the reaction time from several hours to 30 minutes, and the yield and purity were substantially higher. This procedure has been applied to other glycans synthesized in our group (**G3_{SH}**, **G29_{SH}**, **G32_{SH}**, and **G33_{SH}**) with excellent results and high reproducibility.

Additionally, the most dramatic improvement was accomplished in the final deacylation step in the synthesis of **G27_{SH}** and **G28_{SH}**. This is significant because an inefficient last step in a multi-step synthesis is particularly devastating for the overall efficiency of the synthesis. The deprotection of acylated glycans was optimized by carefully controlling the amounts of NaOMe following a standard Zemplen deacylation procedure. We came up with a simple formula that allows us to calculate the optimized quantity of NaOMe. Following the new conditions, we were able to get the unprotected sugars in a quantitative yield.

Finally, a novel series of neoglycolipids (NGL) has been successfully synthesized through the conjugation of thiol-modified glycans to maleimide-functionalized phospholipids. This innovative method has demonstrated significant advancements over our prior neoglycoprotein (NGP) approach, particularly in enhancing their shelf stability and reducing synthesis costs.

Although promising, further investigation is required to refine and determine the optimal conditions for maximizing the efficacy of these neoglycolipids in cELISA.

2.7. ADDITIONAL PROJECT: CONJUGATION OF G28_{SH} TO CRM197 PROTEIN

In order to test a preliminary vaccine against cutaneous leishmaniasis, our group was asked to develop a conjugation protocol that would allow us to conjugate our thiol-derivatized glycans to the CRM197 protein, a non-toxic variant of diphtheria toxin.

In contrast to other frequently employed carrier proteins such as diphtheria toxoid (DT) or tetanus toxoid (TT), **CRM197** does not necessitate detoxification with formaldehyde.¹⁸⁵ This allows for the straightforward acquisition of homogeneous preparations of purified antigens. **CRM197** is a meticulously characterized protein, maintaining consistency across batches. Moreover, it holds licensure for human application in numerous effective conjugate vaccines already administered to hundreds of millions of children.¹⁸⁶⁻¹⁸⁸ Our unconjugated **CRM197** was sourced directly from its manufacturer, Fina Biosolutions.

For this project, we developed a two-step conjugation procedure. Initially, we modified some of the accessible lysine amino acids on the **CRM197** protein by attaching the heterobifunctional crosslinker Sulfo-GMBS (**Figure 27**) to install the maleimide moiety on the protein surface. Subsequently, the freshly reduced glycan, in its free thiol form, was easily linked to the carrier protein through thiol-maleimide click coupling.

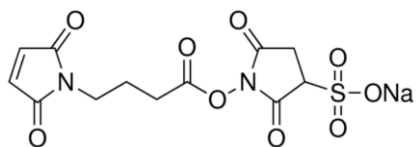


Figure 27. Chemical structure of the heterobifunctional crosslinker Sulfo-GMBS.

Derivatization of the CRM197 protein with the GMBS crosslinker to yield the maleimide derivatized CRM197-Mal. 200 μ L of commercial **CRM197** solution (10 mg/mL) were added to a microcentrifuge with Sulfo-GMBS (0.4 mg, 1:30 weight ratio) dissolved in fresh prepared HEPES Buffer 0.1 M (pH 7.2, 300 μ L). The reaction was stirred at rt for 30 min, and the

mixture was purified by Amicon Ultra-0.5 (10 kDa, 14 000x g, 15 min) five times using 1X PBS/ 5% sucrose/ 10 mM EDTA pH 6.8 buffer.

Reduction of (G28s)₂ to yield G28_{SH} and its conjugation to the maleimide derivatized CRM197-Mal to yield the neoglycoprotein CRM197-G28. Consecutively, a 0.05 M TCEP solution was prepared by diluting a neutral TCEP solution with the conjugation buffer (1X PBS/ 5% sucrose/ 10 mM EDTA buffer). 0.9 equivalents of the diluted TCEP solution were added to a 1.5 mL micro-centrifuge tube that contained disulfide (**G28s**)₂ (0.6 mg, 3.0 μmol), the final volume was adjusted to 200 μL, and the mixture was stirred on a shaker for 30 min to yield the free thiol glycan **G28_{SH}**. The conjugation was performed by adding the glycan solution into the maleimide-derivatized **CRM197-Mal** (~350 μL) solution in a glycan-to-protein ratio of 1:40, and stirring at rt for 1 h. After conjugation, the reaction mixture was diluted with 20 mM HEPES/ 10 % sucrose/ 0.005% tween 80 pH 8.0 buffer to a volume of 1 mL, filtered using an Amicon Ultra-0.5 10K centrifugal filter, and was centrifuged for 15 min at 14 000× g, rt. The mixture was washed with 0.4 mL of the same buffer three times to yield the conjugated **CRM197-G28**. The final NGPs were stored in a frozen solution in 20 Mm HEPES 10 % sucrose/ 0.005% tween 80 buffer (pH 8.0) for further use at -80°C.

To determine the glycan-to-protein ratio in the NGP **CRM197-G28**, a SHIMADZU MALDI-8020 MS was used. Samples were washed using an Amicon Ultra0.5, 3000 Da filter, and washed once with 200μL Optima grade water. Samples were spotted with 10 mg/mL sinapinic acid, 0.05% TFA. Spiked **CRM197** and **CRM197-G28** resulted in one spectral peak, in addition to **BSA+CRM197-G28**. Therefore, the instrument was calibrated with **CRM197** and **CRM197-G28** was measured immediately after. **CRM197** happened to have a mass of 58765.66 m/z; the conjugated **CRM197-G28** appeared at 63583.13 m/z. The difference between the masses

represents an average glycan-to-protein ratio of 6.5. This value is consistent with the reported values for similar approaches in the literature.¹⁸⁵ The MALDI-TOF MS measurements were accomplished by Dr. Cameron C. Ellis from Dr. Almeida's Lab and are illustrated in **Figure 28**.

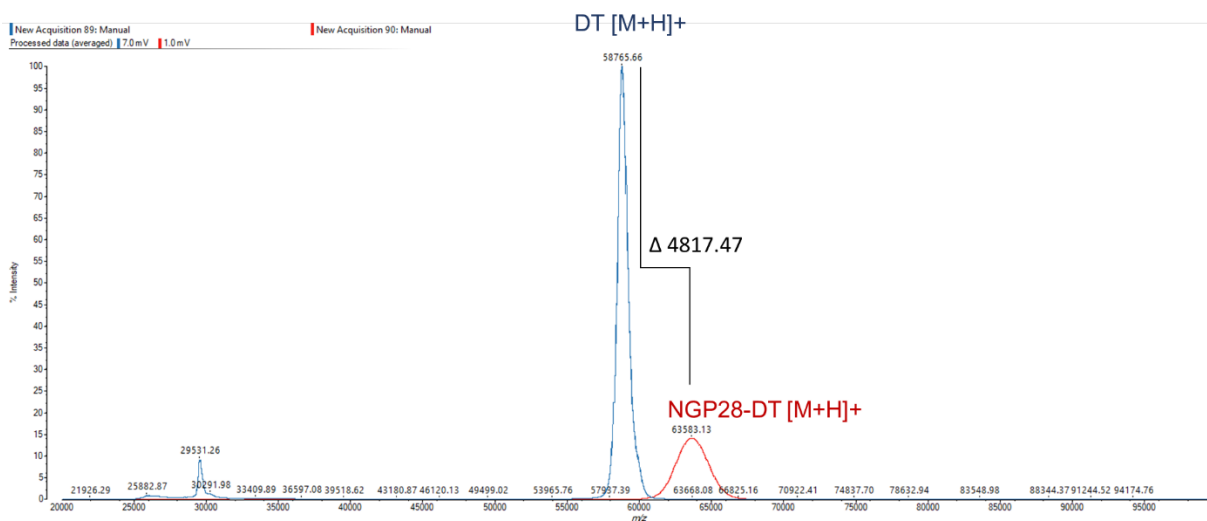


Figure 28. MALDI-TOF MS of CRM197 (blue) and CRM197-G28 (red).

REFERENCES

- (1) Sayed, N.; Allawadhi, P.; Khurana, A.; Singh, V.; Navik, U.; Pasumarthi, S. K.; Khurana, I.; Banothu, A. K.; Weiskirchen, R.; Bharani, K. K. Gene therapy: Comprehensive overview and therapeutic applications. *Life Sci* **2022**, *294*, 120375.
- (2) Polack, F. P.; Thomas, S. J.; Kitchin, N.; Absalon, J.; Gurtman, A.; Lockhart, S.; Perez, J. L.; Pérez Marc, G.; Moreira, E. D.; Zerbini, C.; et al. Safety and Efficacy of the BNT162b2 mRNA Covid-19 Vaccine. *N Engl J Med* **2020**, *383* (27), 2603-2615. From NLM.
- (3) Baden, L. R.; El Sahly, H. M.; Essink, B.; Kotloff, K.; Frey, S.; Novak, R.; Diemert, D.; Spector, S. A.; Rouphael, N.; Creech, C. B.; et al. Efficacy and Safety of the mRNA-1273 SARS-CoV-2 Vaccine. *N Engl J Med* **2021**, *384* (5), 403-416. From NLM.
- (4) Kirtane, A. R.; Verma, M.; Karandikar, P.; Furin, J.; Langer, R.; Traverso, G. Nanotechnology approaches for global infectious diseases. *Nat Nanotechnol* **2021**, *16* (4), 369-384. From NLM.
- (5) Huang, X.; Kon, E.; Han, X.; Zhang, X.; Kong, N.; Mitchell, M. J.; Peer, D.; Tao, W. Nanotechnology-based strategies against SARS-CoV-2 variants. *Nat Nanotechnol* **2022**, *17* (10), 1027-1037. From NLM.
- (6) Chavda, V. P.; Pandya, R.; Apostolopoulos, V. DNA vaccines for SARS-CoV-2: toward third-generation vaccination era. *Expert Rev Vaccines* **2021**, *20* (12), 1549-1560. From NLM.
- (7) Mallapaty, S. India's DNA COVID vaccine is a world first - more are coming. *Nature* **2021**, *597* (7875), 161-162. From NLM.
- (8) Schlosser, K.; Li, Y. Biologically inspired synthetic enzymes made from DNA. *Chem Biol* **2009**, *16* (3), 311-322.

- (9) Guimaraes, L. C.; Costa, P. A. C.; Scalzo Júnior, S. R. A.; Ferreira, H. A. S.; Braga, A. C. S.; de Oliveira, L. C.; Figueiredo, M. M.; Shepherd, S.; Hamilton, A.; Queiroz-Junior, C. M.; et al. Nanoparticle-based DNA vaccine protects against SARS-CoV-2 variants in female preclinical models. *Nat Commun* **2024**, *15* (1), 590. From NLM.
- (10) Huang, K.; Zapata, D.; Tang, Y.; Teng, Y.; Li, Y. In vivo delivery of CRISPR-Cas9 genome editing components for therapeutic applications. *Biomaterials* **2022**, *291*, 121876. From NLM.
- (11) Dilliard, S. A.; Cheng, Q.; Siegwart, D. J. On the mechanism of tissue-specific mRNA delivery by selective organ targeting nanoparticles. *Proc Natl Acad Sci U S A* **2021**, *118* (52), e2109256118.
- (12) Wang, X.; Liu, S.; Sun, Y.; Yu, X.; Lee, S. M.; Cheng, Q.; Wei, T.; Gong, J.; Robinson, J.; Zhang, D. Preparation of selective organ-targeting (SORT) lipid nanoparticles (LNPs) using multiple technical methods for tissue-specific mRNA delivery. *Nat Protoc* **2023**, *18* (1), 265-291.
- (13) Kularatne, R. N.; Crist, R. M.; Stern, S. T. The future of tissue-targeted lipid nanoparticle-mediated nucleic acid delivery. *Pharmaceuticals (Basel)* **2022**, *15* (7), 897.
- (14) Daniels, T. R.; Bernabeu, E.; Rodríguez, J. A.; Patel, S.; Kozman, M.; Chiappetta, D. A.; Holler, E.; Ljubimova, J. Y.; Helguera, G.; Penichet, M. L. The transferrin receptor and the targeted delivery of therapeutic agents against cancer. *Biochim Biophys Acta* **2012**, *1820* (3), 291-317.
- (15) Daniels, T. R.; Delgado, T.; Rodriguez, J. A.; Helguera, G.; Penichet, M. L. The transferrin receptor part I: Biology and targeting with cytotoxic antibodies for the treatment of cancer. *Clin Immunol* **2006**, *121* (2), 144-158.

- (16) Dong, X. Current strategies for brain drug delivery. *Theranostics* **2018**, 8 (6), 1481.
- (17) Ulbrich, K.; Hekmatara, T.; Herbert, E.; Kreuter, J. Transferrin-and transferrin-receptor-antibody-modified nanoparticles enable drug delivery across the blood–brain barrier (BBB). *Eur J Pharm Biopharm* **2009**, 71 (2), 251-256.
- (18) Tang, J.; Wang, Q.; Yu, Q.; Qiu, Y.; Mei, L.; Wan, D.; Wang, X.; Li, M.; He, Q. A stabilized retro-inverso peptide ligand of transferrin receptor for enhanced liposome-based hepatocellular carcinoma-targeted drug delivery. *Acta Biomater* **2019**, 83, 379-389.
- (19) Society, A. C. *American Cancer Society. Facts & Figures 2024*. American Cancer Society, 2024. <https://www.cancer.org/cancer/types/melanoma-skin-cancer/about/key-statistics.html> (accessed 2024 04/15/2024).
- (20) Hamid, O.; Robert, C.; Daud, A.; Hodi, F. S.; Hwu, W. J.; Kefford, R.; Wolchok, J. D.; Hersey, P.; Joseph, R.; Weber, J. S.; et al. Five-year survival outcomes for patients with advanced melanoma treated with pembrolizumab in KEYNOTE-001. *Ann Oncol* **2019**, 30 (4), 582-588. DOI: 10.1093/annonc/mdz011 From NLM.
- (21) Soiffer, R.; Lynch, T.; Mihm, M.; Jung, K.; Rhuda, C.; Schmollinger, J. C.; Hodi, F. S.; Liebster, L.; Lam, P.; Mentzer, S.; et al. Vaccination with irradiated autologous melanoma cells engineered to secrete human granulocyte-macrophage colony-stimulating factor generates potent antitumor immunity in patients with metastatic melanoma. *Proc Natl Acad Sci U S A* **1998**, 95 (22), 13141-13146. DOI: 10.1073/pnas.95.22.13141 From NLM.
- (22) Soiffer, R.; Hodi, F. S.; Haluska, F.; Jung, K.; Gillessen, S.; Singer, S.; Tanabe, K.; Duda, R.; Mentzer, S.; Jaklitsch, M.; et al. Vaccination with irradiated, autologous melanoma cells engineered to secrete granulocyte-macrophage colony-stimulating factor by adenoviral-

- mediated gene transfer augments antitumor immunity in patients with metastatic melanoma. *J Clin Oncol* **2003**, 21 (17), 3343-3350. DOI: 10.1200/jco.2003.07.005 From NLM.
- (23) Rossi, G. R.; Mautino, M. R.; Unfer, R. C.; Seregina, T. M.; Vahanian, N.; Link, C. J. Effective treatment of preexisting melanoma with whole cell vaccines expressing alpha(1,3)-galactosyl epitopes. *Cancer Res* **2005**, 65 (22), 10555-10561. DOI: 10.1158/0008-5472.Can-05-0627 From NLM.
- (24) Galili, U.; Wigglesworth, K.; Abdel-Motal, U. M. Intratumoral injection of alpha-gal glycolipids induces xenograft-like destruction and conversion of lesions into endogenous vaccines. *J Immunol* **2007**, 178 (7), 4676-4687. DOI: 10.4049/jimmunol.178.7.4676 From NLM.
- (25) Albertini, M. R.; Ranheim, E. A.; Zuleger, C. L.; Sondel, P. M.; Hank, J. A.; Bridges, A.; Newton, M. A.; McFarland, T.; Collins, J.; Clements, E.; et al. Phase I study to evaluate toxicity and feasibility of intratumoral injection of α -gal glycolipids in patients with advanced melanoma. *Cancer Immunol Immunother* **2016**, 65 (8), 897-907. DOI: 10.1007/s00262-016-1846-1 From NLM.
- (26) Deriy, L.; Ogawa, H.; Gao, G. P.; Galili, U. In vivo targeting of vaccinating tumor cells to antigen-presenting cells by a gene therapy method with adenovirus containing the alpha1,3galactosyltransferase gene. *Cancer Gene Ther* **2005**, 12 (6), 528-539. DOI: 10.1038/sj.cgt.7700812 From NLM.
- (27) Galili, U. Autologous tumor vaccines processed to express alpha-gal epitopes: a practical approach to immunotherapy in cancer. *Cancer Immunol Immunother* **2004**, 53 (11), 935-945. DOI: 10.1007/s00262-004-0524-x.

- (28) Furukawa, K.; Tanemura, M.; Miyoshi, E.; Eguchi, H.; Nagano, H.; Matsunami, K.; Nagaoka, S.; Yamada, D.; Asaoka, T.; Noda, T.; et al. A practical approach to pancreatic cancer immunotherapy using resected tumor lysate vaccines processed to express α -gal epitopes. *PLoS One* **2017**, *12* (10), e0184901. DOI: 10.1371/journal.pone.0184901 From NLM.
- (29) Whalen, G. F.; Sullivan, M.; Piperdi, B.; Wasseff, W.; Galili, U. Cancer immunotherapy by intratumoral injection of α -gal glycolipids. *Anticancer Res* **2012**, *32* (9), 3861-3868. From NLM.
- (30) Galili, U. Interaction of the natural anti-Gal antibody with alpha-galactosyl epitopes: a major obstacle for xenotransplantation in humans. *Immunol. Today* **1993**, *14*, 480-482. DOI: 10.1016/0167-5699(93)90261-i.
- (31) Galili, U. *The Natural Anti-Gal Antibody As Foe Turned Friend In Medicine*; Elsevier Academic Press, 2018. DOI: 1016/B978-0-12-813362-0.00001-4.
- (32) Sheridan, R. T. C.; Hudon, J.; Hank, J. A.; Sondel, P. M.; Kiessling, L. L. Rhamnose Glycoconjugates for the Recruitment of Endogenous Anti-carbohydrate Antibodies to Tumor Cells. *Chembiochem*. **2014**, *15* (10), 1393-1398. DOI: 10.1002/cbic.201402019.
- (33) Carlson, C. B.; Mowery, P.; Owen, R. M.; Dykhuizen, E. C.; Kiessling, L. L. Selective Tumor Cell Targeting Using Low-Affinity, Multivalent Interactions. *ACS Chem. Biol.* **2007**, *2* (2), 119-127.
- (34) Sianturi, J.; Manabe, Y.; Li, H.-S.; Chiu, L.-T.; Chang, T.-C.; Tokunaga, K.; Kabayama, K.; Tanemura, M.; Takamatsu, S.; Miyoshi, E.; et al. Development of α -Gal–Antibody Conjugates to Increase Immune Response by Recruiting Natural Antibodies. *Angew. Chem. Int. Ed. Engl.* **2019**, *58* (14), 4526-4530. DOI: 10.1002/anie.201812914.

- (35) Harrington, D.; Steuben, F.; Lenahan, C. Chagas Disease in the United States: A Growing Public Health Concern. *Clinical Advisor* **July 18, 2018**.
- (36) Bulcha, J. T.; Wang, Y.; Ma, H.; Tai, P. W.; Gao, G. Viral vector platforms within the gene therapy landscape. *Signal Transduct Target Ther* **2021**, 6 (1), 53.
- (37) Frangoul, H.; Altshuler, D.; Cappellini, M. D.; Chen, Y.-S.; Domm, J.; Eustace, B. K.; Foell, J.; de la Fuente, J.; Grupp, S.; Handgretinger, R. CRISPR-Cas9 gene editing for sickle cell disease and β -thalassemia. *N Engl J Med* **2021**, 384 (3), 252-260.
- (38) Butt, M. H.; Zaman, M.; Ahmad, A.; Khan, R.; Mallhi, T. H.; Hasan, M. M.; Khan, Y. H.; Hafeez, S.; Massoud, E. E. S.; Rahman, M. H. Appraisal for the potential of viral and nonviral vectors in gene therapy: A review. *Genes (Basel)* **2022**, 13 (8), 1370.
- (39) Kotterman, M. A.; Schaffer, D. V. Engineering adeno-associated viruses for clinical gene therapy. *Nat Rev Genet* **2014**, 15 (7), 445-451.
- (40) Fu, Q.; Polanco, A.; Lee, Y. S.; Yoon, S. Critical challenges and advances in recombinant adeno-associated virus (rAAV) biomanufacturing. *Biotechnol Bioeng* **2023**, 120 (9), 2601-2621. From NLM.
- (41) Song, C.-Q.; Jiang, T.; Richter, M.; Rhym, L. H.; Koblan, L. W.; Zafra, M. P.; Schatoff, E. M.; Doman, J. L.; Cao, Y.; Dow, L. E. Adenine base editing in an adult mouse model of tyrosinaemia. *Nat Biomed Eng* **2020**, 4 (1), 125-130.
- (42) Fu, Q.; Polanco, A.; Lee, Y. S.; Yoon, S. Critical challenges and advances in recombinant adeno-associated virus (rAAV) biomanufacturing. *Biotechnol Bioeng* **2023**.
- (43) Raimondo, T. M.; Reed, K.; Shi, D.; Langer, R.; Anderson, D. G. Delivering the next generation of cancer immunotherapies with RNA. *Cell* **2023**, 186 (8), 1535-1540.

- (44) Menon, I.; Zaroudi, M.; Zhang, Y.; Aisenbrey, E.; Hui, L. Fabrication of active targeting lipid nanoparticles: Challenges and perspectives. *Mater Today Adv* **2022**, *16*, 100299.
- (45) Kulkarni, J. A.; Myhre, J. L.; Chen, S.; Tam, Y. Y. C.; Danescu, A.; Richman, J. M.; Cullis, P. R. Design of lipid nanoparticles for in vitro and in vivo delivery of plasmid DNA. *Nanomedicine* **2017**, *13* (4), 1377-1387.
- (46) Algarni, A.; Pilkington, E. H.; Suys, E. J.; Al-Wassiti, H.; Pouton, C. W.; Truong, N. P. In vivo delivery of plasmid DNA by lipid nanoparticles: the influence of ionizable cationic lipids on organ-selective gene expression. *Biomater Sci* **2022**, *10* (11), 2940-2952.
- (47) Li, Y.; Breaker, R. R. Kinetics of RNA Degradation by Specific Base Catalysis of Transesterification Involving the 2'-Hydroxyl Group. *J Am Chem Soc* **1999**, *121* (23), 5364-5372.
- (48) Wang, S.; Zhang, J.; Zhou, H.; Lu, Y. C.; Jin, X.; Luo, L.; You, J. The role of protein corona on nanodrugs for organ-targeting and its prospects of application. *J Control Release* **2023**, *360*, 15-43.
- (49) Nakamura, T.; Kawai, M.; Sato, Y.; Maeki, M.; Tokeshi, M.; Harashima, H. The effect of size and charge of lipid nanoparticles prepared by microfluidic mixing on their lymph node transitivity and distribution. *Mol Pharm* **2020**, *17* (3), 944-953.
- (50) Cheng, Q.; Wei, T.; Farbiak, L.; Johnson, L. T.; Dilliard, S. A.; Siegwart, D. J. Selective organ targeting (SORT) nanoparticles for tissue-specific mRNA delivery and CRISPR–Cas gene editing. *Nat Nanotechnol* **2020**, *15* (4), 313-320.
- (51) Kimura, S.; Khalil, I. A.; Elewa, Y. H.; Harashima, H. Novel lipid combination for delivery of plasmid DNA to immune cells in the spleen. *J Control Release* **2021**, *330*, 753-764.

- (52) Li, Q.; Chan, C.; Peterson, N.; Hanna, R. N.; Alfaro, A.; Allen, K. L.; Wu, H.; Dall'Acqua, W. F.; Borrok, M. J.; Santos, J. L. Engineering caveolae-targeted lipid nanoparticles to deliver mRNA to the lungs. *ACS Chem Biol* **2020**, *15* (4), 830-836.
- (53) Kedmi, R.; Veiga, N.; Ramishetti, S.; Goldsmith, M.; Rosenblum, D.; Dammes, N.; Hazan-Halevy, I.; Nahary, L.; Leviatan-Ben-Arye, S.; Harlev, M. A modular platform for targeted RNAi therapeutics. *Nat Nanotechnol* **2018**, *13* (3), 214-219.
- (54) Rosenblum, D.; Gutkin, A.; Kedmi, R.; Ramishetti, S.; Veiga, N.; Jacobi, A. M.; Schubert, M. S.; Friedmann-Morvinski, D.; Cohen, Z. R.; Behlke, M. A. CRISPR-Cas9 genome editing using targeted lipid nanoparticles for cancer therapy. *Sci Adv* **2020**, *6* (47), eabc9450.
- (55) Kim, M.; Jeong, M.; Hur, S.; Cho, Y.; Park, J.; Jung, H.; Seo, Y.; Woo, H.; Nam, K.; Lee, K. Engineered ionizable lipid nanoparticles for targeted delivery of RNA therapeutics into different types of cells in the liver. *Sci Adv* **2021**, *7* (9), eabf4398.
- (56) Gomme, P. T.; McCann, K. B.; Bertolini, J. Transferrin: structure, function and potential therapeutic actions. *Drug Discov Today* **2005**, *10* (4), 267-273.
- (57) Mojarad-Jabali, S.; Mahdinloo, S.; Farshbaf, M.; Sarfraz, M.; Fatahi, Y.; Atyabi, F.; Valizadeh, H. Transferrin receptor-mediated liposomal drug delivery: Recent trends in targeted therapy of cancer. *Expert Opin Drug Deliv* **2022**, *19* (6), 685-705.
- (58) Anderson, G. J.; Vulpe, C. D. Mammalian iron transport. *Cell Mol Life Sci* **2009**, *66*, 3241-3261.
- (59) Smith, G. P.; Petrenko, V. A. Phage Display. *Chem Rev* **1997**, *97* (2), 391-410.
- (60) Lee, J. H.; Engler, J. A.; Collawn, J. F.; Moore, B. A. Receptor mediated uptake of peptides that bind the human transferrin receptor. *Eur J Biochem* **2001**, *268* (7), 2004-2012.

- (61) Liu, D.-z.; Cheng, Y.; Cai, R.-q.; Wang, W.-w.; Cui, H.; Liu, M.; Mei, Q.-b.; Zhou, S.-y. The enhancement of siPLK1 penetration across BBB and its anti glioblastoma activity in vivo by magnet and transferrin co-modified nanoparticle. *Nanomedicine* **2018**, *14* (3), 991-1003.
- (62) Zhang, S.; Sun, Q.; Peng, X.; Gan, N.; Zhao, L.; Suo, Z.; Zhao, G.; Li, H. A pH-sensitive T7 peptide-decorated liposome system for HER2 inhibitor extracellular delivery: an application for the efficient suppression of HER2+ breast cancer. *J Mater Chem B* **2021**, *9* (42), 8768-8778.
- (63) Guichard, G.; Benkirane, N.; Zeder-Lutz, G.; Van Regenmortel, M.; Briand, J.-P.; Muller, S. Antigenic mimicry of natural L-peptides with retro-inverso-peptidomimetics. *Proc Natl Acad Sci U S A* **1994**, *91* (21), 9765-9769.
- (64) Patra, J. K.; Das, G.; Fraceto, L. F.; Campos, E. V. R.; Rodriguez-Torres, M. d. P.; Acosta-Torres, L. S.; Diaz-Torres, L. A.; Grillo, R.; Swamy, M. K.; Sharma, S. Nano based drug delivery systems: recent developments and future prospects. *J Nanobiotechnology* **2018**, *16* (1), 1-33.
- (65) Mendonça, M. C.; Kont, A.; Kowalski, P. S.; O'Driscoll, C. M. Design of lipid-based nanoparticles for delivery of therapeutic nucleic acids. *Drug Discov Today* **2023**, 103505.
- (66) Witzigmann, D.; Kulkarni, J. A.; Leung, J.; Chen, S.; Cullis, P. R.; van der Meel, R. Lipid nanoparticle technology for therapeutic gene regulation in the liver. *Adv Drug Deliv Rev* **2020**, *159*, 344-363.
- (67) Poon, W.; Zhang, Y.-N.; Ouyang, B.; Kingston, B. R.; Wu, J. L.; Wilhelm, S.; Chan, W. C. Elimination pathways of nanoparticles. *ACS Nano* **2019**, *13* (5), 5785-5798.

- (68) Tilstra, G.; Couture-Sen cal, J.; Lau, Y. M. A.; Manning, A. M.; Wong, D. S.; Janaeska, W. W.; Wuraola, T. A.; Pang, J.; Khan, O. F. Iterative Design of Ionizable Lipids for Intramuscular mRNA Delivery. *J Am Chem Soc* **2023**, *145* (4), 2294-2304.
- (69) Tenchov, R.; Bird, R.; Curtze, A. E.; Zhou, Q. Lipid nanoparticles— from liposomes to mRNA vaccine delivery, a landscape of research diversity and advancement. *ACS Nano* **2021**, *15* (11), 16982-17015.
- (70) Dhiman, N.; Awasthi, R.; Sharma, B.; Kharkwal, H.; Kulkarni, G. T. Lipid nanoparticles as carriers for bioactive delivery. *Front Chem* **2021**, *9*, 580118.
- (71) Kalita, T.; Dezfouli, S. A.; Pandey, L. M.; Uludag, H. siRNA functionalized lipid nanoparticles (LNPs) in management of diseases. *Pharmaceutics* **2022**, *14* (11), 2520.
- (72) Roces, C. B.; Lou, G.; Jain, N.; Abraham, S.; Thomas, A.; Halbert, G. W.; Perrie, Y. Manufacturing considerations for the development of lipid nanoparticles using microfluidics. *Pharmaceutics* **2020**, *12* (11), 1095.
- (73) Judge, A. D.; Robbins, M.; Tavakoli, I.; Levi, J.; Hu, L.; Fronda, A.; Ambegia, E.; McClintock, K.; MacLachlan, I. Confirming the RNAi-mediated mechanism of action of siRNA-based cancer therapeutics in mice. *J Clin Invest* **2009**, *119* (3), 661-673.
- (74) Gomes-da-Silva, L. C.; Fonseca, N. A.; Moura, V.; Pedroso de Lima, M. C.; Sim es, S.; Moreira, J. N. Lipid-based nanoparticles for siRNA delivery in cancer therapy: paradigms and challenges. *Acc Chem Res* **2012**, *45* (7), 1163-1171.
- (75) Zalba, S.; Ten Hagen, T. L. M.; Burgui, C.; Garrido, M. J. Stealth nanoparticles in oncology: Facing the PEG dilemma. *J Control Release* **2022**, *351*, 22-36. From NLM.
- (76) Rohner, E.; Yang, R.; Foo, K. S.; Goedel, A.; Chien, K. R. Unlocking the promise of mRNA therapeutics. *Nat Biotechnol* **2022**, *40* (11), 1586-1600. From NLM.

- (77) Zhu, Y.; Shen, R.; Vuong, I.; Reynolds, R. A.; Shears, M. J.; Yao, Z.-C.; Hu, Y.; Cho, W. J.; Kong, J.; Reddy, S. K. Multi-step screening of DNA/lipid nanoparticles and co-delivery with siRNA to enhance and prolong gene expression. *Nat Commun* **2022**, *13* (1), 4282.
- (78) Campbell, B. C.; Nabel, E. M.; Murdock, M. H.; Lao-Peregrin, C.; Tsoulfas, P.; Blackmore, M. G.; Lee, F. S.; Liston, C.; Morishita, H.; Petsko, G. A. mGreenLantern: a bright monomeric fluorescent protein with rapid expression and cell filling properties for neuronal imaging. *Proc Natl Acad Sci U S A* **2020**, *117* (48), 30710-30721.
- (79) McGraw, T. E.; Greenfield, L.; Maxfield, F. R. Functional expression of the human transferrin receptor cDNA in Chinese hamster ovary cells deficient in endogenous transferrin receptor. *J Cell Biol* **1987**, *105* (1), 207-214.
- (80) Rodríguez, J. A.; Helguera, G.; Daniels, T. R.; Neacato, I. I.; López-Valdés, H. E.; Charles, A. C.; Penichet, M. L. Binding specificity and internalization properties of an antibody–avidin fusion protein targeting the human transferrin receptor. *J Control Release* **2007**, *124* (1-2), 35-42.
- (81) Zhang, H.; You, X.; Wang, X.; Cui, L.; Wang, Z.; Xu, F.; Li, M.; Yang, Z.; Liu, J.; Huang, P. Delivery of mRNA vaccine with a lipid-like material potentiates antitumor efficacy through Toll-like receptor 4 signaling. *Proc Natl Acad Sci U S A* **2021**, *118* (6), e2005191118.
- (82) Templeton, N. S.; Lasic, D. D.; Frederik, P. M.; Strey, H. H.; Roberts, D. D.; Pavlakis, G. N. Improved DNA: liposome complexes for increased systemic delivery and gene expression. *Nat Biotechnol* **1997**, *15* (7), 647-652.
- (83) Jayaraman, M.; Ansell, S. M.; Mui, B. L.; Tam, Y. K.; Chen, J.; Du, X.; Butler, D.; Eltepu, L.; Matsuda, S.; Narayanannair, J. K. Maximizing the potency of siRNA lipid nanoparticles for hepatic gene silencing in vivo. *Angew Chem Int Ed Engl* **2012**, *124* (34), 8657-8661.

- (84) Akinc, A.; Maier, M. A.; Manoharan, M.; Fitzgerald, K.; Jayaraman, M.; Barros, S.; Ansell, S.; Du, X.; Hope, M. J.; Madden, T. D. The Onpattro story and the clinical translation of nanomedicines containing nucleic acid-based drugs. *Nat Nanotechnol* **2019**, *14* (12), 1084-1087.
- (85) Adams, D.; Gonzalez-Duarte, A.; O’Riordan, W. D.; Yang, C.-C.; Ueda, M.; Kristen, A. V.; Tournev, I.; Schmidt, H. H.; Coelho, T.; Berk, J. L. Patisiran, an RNAi therapeutic, for hereditary transthyretin amyloidosis. *N Engl J Med* **2018**, *379* (1), 11-21.
- (86) Patel, S.; Ashwanikumar, N.; Robinson, E.; Xia, Y.; Mihai, C.; Griffith III, J. P.; Hou, S.; Esposito, A. A.; Ketova, T.; Welsher, K. Naturally-occurring cholesterol analogues in lipid nanoparticles induce polymorphic shape and enhance intracellular delivery of mRNA. *Nat Commun* **2020**, *11* (1), 983.
- (87) Cheng, X.; Lee, R. J. The role of helper lipids in lipid nanoparticles (LNPs) designed for oligonucleotide delivery. *Adv Drug Deliv Rev* **2016**, *99*, 129-137.
- (88) Tenchov, R.; Sasso, J. M.; Zhou, Q. A. PEGylated Lipid Nanoparticle Formulations: Immunological Safety and Efficiency Perspective. *Bioconjug Chem* **2023**, *34* (6), 941-960. From NLM.
- (89) Harris, J. M.; Martin, N. E.; Modi, M. Pegylation: a novel process for modifying pharmacokinetics. *Clin Pharmacokinet* **2001**, *40*, 539-551.
- (90) Kulkarni, J. A.; Darjuan, M. M.; Mercer, J. E.; Chen, S.; Van Der Meel, R.; Thewalt, J. L.; Tam, Y. Y. C.; Cullis, P. R. On the formation and morphology of lipid nanoparticles containing ionizable cationic lipids and siRNA. *ACS Nano* **2018**, *12* (5), 4787-4795.
- (91) Whitfield, R.; Anastasaki, A.; Truong, N. P.; Cook, A. B.; Omedes-Pujol, M.; Loczenski Rose, V.; Nguyen, T. A.; Burns, J. A.; Perrier, S.; Davis, T. P. Efficient binding, protection,

- and self-release of dsrna in soil by linear and star cationic polymers. *ACS Macro Lett* **2018**, 7 (8), 909-915.
- (92) Crawford, R.; Dogdas, B.; Keough, E.; Haas, R. M.; Wepukhulu, W.; Krotzer, S.; Burke, P. A.; Sepp-Lorenzino, L.; Bagchi, A.; Howell, B. J. Analysis of lipid nanoparticles by Cryo-EM for characterizing siRNA delivery vehicles. *Int J Pharm* **2011**, 403 (1-2), 237-244.
- (93) Edwards, K. A.; Baeumner, A. J. Analysis of liposomes. *Talanta* **2006**, 68 (5), 1432-1441.
- (94) Ingebrigtsen, L.; Brandl, M. Determination of the size distribution of liposomes by SEC fractionation, and PCS analysis and enzymatic assay of lipid content. *AAPS PharmSciTech* **2002**, 3, 9-15.
- (95) Chazotte, B. Labeling nuclear DNA with hoechst 33342. *Cold Spring Harb Protoc* **2011**, 2011 (1), pdb prot5557.
- (96) Lai, T.-Y.; Cao, J.; Ou-Yang, P.; Tsai, C.-Y.; Lin, C.-W.; Chen, C.-C.; Tsai, M.-K.; Lee, C.-Y. Different methods of detaching adherent cells and their effects on the cell surface expression of Fas receptor and Fas ligand. *Sci Rep* **2022**, 12 (1), 5713.
- (97) Cui, L.; Renzi, S.; Quagliarini, E.; Digiacomo, L.; Amenitsch, H.; Masuelli, L.; Bei, R.; Ferri, G.; Cardarelli, F.; Wang, J. Efficient delivery of DNA using lipid nanoparticles. *Pharmaceutics* **2022**, 14 (8), 1698.
- (98) Prazeres, P. H. D. M.; Ferreira, H.; Costa, P. A. C.; da Silva, W.; Alves, M. T.; Padilla, M.; Thatte, A.; Santos, A. K.; Lobo, A. O.; Sabino, A. Delivery of Plasmid DNA by Ionizable Lipid Nanoparticles to Induce CAR Expression in T Cells. *Int J Nanomedicine* **2023**, 5891-5904.

- (99) Huang, R.-Q.; Qu, Y.-H.; Ke, W.-L.; Zhu, J.-H.; Pei, Y.-Y.; Jiang, C. Efficient gene delivery targeted to the brain using a transferrin-conjugated polyethyleneglycol-modified polyamidoamine dendrimer. *FASEB J* **2007**, *21* (4), 1117-1125.
- (100) Yu, M.; Su, D.; Yang, Y.; Qin, L.; Hu, C.; Liu, R.; Zhou, Y.; Yang, C.; Yang, X.; Wang, G. D-T7 peptide-modified PEGylated bilirubin nanoparticles loaded with cediranib and paclitaxel for antiangiogenesis and chemotherapy of glioma. *ACS Appl Mater Interfaces* **2018**, *11* (1), 176-186.
- (101) Khamisi, J.; Ashmus, R. A.; Schocker, N. S.; Michael, K. A high-yielding synthesis of allyl glycosides from peracetylated glycosyl donors. *Carbohydr Res* **2012**, *357*, 147-150. From NLM.
- (102) Ashmus, R. A.; Schocker, N. S.; Cordero-Mendoza, Y.; Marques, A. F.; Monroy, E. Y.; Pardo, A.; Izquierdo, L.; Gállego, M.; Gascon, J.; Almeida, I. C.; et al. Potential use of synthetic α -galactosyl-containing glycotopes of the parasite *Trypanosoma cruzi* as diagnostic antigens for Chagas disease. *Org Biomol Chem* **2013**, *11* (34), 5579-5583. From NLM.
- (103) Schocker, N. S.; Portillo, S.; Ashmus, R. A.; Brito, C. R.; Silva, I. E.; Mendoza, Y. C.; Marques, A. F.; Monroy, E. Y.; Pardo, A.; Izquierdo, L. *Probing for Trypanosoma cruzi cell surface glycobiomarkers for the diagnosis and follow-up of chemotherapy of Chagas disease*; Springer Verlag, 2018.
- (104) Iniguez, E.; Schocker, N. S.; Subramaniam, K.; Portillo, S.; Montoya, A. L.; Al-Salem, W. S.; Torres, C. L.; Rodriguez, F.; Moreira, O. C.; Acosta-Serrano, A.; et al. An α -Gal-containing neoglycoprotein-based vaccine partially protects against murine cutaneous leishmaniasis caused by *Leishmania major*. *PLoS Negl Trop Dis* **2017**, *11* (10), e0006039. From NLM.

- (105) Ortega-Rodriguez, U.; Portillo, S.; Ashmus, R. A.; Duran, J. A.; Schocker, N. S.; Iniguez, E.; Montoya, A. L.; Zepeda, B. G.; Olivas, J. J.; Karimi, N. H.; et al. Purification of Glycosylphosphatidylinositol-Anchored Mucins from *Trypanosoma cruzi* Trypomastigotes and Synthesis of α -Gal-Containing Neoglycoproteins: Application as Biomarkers for Reliable Diagnosis and Early Assessment of Chemotherapeutic Outcomes of Chagas Disease. *Methods Mol Biol* **2019**, *1955*, 287-308. From NLM.
- (106) Alonso-Vega, C.; Urbina, J. A.; Sanz, S.; Pinazo, M. J.; Pinto, J. J.; Gonzalez, V. R.; Rojas, G.; Ortiz, L.; Garcia, W.; Lozano, D.; et al. New chemotherapy regimens and biomarkers for Chagas disease: the rationale and design of the TESEO study, an open-label, randomised, prospective, phase-2 clinical trial in the Plurinational State of Bolivia. *BMJ Open* **2021**, *11* (12), e052897. From NLM.
- (107) Montoya, A. L.; Carvajal, E. G.; Ortega-Rodriguez, U.; Estevao, I. L.; Ashmus, R. A.; Jankuru, S. R.; Portillo, S.; Ellis, C. C.; Knight, C. D.; Alonso-Padilla, J.; et al. A Branched and Double Alpha-Gal-Bearing Synthetic Neoglycoprotein as a Biomarker for Chagas Disease. *Molecules* **2022**, *27* (17). From NLM.
- (108) Knight, C. D.; Estevao, I. L.; Portillo, S.; Farani, P. S. G.; Montoya, A.; Heydemann, E.; Carvajal, E. G.; Vinales, I.; Gil, E. R.; Rodriguez, F. Synthetic glycovaccines elicit cross-protection against Chagas disease and tegumentary leishmaniasis in a murine co-infection model. In *The Journal of Immunology*, 2023; Vol. 210, pp 141.105-141.105.
- (109) Subramaniam, K. S.; Austin, V.; Schocker, N. S.; Montoya, A. L.; Anderson, M. S.; Ashmus, R. A.; Mesri, M.; Al-Salem, W.; Almeida, I. C.; Michael, K. Anti- α -Gal antibodies detected by novel neoglycoproteins as a diagnostic tool for Old World cutaneous leishmaniasis caused by *Leishmania major*. *Parasitology* **2018**, *145* (13), 1758-1764.

- (110) Ashmus, R. A.; Schocker, N. S.; Cordero-Mendoza, Y.; Marques, A. F.; Monroy, E. Y.; Pardo, A.; Izquierdo, L.; Gállego, M.; Gascon, J.; Almeida, I. C. Potential use of synthetic α -galactosyl-containing glycotopes of the parasite *Trypanosoma cruzi* as diagnostic antigens for Chagas disease. *Organic & biomolecular chemistry* **2013**, *11* (34), 5579-5583.
- (111) Schocker, N. S.; Portillo, S.; Brito, C. R.; Marques, A. F.; Almeida, I. C.; Michael, K. Synthesis of Gal α (1, 3) Gal β (1, 4) GlcNAc α -, Gal β (1, 4) GlcNAc α -and GlcNAc-containing neoglycoproteins and their immunological evaluation in the context of Chagas disease. *Glycobiology* **2016**, *26* (1), 39-50.
- (112) Witczak, Z. J.; Bielski, R. *Coupling and decoupling of diverse molecular units in glycosciences*; Springer, 2017.
- (113) Portillo, S.; Zepeda, B. G.; Iniguez, E.; Olivas, J. J.; Karimi, N. H.; Moreira, O. C.; Marques, A. F.; Michael, K.; Maldonado, R. A.; Almeida, I. C. A prophylactic α -Gal-based glycovaccine effectively protects against murine acute Chagas disease. *Npj Vaccines* **2019**, *4* (1), 1-15.
- (114) Montoya, A. L.; Gil, E. R.; Heydemann, E. L.; Estevao, I. L.; Luna, B. E.; Ellis, C. C.; Jankuru, S. R.; Alarcón de Noya, B.; Noya, O.; Zago, M. P. Specific Recognition of β -Galactofuranose-Containing Glycans of Synthetic Neoglycoproteins by Sera of Chronic Chagas Disease Patients. *Molecules* **2022**, *27* (2), 411.
- (115) Montoya, A. L.; Austin, V. M.; Portillo, S.; Vinales, I.; Ashmus, R. A.; Estevao, I.; Jankuru, S. R.; Alraey, Y.; Al-Salem, W. S.; Acosta-Serrano, Á.; et al. Reversed Immunoglycomics Identifies α -Galactosyl-Bearing Glycotopes Specific for *Leishmania major* Infection. *JACS Au* **2021**, *1* (8), 1275-1287. DOI: 10.1021/jacsau.1c00201 (accessed 2022-01-26T16:42:39).

- (116) Viana, S. M.; Montoya, A. L.; Carvalho, A. M.; de Mendonça, B. S.; Portillo, S.; Olivas, J. J.; Karimi, N. H.; Estevao, I. L.; Ortega-Rodriguez, U.; Carvalho, E. M.; et al. Serodiagnosis and therapeutic monitoring of New-World tegumentary leishmaniasis using synthetic type-2 glycoinositolphospholipid-based neoglycoproteins. *Emerg Microbes Infect* **2022**, *11* (1), 2147-2159. From NLM.
- (117) Bertozzi, C. R.; Kiessling, L. L. Chemical glycobiology. *Science* **2001**, *291* (5512), 2357-2364.
- (118) Rudd, P. M.; Elliott, T.; Cresswell, P.; Wilson, I. A.; Dwek, R. A. Glycosylation and the immune system. *Science* **2001**, *291* (5512), 2370-2376.
- (119) Murrey, H. E.; Hsieh-Wilson, L. C. The chemical neurobiology of carbohydrates. *Chemical reviews* **2008**, *108* (5), 1708-1731.
- (120) Boltje, T. J.; Buskas, T.; Boons, G.-J. Opportunities and challenges in synthetic oligosaccharide and glycoconjugate research. *Nature chemistry* **2009**, *1* (8), 611-622.
- (121) Demarco, M. L.; Woods, R. J. Structural glycobiology: A game of snakes and ladders. *Glycobiology* **2008**, *18* (6), 426-440. DOI: 10.1093/glycob/cwn026 (accessed 2022-01-25T18:06:39).
- (122) Haltiwanger, R. S.; Lowe, J. B. Role of Glycosylation in Development. *Annual Review of Biochemistry* **2004**, *73* (1), 491-537. DOI: 10.1146/annurev.biochem.73.011303.074043 (accessed 2022-01-25T18:32:00).
- (123) Willment, J. A.; Gordon, S.; Brown, G. D. Characterization of the Human β -Glucan Receptor and Its Alternatively Spliced Isoforms. *Journal of Biological Chemistry* **2001**, *276* (47), 43818-43823. DOI: 10.1074/jbc.m107715200 (accessed 2022-01-25T18:33:54).

- (124) Cobb, B. A.; Kasper, D. L. Coming of age: carbohydrates and immunity. *European Journal of Immunology* **2005**, 35 (2), 352-356. DOI: 10.1002/eji.200425889 (accessed 2022-01-25T18:36:08).
- (125) Sarkar, A. K.; Rostand, K. S.; Jain, R. K.; Matta, K. L.; Esko, J. D. Fucosylation of Disaccharide Precursors of Sialyl LewisX Inhibit Selectin-mediated Cell Adhesion. *Journal of Biological Chemistry* **1997**, 272 (41), 25608-25616. DOI: 10.1074/jbc.272.41.25608 (accessed 2022-01-25T18:39:11).
- (126) Dreitlein, W. B.; Maratos, J.; Brocavich, J. Zanamivir and oseltamivir: two new options for the treatment and prevention of influenza. *Clinical Therapeutics* **2001**, 23 (3), 327-355. DOI: 10.1016/s0149-2918(01)80042-4 (accessed 2022-01-25T18:41:29).
- (127) Kelly, D. F.; Moxon, E. R.; Pollard, A. J. Haemophilus influenzae type b conjugate vaccines. *Immunology* **2004**, 113 (2), 163-174. DOI: 10.1111/j.1365-2567.2004.01971.x (accessed 2022-01-25T19:00:32).
- (128) Geyer, H.; Geyer, R. Strategies for analysis of glycoprotein glycosylation. *Biochimica et Biophysica Acta (BBA)-Proteins and Proteomics* **2006**, 1764 (12), 1853-1869.
- (129) Guo, J.; Ye, X.-S. Protecting groups in carbohydrate chemistry: influence on stereoselectivity of glycosylations. *Molecules* **2010**, 15 (10), 7235-7265.
- (130) Wu, Y.; Xiong, D.-C.; Chen, S.-C.; Wang, Y.-S.; Ye, X.-S. Total synthesis of mycobacterial arabinogalactan containing 92 monosaccharide units. *Nature communications* **2017**, 8 (1), 1-7.
- (131) Smoot, J. T.; Demchenko, A. V. Oligosaccharide synthesis: from conventional methods to modern expeditious strategies. *Advances in carbohydrate chemistry and biochemistry* **2009**, 62, 161-250.

- (132) Joseph, A. A.; Pardo-Vargas, A.; Seeberger, P. H. Total synthesis of polysaccharides by automated glycan assembly. *Journal of the American Chemical Society* **2020**, *142* (19), 8561-8564.
- (133) Krasnova, L.; Wong, C.-H. Oligosaccharide synthesis and translational innovation. *Journal of the American Chemical Society* **2019**, *141* (9), 3735-3754.
- (134) Varki, A.; Cummings, R. D.; Esko, J. D.; Stanley, P.; Hart, G. W.; Aebi, M.; Darvill, A. G.; Kinoshita, T.; Packer, N. H.; Prestegard, J. H. Essentials of Glycobiology [internet]. **2015**.
- (135) Neelamegham, S.; Aoki-Kinoshita, K.; Bolton, E.; Frank, M.; Lisacek, F.; Lütteke, T.; O'Boyle, N.; Packer, N. H.; Stanley, P.; Toukach, P. Updates to the symbol nomenclature for glycans guidelines. *Glycobiology* **2019**, *29* (9), 620-624.
- (136) Ramírez, J. L.; Guevara, P. Persistent infections by Leishmania (Viannia) braziliensis. *Mem Inst Oswaldo Cruz* **1997**, *92* (3), 333-338. From NLM.
- (137) Bailey, M. S.; Lockwood, D. N. Cutaneous leishmaniasis. *Clinics in dermatology* **2007**, *25* (2), 203-211.
- (138) Hong, A.; Zampieri, R. A.; Shaw, J. J.; Floeter-Winter, L. M.; Laranjeira-Silva, M. F. One Health Approach to Leishmaniases: Understanding the Disease Dynamics through Diagnostic Tools. *Pathogens* **2020**, *9* (10). DOI: 10.3390/pathogens9100809 From NLM.
- (139) de Vries, H. J.; Reedijk, S. H.; Schallig, H. D. Cutaneous leishmaniasis: recent developments in diagnosis and management. *American journal of clinical dermatology* **2015**, *16* (2), 99-109.
- (140) WHO. *Leishmaniasis*. World Health Organization, 2022. (accessed).
- (141) Mcgwire, B. S.; Satoskar, A. R. Leishmaniasis: clinical syndromes and treatment. *QJM* **2014**, *107* (1), 7-14. DOI: 10.1093/qjmed/hct116 (accessed 2022-01-25T23:05:05).

- (142) Bailey, F.; Mondragon-Shem, K.; Haines, L. R.; Olabi, A.; Alorfi, A.; Ruiz-Postigo, J. A.; Alvar, J.; Hotez, P.; Adams, E. R.; Vélez, I. D. Cutaneous leishmaniasis and co-morbid major depressive disorder: a systematic review with burden estimates. *PLoS neglected tropical diseases* **2019**, *13* (2), e0007092.
- (143) Zulfikar, B.; Shelper, T. B.; Avery, V. M. Leishmaniasis drug discovery: recent progress and challenges in assay development. *Drug Discov Today* **2017**, *22* (10), 1516-1531. From NLM.
- (144) Machado, P. R.; Rosa, M. E.; Guimarães, L. H.; Prates, F. V.; Queiroz, A.; Schrieffer, A.; Carvalho, E. M. Treatment of Disseminated Leishmaniasis With Liposomal Amphotericin B. *Clin Infect Dis* **2015**, *61* (6), 945-949. From NLM.
- (145) Gomes, C. M.; Paula, N. A.; Morais, O. O.; Soares, K. A.; Roselino, A. M.; Sampaio, R. N. Complementary exams in the diagnosis of American tegumentary leishmaniasis. *An Bras Dermatol* **2014**, *89* (5), 701-709. From NLM.
- (146) Goto, H.; Lindoso, J. A. Current diagnosis and treatment of cutaneous and mucocutaneous leishmaniasis. *Expert Rev Anti Infect Ther* **2010**, *8* (4), 419-433. From NLM.
- (147) Maia, Z.; Lírio, M.; Mistro, S.; Mendes, C. M.; Mehta, S. R.; Badaro, R. Comparative study of rK39 Leishmania antigen for serodiagnosis of visceral leishmaniasis: systematic review with meta-analysis. *PLoS Negl Trop Dis* **2012**, *6* (1), e1484. From NLM.
- (148) Sánchez-Ovejero, C.; Benito-Lopez, F.; Díez, P.; Casulli, A.; Siles-Lucas, M.; Fuentes, M.; Manzano-Román, R. Sensing parasites: Proteomic and advanced bio-detection alternatives. *J Proteomics* **2016**, *136*, 145-156. From NLM.
- (149) Zanetti, A. D. S.; Sato, C. M.; Longhi, F. G.; Ferreira, S. M. B.; Espinosa, O. A. Diagnostic accuracy of Enzyme-Linked Immunosorbent Assays to detect anti-Leishmania antibodies in

- patients with American Tegumentary Leishmaniasis: a systematic review. *Rev Inst Med Trop Sao Paulo* **2019**, 61, e42. From NLM.
- (150) Zawadzki, J.; Scholz, C.; Currie, G.; Coombs, G. H.; McConville, M. J. The glycoinositolphospholipids from *Leishmania panamensis* contain unusual glycan and lipid moieties. *J Mol Biol* **1998**, 282 (2), 287-299. From NLM.
- (151) McConville, M. J.; Ferguson, M. A. The structure, biosynthesis and function of glycosylated phosphatidylinositols in the parasitic protozoa and higher eukaryotes. *Biochemical Journal* **1993**, 294 (2), 305-324.
- (152) McConville, M. J.; Homans, S. W.; Thomas-Oates, J. E.; Dell, A.; Bacic, A. Structures of the glycoinositolphospholipids from *Leishmania major*. A family of novel galactofuranose-containing glycolipids. *J Biol Chem* **1990**, 265 (13), 7385-7394. From NLM.
- (153) de Lederkremer, R. M.; Giorgi, M. E.; Marino, C. The α -Galactosyl Carbohydrate Epitope in Pathogenic Protozoa. *ACS Infect Dis* **2022**, 8 (11), 2207-2222. From NLM.
- (154) de Lederkremer, R. M.; Colli, W. Galactofuranose-containing glycoconjugates in trypanosomatids. *Glycobiology* **1995**, 5 (6), 547-552. From NLM.
- (155) Travassos, L. R.; Almeida, I. C. Carbohydrate immunity in American trypanosomiasis. *Springer Semin Immunopathol* **1993**, 15 (2-3), 183-204. From NLM.
- (156) McConville, M. J.; Ferguson, M. A. The structure, biosynthesis and function of glycosylated phosphatidylinositols in the parasitic protozoa and higher eukaryotes. *Biochem J* **1993**, 294 (Pt 2), 305-324.
- (157) McConville, M. J.; Bacic, A. A family of glycoinositol phospholipids from *Leishmania major*. Isolation, characterization, and antigenicity. *J Biol Chem* **1989**, 264 (2), 757-766.

- (158) Avila, J. L.; Rojas, M.; Acosta, A. Glycoinositol phospholipids from American Leishmania and Trypanosoma spp: partial characterization of the glycan cores and the human humoral immune response to them. *J Clin Microbiol* **1991**, *29* (10), 2305-2312.
- (159) Rosen, G.; Londner, M. V.; Seveler, D.; Greenblatt, C. L. Leishmania major: glycolipid antigens recognized by immune human sera. *Mol Biochem Parasitol* **1988**, *27* (1), 93-99. DOI: 10.1016/0166-6851(88)90028-x.
- (160) Cabezas, Y.; Legentil, L.; Robert-Gangneux, F.; Daligault, F.; Belaz, S.; Nugier-Chauvin, C.; Tranchimand, S.; Tellier, C.; Gangneux, J. P.; Ferrières, V. Leishmania cell wall as a potent target for antiparasitic drugs. A focus on the glycoconjugates. *Org Biomol Chem* **2015**, *13* (31), 8393-8404. DOI: 10.1039/c5ob00563a.
- (161) Montoya Arias, A. L. Discovery of glycan-based biomarkers for cutaneous leishmaniasis and chagas disease by reversed immunoglycomics. University of Texas at El Paso, El Paso, Texas, 2020.
- (162) Completo, G. C.; Lowary, T. L. Synthesis of galactofuranose-containing acceptor substrates for mycobacterial galactofuranosyltransferases. *J Org Chem* **2008**, *73* (12), 4513-4525. DOI: 10.1021/jo800457j.
- (163) Bai, Y.; Lowary, T. L. 2,3-Anhydrosugars in glycoside bond synthesis. Application to alpha-D-galactofuranosides. *J Org Chem* **2006**, *71* (26), 9658-9671. DOI: 10.1021/jo061713o.
- (164) Zemplén, G.; Kunz, A. Studien über Amygdalin, IV: Synthese des natürlichen l-Amygdalins. *Berichte der deutschen chemischen Gesellschaft (A and B Series)* **1924**, *57* (8), 1357-1359.
- (165) Fischer, E. Ueber die glucoside der alkohole. In *Untersuchungen Über Kohlenhydrate und Fermente (1884–1908)*, Springer, 1909; pp 682-694.

- (166) Fischer, E. Ueber die verbindungen der zucker mit den alkoholen und ketonen. In *Untersuchungen Über Kohlenhydrate und Fermente (1884–1908)*, Springer, 1909; pp 734-757.
- (167) Fischer, E.; Beensch, L. Ueber einige synthetische Glucoside «. *Berichte der deutschen chemischen Gesellschaft* **1894**, 27 (2), 2478-2486.
- (168) Lubineau, A.; Fischer, J.-C. High-yielding one-Step conversion of D-glucose and D-galactose to the corresponding α and β methyl-D-glucofuranosides and galactofuranosides. *Synthetic communications* **1991**, 21 (6), 815-818.
- (169) Plietker, B. *Iron catalysis in organic chemistry: reactions and applications*; John Wiley & Sons, 2008.
- (170) Goulart, T. A.; Kazmirski, J. A.; Back, D. F.; Zeni, G. Iron (III)-promoted synthesis of 3-(organoselanyl)-1, 2-dihydroquinolines from diorganyl diselenides and N-arylpropargylamines by sequential carbon-carbon and carbon-selenium bond formation. *Advanced Synthesis & Catalysis* **2019**, 361 (1), 96-104.
- (171) Halfen, J. A. Recent advances in metal-mediated carbon-nitrogen bond formation reactions: Aziridination and amidation. *Current Organic Chemistry* **2005**, 9 (7), 657-669.
- (172) Sarkar, S.; Maiti, S.; Bera, K.; Jalal, S.; Jana, U. Highly efficient synthesis of polysubstituted fluorene via iron-catalyzed intramolecular Friedel–Crafts alkylation of biaryl alcohols. *Tetrahedron Letters* **2012**, 53 (41), 5544-5547.
- (173) Diaz, D. D.; Miranda, P. O.; Padron, J. I.; Martin, V. S. Recent uses of Iron (III) chloride in organic synthesis. *Current Organic Chemistry* **2006**, 10 (4), 457-476.
- (174) Hoyle, C. E.; Bowman, C. N. Thiol–ene click chemistry. *Angewandte Chemie International Edition* **2010**, 49 (9), 1540-1573.

- (175) Biermann, U.; Butte, W.; Koch, R.; Fokou, P. A.; Türlüç, O.; Meier, M. A.; Metzger, J. O. Initiation of radical chain reactions of thiol compounds and alkenes without any added initiator: thiol-catalyzed cis/trans isomerization of methyl oleate. *Chemistry-A European Journal* **2012**, *18* (26), 8201.
- (176) Firdaus, M. Thiol-Ene (Click) Reactions as Efficient Tools for Terpene Modification. *Asian Journal of Organic Chemistry* **2017**, *6* (12), 1702-1714. DOI: 10.1002/ajoc.201700387 (accessed 2022-01-27T16:26:36).
- (177) Mijangos, I.; Navarro-Villoslada, F.; Guerreiro, A.; Piletska, E.; Chianella, I.; Karim, K.; Turner, A.; Piletsky, S. Influence of initiator and different polymerisation conditions on performance of molecularly imprinted polymers. *Biosensors and Bioelectronics* **2006**, *22* (3), 381-387. DOI: 10.1016/j.bios.2006.05.012 (accessed 2022-01-27T16:59:03).
- (178) Govindarajan, M. Protecting group migrations in carbohydrate chemistry. *Carbohydrate Research* **2020**, 108151.
- (179) Volbeda, A. G.; van der Marel, G. A.; Codée, J. D. Protecting group strategies in carbohydrate chemistry. *Protecting Groups: Strategies and Applications in Carbohydrate Chemistry* **2019**, 1-27.
- (180) Ren, B.; Wang, M.; Liu, J.; Ge, J.; Zhang, X.; Dong, H. Zemplén transesterification: a name reaction that has misled us for 90 years. *Green Chemistry* **2015**, *17* (3), 1390-1394.
- (181) Montoya, A. L.; Gil, E. R.; Vinales, I.; Estevao, I. L.; Taboada, P.; Torrico, M. C.; Torrico, F.; Marco, J. D.; Almeida, I. C.; Michael, K. Big is not better: Comparing two alpha-Gal-bearing glycotopes in neoglycoproteins as biomarkers for *Leishmania (Viannia) braziliensis* infection. *Carbohydr Res* **2023**, *536*, 109015. From NLM.

- (182) Rogozea, A.; Matei, I.; Turcu, I. M.; Ionita, G.; Sahini, V. E.; Salifoglou, A. EPR and circular dichroism solution studies on the interactions of bovine serum albumin with ionic surfactants and β -cyclodextrin. *J Phys Chem B* **2012**, *116* (49), 14245-14253. From NLM.
- (183) Stoll, M. S.; Feizi, T.; Loveless, R. W.; Chai, W.; Lawson, A. M.; Yuen, C. T. Fluorescent neoglycolipids. Improved probes for oligosaccharide ligand discovery. *Eur J Biochem* **2000**, *267* (6), 1795-1804. From NLM.
- (184) Liu, Y.; Palma, A. S.; Feizi, T.; Chai, W. Insights Into Glucan Polysaccharide Recognition Using Glucooligosaccharide Microarrays With Oxime-Linked Neoglycolipid Probes. *Methods Enzymol* **2018**, *598*, 139-167. From NLM.
- (185) Micoli, F.; Rondini, S.; Pisoni, I.; Proietti, D.; Berti, F.; Costantino, P.; Rappuoli, R.; Szu, S.; Saul, A.; Martin, L. B. Vi-CRM 197 as a new conjugate vaccine against Salmonella Typhi. *Vaccine* **2011**, *29* (4), 712-720. From NLM.
- (186) Rennels, M. B.; Edwards, K. M.; Keyserling, H. L.; Reisinger, K. S.; Hogerman, D. A.; Madore, D. V.; Chang, I.; Paradiso, P. R.; Malinoski, F. J.; Kimura, A. Safety and immunogenicity of heptavalent pneumococcal vaccine conjugated to CRM197 in United States infants. *Pediatrics* **1998**, *101* (4 Pt 1), 604-611. From NLM.
- (187) Shinefield, H. R.; Black, S.; Ray, P.; Chang, I.; Lewis, N.; Fireman, B.; Hackell, J.; Paradiso, P. R.; Siber, G.; Kohberger, R.; et al. Safety and immunogenicity of heptavalent pneumococcal CRM197 conjugate vaccine in infants and toddlers. *Pediatr Infect Dis J* **1999**, *18* (9), 757-763. From NLM.
- (188) Snape, M. D.; Perrett, K. P.; Ford, K. J.; John, T. M.; Pace, D.; Yu, L. M.; Langley, J. M.; McNeil, S.; Dull, P. M.; Ceddia, F.; et al. Immunogenicity of a tetravalent meningococcal

glycoconjugate vaccine in infants: a randomized controlled trial. *Jama* **2008**, 299 (2), 173-184. From NLM.

VITA

Irodiel Vinales was born in Villa Clara, Cuba, in 1994, harboring an early aspiration to contribute to society through medicine and scientific endeavors, likely influenced by his physicist mother. Excelling academically, he graduated with honors from Elementary, Middle, and High School. His prowess in chemistry became evident as he clinched Gold medals in the Cuban National Chemistry Olympics for high school students in 2009, 2010, and 2011. In 2012, he represented Cuba at the XVII Iberoamerican Chemistry Olympics in Santa Fe, Argentina, securing a bronze medal.

In September 2013, meeting all prerequisites, he enrolled at the University of Havana as a chemistry major. The same year marked the commencement of his research journey at the Center for the Study of Natural Products under Dr. Fidel E. Morales Vicente's guidance, focusing on multicomponent reactions. Transitioning to the Peptide Synthesis Group at the Center for Genetic Engineering and Biotechnology (CIGB) in 2016, he honed his skills in synthesizing multivalent peptides with biomedical applications.

After completing his undergraduate studies in Chemistry at the University of Havana in July 2018, he promptly applied to the Chemistry Doctoral Program at UTEP and embarked on his Ph.D. journey in the Michael Lab in January 2019. His research spans synthetic carbohydrate chemistry for biomarker discovery, assay development for infectious diseases, and pioneering cancer immunotherapy using lipid nanoparticles. Collaborating closely with glycoimmunologists, his work embodies interdisciplinary excellence.

Outside academia, Irodiel finds solace in hiking, exploring new landscapes, and immersing himself in nature through camping, embracing a lifestyle disconnected from modern amenities.